ADVANCING DIESEL ENGINES VIA CYLINDER DEACTIVATION

A Dissertation

Submitted to the Faculty

of

Purdue University

by

Cody M. Allen

In Partial Fulfillment of the

Requirements for the Degree

of

Doctor of Philosophy

May 2019

Purdue University

West Lafayette, Indiana

THE PURDUE UNIVERSITY GRADUATE SCHOOL
STATEMENT OF DISSERTATION APPROVAL

Dr. Gregory M. Shaver, Chair

   School of Mechanical Engineering

Dr. Peter H. Meckl

   School of Mechanical Engineering

Dr. Steven F. Son

   School of Mechanical Engineering

Dr. Li Qiao

   School of Aeronautics and Astronautics

Approved by:

   Dr. Jay P. Gore

      Head of the School Graduate Program

ACKNOWLEDGMENTS

TABLE OF CONTENTS

LIST OF TABLES

LIST OF FIGURES

ABBREVIATIONS

AFR	Air-Fuel Ratio
BDC	Bottom Dead Center
BMEP	Brake Mean Effective Pressure
BSFC	Brake Specific Fuel Consumption
BTDC	Before Top Dead Center
BTE	Brake Thermal Efficiency
CAC	Charge Air Cooler
CAD	Crank Angle Degree
CCE	Closed Cycle Efficiency
CDA	Cylinder Deactivation
CDA-2CF	CDA with 2 cylinders firing
CDA-3CF	CDA with 3 cylinders firing
CDA-4CF	CDA with 4 cylinders firing
CITT	Curb Idle Transmission Torque
CO	Carbon Monoxide
CO_2	Carbon Dioxide
DCA	Dynamic Cylinder Activation
DOC	Diesel Oxidation Catalyst
DOE	Design of Experiment
DPF	Diesel Particulate Filter
ECM	Engine Control Module
ECR	Effective Compression Ratio
EGR	Exhaust Gas Recirculation
EIVC	Early Intake Valve Closing
EPA	Environmental Protection Agency

FE-6CF	Fuel efficiency mode with 6 cylinders firing
GHG	Greenhouse Gas
HD-FTP	Heavy-Duty Federal Test Procedure
HSDA	High-Speed Data Acquisition
IVC	Intake Valve Closing
LIVC	Late Intake Valve Closing
ME	Mechanical Efficiency
MEP	Mean Effective Pressure
NIMEP	Net Indicated Mean Effective Pressure
NOx	Oxides of Nitrogen
NVH	Noise, Vibration, and Harshness
OASPL	Overall Sound Pressure Level
OCE	Open Cycle Efficiency
PM	Particulate Matter
PV	Pressure-Volume
RPM	Revolutions per Minute
SCR	Selective Catalytic Reduction
SOI	Start of Injection
SPL	Sound Pressure Level
TDC	Top Dead Center
TM-6CF	Thermal management mode with 6 cylinders firing
TOT	Turbine Outlet Temperature
UHC	Unburned Hydrocarbons
VGT	Variable Geometry Turbocharger
VVA	Variable Valve Actuation

ABSTRACT

Allen, Cody M. Ph.D., Purdue University, May 2019. Advancing Diesel Engines via Cylinder Deactivation. Major Professor: Gregory M. Shaver, School of Mechanical Engineering.

The transportation sector continues to be a primary source of greenhouse gas (GHG) emissions, contributing more than any other sector in the United States in 2017. Medium-duty and heavy-duty trucks trail only passenger cars as the largest GHG contributor in this sector [1]. The intense operating requirements of these vehicles create a reliance on the diesel engine that is projected to last for many decades. Therefore, it is vital that the efficiency and environmental sustainability of diesel engines continue to be advanced.

Cylinder deactivation (CDA) is a promising technology to improve diesel engine fuel efficiency and aftertreatment thermal management for emissions reduction. This work presents original experimental results demonstrating fuel efficiency improvements of CDA implemented on a modern engine at idle operating conditions through testing of various CDA configurations. Idle calibration optimizations result in up to 28% fuel consumption reduction at steady-state unloaded idle operation and 0.7% fuel consumption reduction over HD-FTP drive cycles at equivalent emissions levels. The low-load thermal management performance of CDA is also investigated through creep and extended idle transient cycles, during which CDA is shown to reduce fuel consumption by up to 40% with similar thermal management performance and reduced NOx and soot emissions.

Variants of CDA implementation are explored through an experimental comparison of deactivation strategies. The effort described here compares charge trapping strategies through examination of in-cylinder pressures following deactivation because: (1) choice of trapping strategy dictates the in-cylinder pressure character-

istics of the deactivated cylinders, and (2) deactivated cylinders can affect torque, oil consumption, and emissions upon reactivation. Results discussed here suggest no significant differences between the strategies. As an example, the in-cylinder pressures of both trapping strategies are shown to converge as quickly as 0.8 seconds after deactivation.

Finally, the NVH effects of CDA are characterized through studies of torsional vibration, linear vibration, and acoustics. CDA causes frequency content at reduced frequencies compared to conventional operation, which has effects on all aspects of NVH. This creates possible constraints on achievable fuel efficiency and thermal management performance by restricting CDA usage. An alternate form of CDA, dynamic cylinder activation (DCA), is explored as a possible option of avoiding undesirable frequency output while maintaining the desired engine performance.

1. INTRODUCTION

1.1 Motivation

Global and national fossil fuel reduction can be motivated by noting environmental impact on both breathable air and the climate, cheaper consumer input costs, improved energy security, and prolonged oil reserves. While the eventual goal should be a reduced reliance on non-renewable energy sources in favor of alternative renewable sources, a large focus must also remain on improving the efficiency of current energy pathways. Though this effort is certainly a multi-level approach from all industries, one of the largest potential areas for improvement is the transportation sector. As depicted in Figure 1.1, the transportation sector was the largest source of CO_2 emissions in the United States in 2017, contributing 28.7% of the total GHG emissions [1].

Medium-duty and heavy-duty trucks contribute 22.7% of the transportation-related GHG emissions in 2017, trailing only light passenger car. This makes medium- and heavy-duty trucks one of the largest areas for improvement within the transportation sector. As shown in Figure 1.2, freight trucks output significantly greater GHG emissions than other forms of freight transportation. According to the U.S. Department of Transportation, these trucks account for 64% of all freight transported in 2015 by weight and 69% of all freight transported by value [2]. Government forecasts indicate an increase of 44% in tonnage moved by truck by 2045. This would mean trucks account for 16.5 billion tons out of a total of 25.3 billion tons of freight moved annually [3].

There are a variety of approaches to reduce the fuel consumption and GHG impact of the medium- and heavy-duty trucking industry. Many of these, such as electrification and downsizing, are currently being researched by industry and academia. While these approaches have been increasingly successful in reducing fuel consumption of
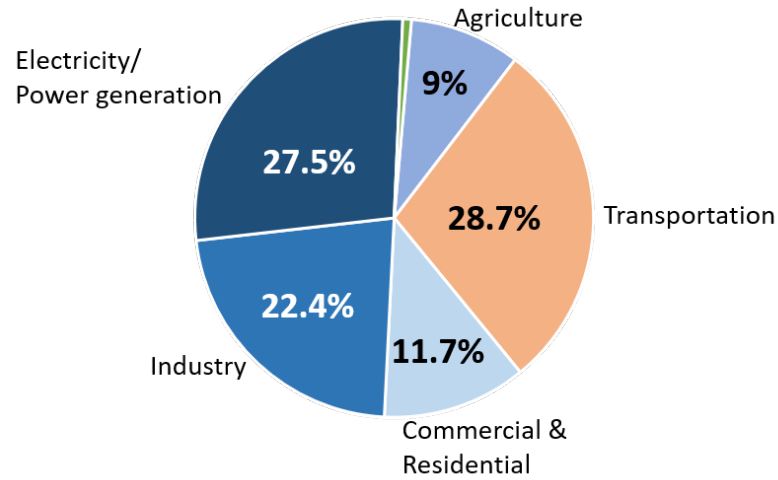
Figure 1.1. Total U.S. greenhouse gas emissions by economic sector in 2017 [1].
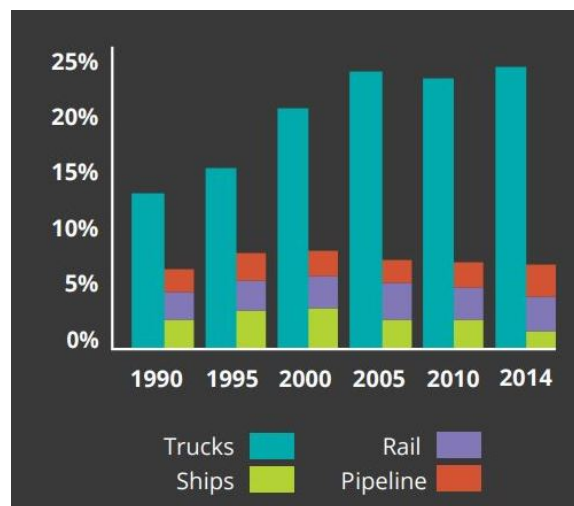
Figure 1.2. Freight GHG emissions as a percentage of transportation sector emissions [3].

the light-duty applications, the medium- and heavy-duty industry will likely remain reliant on fossil fuels for a longer period of time than its lighter counterparts, even with a more complete alternative energy infrastructure. The high power, extended operating requirements of the medium- and heavy-duty trucking industry simply make it less suitable for the adoption of full electrification with the current technology. For

this reason, innovations and improvements to engine efficiency in this segment will make an impact for many years to come. Alternative fuel sources to traditionally used diesel is another pathway to reduced medium- and heavy-duty trucking emissions. Natural gas usage in these applications is an increasingly promising approach. Adoption is expected to be slow, however, as a report by the National Petroleum Council predicts between 61%-100%, depending on oil price, of Class 7 and Class 8 fleets in 2050 will still utilize diesel fuel [4]. The focus on these larger class vehicles is important due to the relative magnitude of fuel consumed compared to other classes, as shown in Figure 1.3.
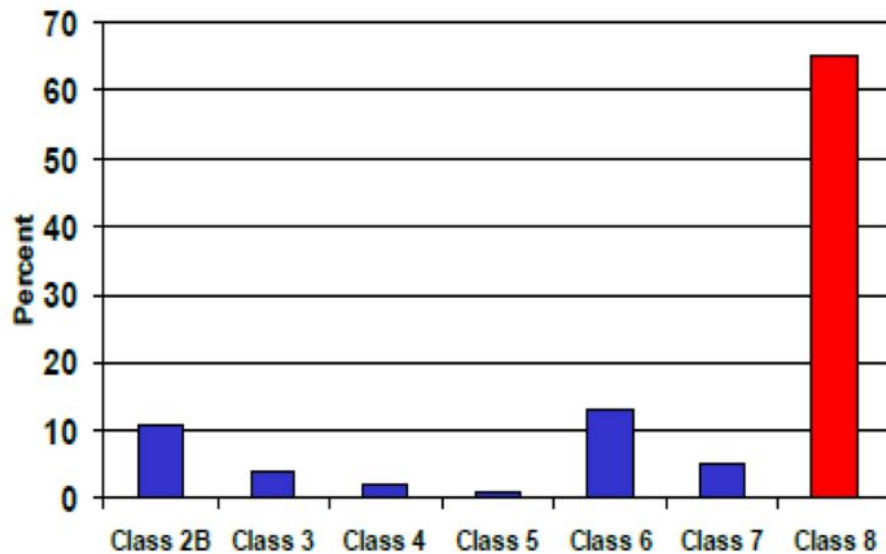
Figure 1.3. U.S. commercial vehicle fuel usage by weight class [5].

The diesel engine has been continually advanced over the last century, so efficiency improvements are a function of innovation. Creating completely new technologies, improving the current state of the art, lowering manufacturing costs to make known potentials realizable in the market, and adopting advancements from other industry segments are all paths that must be considered to enable progress. This work focuses on enabling cylinder deactivation (CDA), a technology that has been used for the past decade in gasoline engines but has yet to penetrate the diesel market. The remainder

of Chapter 1 provides a background on the current state of the art for diesel engines and previous work in CDA to provide the reader with requisite background for the remainder of the dissertation.

1.2 Background and State of the Art

This section serves to provide the reader with a working knowledge of current standards and technology in the heavy-duty on-road diesel engine realm. Trends of criteria pollutant and greenhouse gas emission regulations are first chronicled in order to give a sense of the pace of change in the industry. Some of the advancements that have been implemented to meet these regulations are then described. This includes on-engine technology and downstream aftertreatment technology.

1.2.1 Heavy-Duty On-Highway Diesel Emissions and Regulations

The primary pollutant emissions from diesel combustion are oxides of nitrogen (NOx), particulate matter (PM), unburned hydrocarbons (UHC), and carbon monoxide (CO). These emissions are known to have harmful effects on the environment and population. NOx is a primary cause of acid rain, smog, and the formation of tropospheric ozone. PM is known to cause lung cancer and is a carrier for the ingestion of harmful UHC that are also known to cause cancer. CO can cause poisoning and has undetermined long-term effects [6].

For these reasons, the United States Environmental Protection Agency (EPA) has implemented increasingly stringent regulatory limits in the previous decades culminating in the regulations in place today for heavy-duty on-road engines. These engines are certified on an engine dynamometer drive cycle known as the Heavy-Duty Federal Test Procedure (HD-FTP). The current emissions limits began taking effect in 2007 and were completely implemented in 2010. These levels are shown in Table 1.1.

In addition to these pollutant emissions, the EPA and Department of Highway Traffic Safety Administration have given final rule for GHG and fuel efficiency stan-

dards for medium- and heavy-duty engines and vehicles. Phase two of this ruling will cover model years 2021-2027 and is expected to lower carbon dioxide (CO_2) emissions by 1.1 billion metric tons to reduce climate change impact. This GHG reduction is accompanied by an estimated savings to vehicle owners of approximately \$170 billion on fuel costs and a reduction of up to two billion barrels of oil consumption over the program lifetime [7]. These regulations can be found in [8] and place a renewed focus on fuel efficiency in combination with emissions reduction.

Table 1.1. U.S. EPA emissions standards for heavy-duty on-road engines in g/bhp-hr

CO	UHC	NOx	PM
15.5	0.14	0.20	0.01

1.2.2   On-engine technology

The diesel engine has had a number of advancements over the past two decades. Tightening emissions regulations, particularly with respect to NOx and PM, has motivated many of these advancements. Reduction in PM is achieved via more complete combustion and oxidation of the fuel. This requires sufficient oxygen and high temperatures. NOx, however, is formed in high temperature environments containing excess oxygen [9,10]. Therefore, there is an inherent tradeoff between these two emissions in addition to the tradeoff of emissions with efficiency. Figure 1.4 chronicles the introduction of many now commonplace diesel engine technologies implemented to overcome these challenges.

Charge cooling involves routing the compressed fresh air from the turbocharger through a heat exchanger, typically on the front of the vehicle, to reduce charge
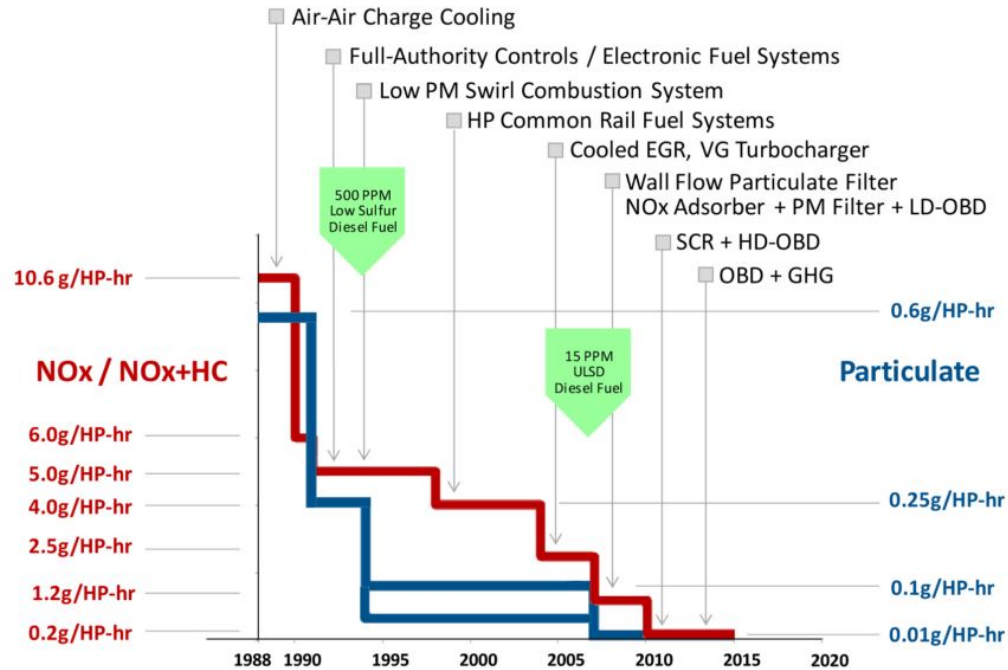
Figure 1.4. Advances of diesel engine and aftertreatment technologies to meet emissions regulations [11].

temperature. The reduction in charge temperature leads to large reductions in NOx emissions via reduced combustion temperatures. Denser air also allows for increased torque and power.

Electronic fuel systems allow for calibration of parameters across the engine operating range via the inclusion of on-board computers known as Engine Control Modules (ECM). These calibrated fueling parameters include injection timing, number of injections, and quantity of fuel in each injection pulse. This allows the combustion to be tailored to the operating condition. For example, early injection timings generally provide more efficient combustion whereas later injection timings lower the combustion temperatures and reduce NOx, as shown in Figure 1.5. Electronic control was eventually extended to a number of actuators and sensors on the engine in the present day. The addition of high pressure common rail fuel systems allows for even further control of the fueling, as the high pressure differential enables precise injections with

even flow. The high fuel pressures (sometimes greater than 2000 bar) also results in an atomized spray, allowing a drastic reduction of particulate emissions [11].
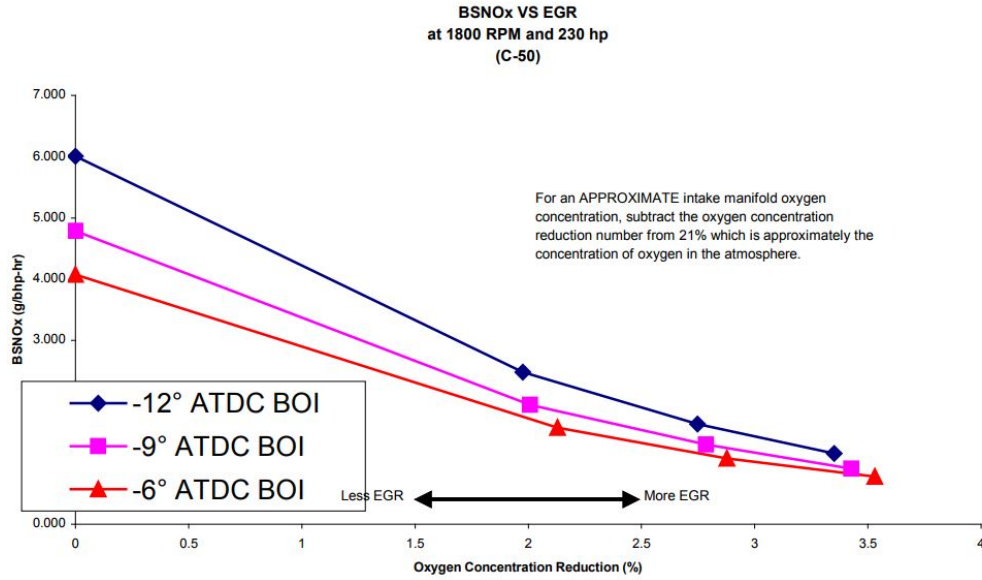
Figure 1.5. Experimental depiction of the relationship between NOx production, oxygen concentration, and injection timing [12].

Other additions, such as variable geometry turbochargers (VGT) and cooled exhaust gas recirculation (EGR), were primarily implemented due to criteria pollutant regulations. The primary function of a turbocharger is to increase charge density, and therefore power, via compression of intake gases. Turbochargers were first introduced on diesel engines in the early 20$^{\text{th}}$ century, however these were fixed geometry turbines with the occasional addition of a wastegate to prevent overspeeding the turbine. Conversely, the VGT involves varying either the geometry of the turbine blades or the width of the entrance to the turbocharger to change the turbine effectiveness via modulation of the swallowing capacity and isentropic efficiency. This, in turn, affects the amount of work extracted for boost [11]. While there are other benefits of the VGT, such as modulated engine braking ability, perhaps the most important reason for the inclusion of a VGT over a fixed geometry turbocharger is EGR control. Varying the geometry of the turbine changes the pressure differential between the exhaust

manifold and intake manifold in order to flow a portion of exhaust gas into the intake. The modulated pressure differential created by the VGT works in conjunction with a valve in the EGR loop to dictate EGR flow. The recirculated gas is routed through a heat exchanger known as an EGR cooler to create cooled high pressure EGR. As described in the previous section, NOx formation requires high temperatures and excess oxygen in the cylinder. The recirculated exhaust gas increases the heat capacity of the charge, resulting in lower combustion temperatures. Moreover, the recirculated gas lowers the oxygen fraction in the cylinder, reducing the available oxygen for NOx formation. This effect is shown in Figure 1.5 for varying levels of EGR and different injection timings.

1.2.3   Aftertreatment

Most modern diesel engines utilize emissions abatement systems including a diesel oxidation catalyst (DOC), diesel particulate filter (DPF), and selective catalytic reduction (SCR) to reduce regulated pollutants [13]. While a variety of configurations and additional components are being studied [14], this is the aftertreatment configuration that is most common today. These aftertreatment components, particularly DOC and SCR, have strong temperature dependencies for performance, and the DPF must be periodically regenerated with high temperatures. Notable is the dependency of NOx conversion on SCR catalyst bed temperature, whose deNOx performance suffers during cold starts and low load operation when inlet gas temperatures are below 200°C-250°C [15, 16].

Engine calibration and performance aspects aimed at controlling the exhaust gas properties, including mass flow rate and exhaust temperature, for efficient aftertreatment operation are commonly collectively known as aftertreatment thermal management [11]. Thermal management techniques that elevate and maintain aftertreatment temperatures typically rely on reduced engine efficiency in order to increase exhaust temperatures [17]. Examples include delayed injection timing, increased en-

gine backpressure from a variable geometry turbine turbocharger (VGT) setting or exhaust throttle, and hydrocarbon dosers. As a result, a complex balance between thermal management, efficiency, and engine-out emissions is required. Advancements in aftertreatment technologies can enable improve efficiency while achieving desired emissions levels or allow for even further emissions reduction. Examples include low-temperature SCR catalysts [18], more efficient aftertreatment configurations, and close coupled or integrated aftertreatments/turbochargers.

A DOC is commonly the first aftertreatment component that the engine exhaust gas flows through. This is because the DOC has a number of conditioning functions for the rest of the aftertreatment. The rare metal DOC catalyst oxidizes UHC and CO from the engine to acceptable levels. Common mechanisms for these reactions are shown in Equation (1.1) and Equation (1.2). The DOC also aids in the DPF functionality via oxidation of NO to NO_2 via Equation (1.3), which is vital for the rest of the aftertreatment.

$$Hydrocarbons + O_2 \rightarrow CO_2 + H_2O \tag{1.1}$$

$$CO + \frac{1}{2}O_2 \rightarrow CO_2 \tag{1.2}$$

$$NO + \frac{1}{2}O_2 \leftrightarrow NO_2 \tag{1.3}$$
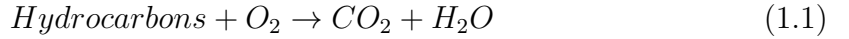
A DPF is a honeycomb filter that physically traps particulate matter to prevent it from exiting the tailpipe to the atmosphere. DPFs typically have high trapping efficiencies reaching almost 95% [19]. However, the particulate trapped in a DPF must periodically be oxidized to reduce the backpressure on the engine and free up space for more particulate to be trapped. When exhaust temperatures are high enough, the NO_2 from the DOC and the excess oxygen in the exhaust stream readily oxidizes the carbon built up on the DPF via Equations (1.4) to (1.7). Soot oxidation with oxygen occurs with notable rates at temperatures above 550°C and with NO_2 at

temperatures above 250°C [20]. When the normal operating condition of the engine is producing temperatures and oxidizer flows to sufficiently oxidize the soot on the DPF, it is known as passive regeneration of the DPF. If the exhaust temperature is too cold for passive regeneration, a common practice is to alter the engine operation to force a regeneration. This is known as active regeneration and can greatly degrade fuel economy.

$$NO_2 + C \rightarrow NO + CO \tag{1.4}$$

$$NO_2 + C \rightarrow \frac{1}{2}N_2 + CO_2 \tag{1.5}$$

$$C + O_2 \rightarrow CO_2 \tag{1.6}$$

$$C + \frac{1}{2}O_2 \rightarrow CO \tag{1.7}$$

The final aftertreatment component is typically the SCR for NOx control. The platinum, vanadia, and/or zeolite based SCR catalysts reduce NO and NO_2 to inert nitrogen gas using ammonia delivered to the exhaust stream in liquid form in an aqueous urea solution. The simplified mechanisms for these reductions are shown in Equations (1.8) to (1.10), with Equation (1.8) representing the dominant mechanism. The NOx conversion efficiency of the catalysts can reach over 95% but is highly temperature dependent [14]. This fact, combined with the component being located downstream of the effective thermal sinks that are the DOC and DPF, can create a challenge for NOx control. NOx control is particularly challenging during cold operation before the engine has time to sufficiently warm up the catalysts. A common engine thermal management strategy is to purposely degrade the fuel efficiency of the engine, either via applying increased backpressure and/or delaying injections, to increase the exhaust temperatures to warm up the SCR. Therefore, strategies that

can increase the exhaust temperature without degrading fuel efficiency are of strong consideration.

$$4NH_3 + 4NO + O_2 \rightarrow 4N_2 + 6H_2O \qquad (1.8)$$

$$2NH_3 + NO + NO_2 \rightarrow 2N_2 + 3H_2O \qquad (1.9)$$

$$8NH_3 + 6NO_2 \rightarrow 7N_2 + 12H_2O \qquad (1.10)$$
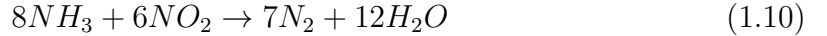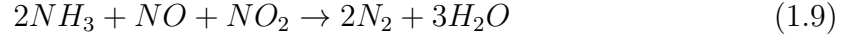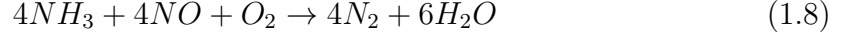
1.3 Literature Review

1.3.1 Cylinder Deactivation

Cylinder deactivation (CDA) is multi-cylinder engine operating strategy in which a fewer number of cylinders than the engine has available are utilized to provide the output power. This reduces the effective displacement of the engine, improving powertrain system efficiency at certain operating conditions. CDA is typically implemented by suspending fueling and valve motion in the deactivated cylinder(s). The technique has proven to be beneficial for fuel efficiency in both gasoline and diesel engines. It also improves diesel engine aftertreatment thermal management.

Manufacturers use CDA on production gasoline engines to improve fuel consumption of vehicles with high power-to-weight ratios [21]. Gasoline engines frequently operate well below their peak power, requiring intake throttling to reduce airflow in order to maintain fuel-air stoichiometry. Throttling increases fuel consumption as a result of higher pumping losses. CDA reduces airflow without incurring increased pumping losses, thereby reducing the amount of throttling required to maintain stoichiometric operation [22]. Firing in less cylinders also means less surface area for heat loss, which improves efficiency [23]. Fuel consumption improvements between 5% to 14% have also been demonstrated [23–26]. 2.7% of U.S. MY2015 passenger

cars and 27.4% of MY2015 light duty gasoline trucks employ CDA. Overall, nearly 13% of light vehicles sold in the U.S. utilize some variant of CDA [27].

CDA is also becoming an increasingly promising option for diesel engines to improve fuel efficiency and aftertreatment thermal management. While there are currently no production examples of CDA implemented on a diesel application, researchers have shown that it has merit. Conventional diesel engines operate lean and typically without an intake throttle. The highest air-fuel ratios (AFR) are generally found at low loads where the engine pumps a large amount of excess air, reducing exhaust temperatures and increasing pumping work. This is problematic for aftertreatment thermal management. Common scenarios of extended low-load operations include hoteling, refuse hauling, urban driving, and drayage operation around ports [17]. Drayage operation, for example, involves idling for an average of 46% of the time [28] with queuing times at ports ranging from 30 minutes to over two hours in some locations [29], during which time the aftertreatment is generally not at temperatures required for effective emissions control. CDA has the potential to increase exhaust temperatures in a fuel efficient manner by lowering the AFR of the engine. This can provide an improved trade-off between fuel economy and thermal management, since the reduction in excess air can yield a simultaneous increase in exhaust gas temperatures [30].

Reference [31] describes experimentally demonstrated 3.4% fuel savings over the Heavy-Duty FTP transient cycle by implementing CDA on a diesel engine during idle. Reference [32] shows analytical and experimental steady-state fuel consumption benefits between 10% to 30% without compromising engine emissions. This fuel consumption improvement was combined with a 40°C-160°C increase in exhaust temperatures. Authors of [30] and [33] found similar results for CDA, each demonstrating fuel consumption improvements of approximately 25% at idle conditions with increased exhaust temperatures. The authors of [34] showed that implementing CDA at and around idle conditions results in no transient response deterioration.

Increases in exhaust temperature can allow more efficient aftertreatment operation during engine operating conditions that would otherwise be too cold for efficient operation [35]. Reference [36] describes simulations to compare CDA and other variable valve actuation strategies and determined it to be the best strategy for near-idle operation to enable low-temperature combustion. They concluded this based on improved fuel economy and superior aftertreatment performance resulting from lower exhaust flow rates and higher exhaust gas temperatures to increase DOC conversion efficiency. The authors of [37] determined experimentally that adopting CDA at highway cruise conditions can enable passive DPF regeneration by elevating the exhaust temperatures by 170-220°C. The authors of [38] found that CDA at high speeds and low loads enabled exhaust temperatures in excess of 450°C, which can be enough to realize DPF regeneration without dosing of the DOC with hydrocarbons. They determined that CDA improves aftertreatment warm-up time and is more effective at maintaining aftertreatment component operating temperatures than conventional operation.

1.3.2 Deactivation Transition Strategies

A cylinder is deactivated when the fueling is suspended and all intake and exhaust valves remain closed. This can increase the overall fuel efficiency and exhaust temperatures of the engine. This technique differs from both cylinder cutout, during which only the fueling is suspended, and other CDA variants discussed below. There are a variety of cylinder combinations that can be deactivated. Cylinders can be deactivated in a configuration that maintains the firing frequency of the engine as close to conventional operation as possible. This helps limit low-frequency torsional vibrations transmitted to the drivetrain. As an example, Figure 1.6 shows a possible half-engine CDA configuration for an inline six-cylinder engine. This configuration, which is used in this study, maintains a periodic firing sequence on the 1-5-3-6-2-4 firing order engine of *fire-inactive-fire-inactive-fire-inactive*.
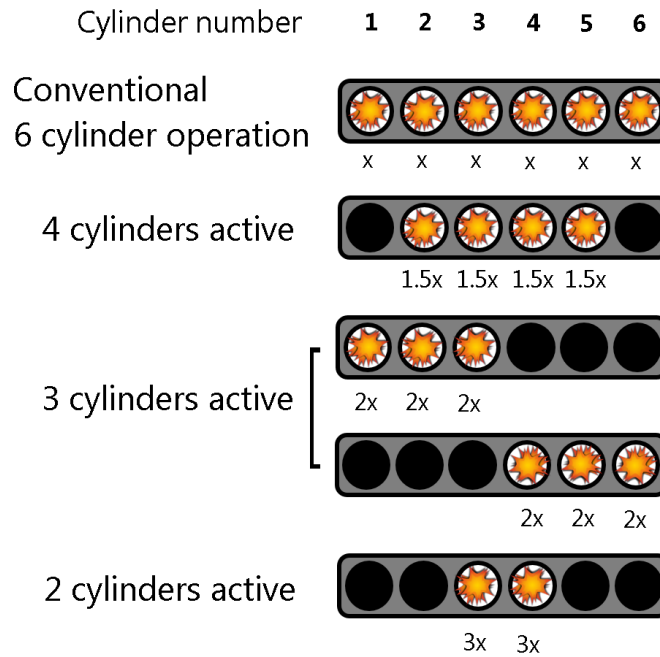
Figure 1.6. Some of the possible cylinder combinations for CDA on the tested engine.

The transition strategy for deactivating a previously firing cylinder is a design consideration that must be made. It is advantageous to have gas in the cylinder once the deactivation occurs in order to keep the minimum cylinder pressure above the crankcase pressure for a longer duration to mitigate oil accumulation in the cylinder and maintain a gas spring [39]. This gas can either be a "fresh" charge mixture of air and recirculated exhaust gas from the intake manifold or a "combusted" charge comprised of burned exhaust gas. Therefore, CDA can be entered by trapping either a fresh charge or a combusted charge.

The implementations of fresh and combusted charge trapping strategies are shown in Figure 1.7. Both trapping strategies deactivate the valve motions with the same timing. The difference between the strategies is the timing of the final fueling and combustion event. In fresh charge trapping, the final intake event occurs without any subsequent fueling events. This leaves a fresh charge trapped in the cylinder

during deactivation. In combusted charge trapping, the final intake event is followed by a fueling and combustion event. This leaves a combusted charge trapped in the cylinder during deactivation. The valves and fueling then remain deactivated until the cylinder is reactivated and conventional engine operation resumes.
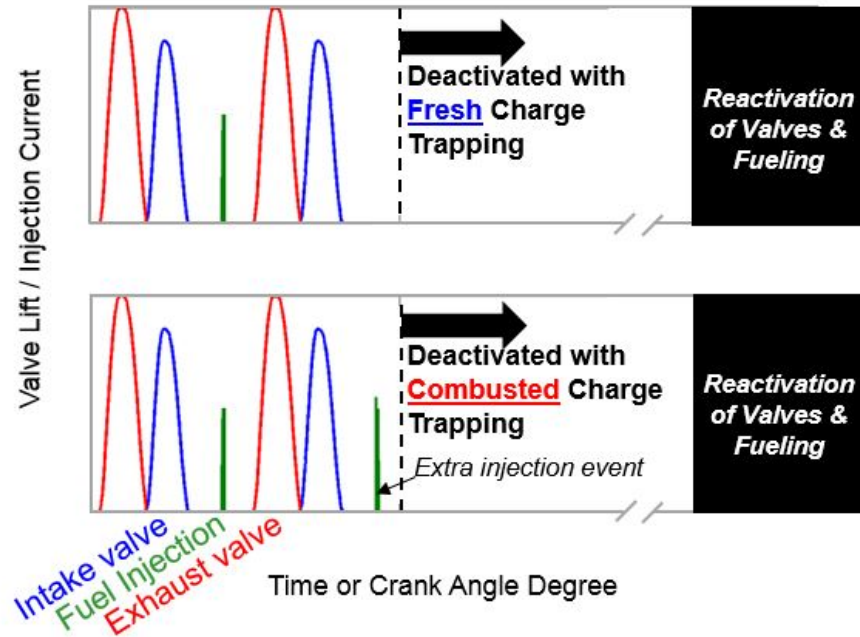
Figure 1.7. Valve and injection event sequences for transitioning into CDA with fresh charge trapping (upper) and combusted charge trapping (lower).

Prior efforts have shown that there are benefits and drawbacks to each trapping strategy. These efforts are variants of CDA [39–41] and skip fire [42]. While works [40–42] focus on gasoline applications, the observations are still worth noting when discussing diesel applications. CDA can be implemented by trapping combusted exhaust gas [22]. CDA can also be implemented by trapping fresh gas. Both trapping strategies will result in the gas spring pressure decaying due to blow-by across the piston rings and heat loss through the cylinder and piston. Authors of [40] claim it to be advisable to trap higher pressure exhaust gas in the cylinder to slow the pressure decay, as maintaining greater cylinder pressures for a longer period of time

will reduce oil consumption. The authors of [39] demonstrated that the mass of oil accumulated in the deactivated cylinder is proportional to the time spent deactivated, and first fire readiness upon reactivation was acceptable for deactivation lengths of up to 20 minutes. Accumulating oil in the cylinder can also lead to increased emissions when the cylinder is reactivated, so a cylinder must be recharged at certain intervals to avoid this effect [41]. Slower pressure decay resulting from combusted charge trapping would allow for less frequent cylinder recharges.

There are also claimed benefits to trapping fresh charge. Fresh charge is claimed to produce less pressure variances and, therefore, less irregularities on the crankshaft [43]. It was also posited that the trapping strategy has an important impact on frictional losses on the deactivated cylinder. The authors of [42] hypothesize lower-pressure gas will have less piston skirt and ring side forces on the cylinder, reducing frictional losses especially immediately after deactivation for skip fire operation. These authors also mention a third strategy of trapping low-pressure gas by deactivating the valves after the exhaust stroke in order to reduce frictional losses. This is likely acceptable since their work focused on skip fire operation where oil accumulation for the small number of deactivation cycles is likely negligible.

1.3.3   CDA and NVH

NVH acceptability is a key design requirement in any automotive product. Multiple components contribute to the NVH of the vehicle, however the powertrain is the dominant contributor. And within the powertrain, the most important source is the engine [44]. The engine is a source of noise and vibration itself due to its dynamic operation. But it can also dictate many NVH characteristics for the rest of the drivetrain due to its torsional vibration contributions.

Diesel engine noise and harshness is perceived by the human ear after the mechanical motion and combustions of the engine create air pressure fluctuations. Harshness generally refers to an unpleasant characteristic of the noise (or vibration), such as

spikes or oscillatory traits [44]. It is an important consideration due to human safety and product quality perception. Humans can perceive noise between 10 Hz-20 kHz, and diesel engines emit a large amount of noise in that range. Engines have direct combustion noise, which is noise originating from the actual combustion, indirect combustion noise, and mechanical noise. Direct combustion noise originates from the pressure increase caused by combustion. Indirect combustion noise stems from a variety of sources and dominates much of the load range [45]. Piston noise is an example of a prominent indirect combustion noise. The pistons changing position are due to combustion but not directly, hence the term indirect combustion noise. Mechanical noise includes the gears and pumps. Inertial forces also create noise, especially at idle [45].

The numerous rotating components, reciprocating pistons, and fast pressure increases mean the diesel engine is also a large source of vibrations. Engine vibrations can be categorized into two types- linear vibrations and torsional vibrations [46]. Linear vibrations refer to the physical motion of the engine in or about the Cartesian directions. Engines are typically designed to minimize linear vibrations via balanced crankshafts and design geometry. Rubberized and hydraulic engine mounts are also commonly used in vehicle applications to dampen these vibrations. The other type of vibrations, torsional vibrations, are an inherent characteristic of any reciprocating engine. These vibrations result from the discontinuous impacts on the crankshaft caused by combustions and are transmitted through the rest of the drivetrain as pulses of varying amplification and frequency through the crankshaft. Driveline boom noise and gear rattle are particularly sensitive to torsional vibrations, especially in manual transmission applications such as heavy-duty vehicles [47]. Driveline boom is objectionable low-frequency noise caused by driveline resonance, which gets excited by the engine torsionals [48]. Gear rattle is a phenomenon caused by the impacts of meshing gear teeth that result in impulsive noise. Both of these are issues that manufacturers must design around and are certainly of concern with respect to customer perception and durability. In order to combat these vibrations, driveline manufacturers typi-

cally design their systems to have resonant frequencies below the lowest fundamental torsional frequencies expected from the engine.

Cylinder deactivation causes lower frequency and higher amplitude torque pulsations on the crankshaft [49]. This can be problematic because many vehicle body and driveline resonant frequencies are already in the low-frequency (0 Hz - 30 Hz) range around idle [23, 48, 50, 51]. The gasoline engine industry encountered this hurdle when CDA started to be implemented on production light-duty vehicles. Reference [23] describes a simulation study on the tradeoff between fuel efficiency improvement and NVH in gasoline vehicles. More frequent CDA usage increases fuel efficiency but has more NVH implications. They posit that NVH and driveability concerns are particularly severe for lower gears and that the low engine speed of idle may be unacceptable for CDA due to NVH. Additionally, human sensitivity to vibration tends to occur between 1 to 18 Hz, with peak sensitivity around 4 Hz [51]. There are key differences between the two scenarios in that gasoline CDA is typically implemented on highway cruise scenarios in drivelines with torque converters, whereas diesel CDA has shown the largest benefits at idle and low-load/speed operation and its applications typically do not have torque converters. Moreover, it has been observed that diesel CDA has larger vibrations than gasoline CDA in general [52]. Some techniques, such as active dampening, additional isolators in the driveline, and increasing inertia of rotating components including the flywheel have potential to mitigate some of the issues [53]. However, these strategies can prove costly and can cause performance degradation. There are also strategies that may be able to help with NVH via the implementation of CDA dynamically. These have been studied on gasoline engines by the authors of [42, 51, 54].

1.4   Contributions

1.4.1   Diesel Engine Variable Valve Actuation

The author led or assisted on a variety of diesel engine VVA-related projects throughout the completion of this dissertation research in support of a research project funded by Cummins and Eaton. Many of these efforts are described below.

CDA Fuel Efficiency Optimizations

The author led an emissions-constrained fuel efficiency optimization for various CDA modes at unloaded idle, demonstrating up to 28% fuel efficiency benefit during experimental testing. The author then led experimental screening to extend the optimized calibration to loaded idle, demonstrating up to 13% fuel efficiency benefit. This work is detailed in Sections 3.2 and 3.3.

Upgraded Transient VVA Testing Capability

The author aided in the migration of the VVA engine and surrounding experimental infrastructure to an upgraded facility with transient AC dynamometer. Then the author co-led an effort with Aswin Ramesh and Dheeraj Gosala to enable transient engine operation with the VVA by enabling seamless transitions between different VVA strategies, including CDA, through coordination of air handling controller, fueling controller, and the VVA system. The results from this effort enabled many other works, including many of the results in this dissertation.

Study of Aftertreatment 'Get-hot' Thermal Management Strategies

The author collaborated with Dheeraj Gosala, Aswin Ramesh, and Mrunal Joshi on an effort to identify VVA strategies that can improve aftertreatment warm-up following cold start engine operation. Steady-state tests were performed to identify

strategies yielding elevated turbine-outlet temperatures and exhaust flow rates. The most promising strategies were then implemented over the HD-FTP drive cycle. A combination of early exhaust valve opening (EEVO) and internal EGR (iEGR) was identified as the most favorable idle strategy. A combination of EEVO and late intake valve closure (LIVC) was implemented at off-idle operating conditions to further expedite the aftertreatment warm-up. Many of the conclusions from this work are detailed in [55].

Study of Aftertreatment 'Stay-hot' Thermal Management Strategies

The author led an effort to characterize the fuel efficiency and thermal management benefits of CDA over low-load operations during extended idle and repeated Heavy Heavy-Duty Diesel Truck (HHDDT) Creep cycles. This work is detailed in Section 3.5. The author co-led experiments with Mrunal Joshi, Dheeraj Gosala, and Kalen Vos to examine the thermal management and fuel efficiency performance of CDA at idle and low loads during HD-FTP operation. Some of these results are presented in Section 3.4, and other results are presented in [31]. Additional thermal management and fuel efficiency results and predictions for various other examined drive cycles are presented in [56]. The author also contributed to the steady-state performance characterization of CDA at various operating conditions, including co-leading an effort at curb idle and assisting Aswin Ramesh on an effort at higher speed low-load operating conditions. The latter effort demonstrated that, depending on load, CDA and IVC modulation can be used to reduce the fuel consumption between 5% and 25%, increase the rate of warm-up of AFT, maintain higher temperatures, or achieve active DPF regeneration without requiring dosing of the DOC. The results from these experiments are summarized in reference [38].

Evaluation of CDA Transient Performance

The author assisted Dheeraj Gosala on a study of transient operation with CDA. This includes handling the transition between CDA and conventional operation during transient engine operation from starting conditions of unloaded idle, loaded idle, and motoring operation during select aggressive transient sections of the HD-FTP cycle. This work is described in reference [34].

IVC Modulation for Improved Efficiency at Elevated Speeds and Loads

The author led an initial literature review and experimental effort to study the impact of dynamic charging via IVC modulation at high speeds in order to improve volumetric efficiency. The author mentored undergraduate student Troy Odstrcil on a GT-Power simulation of these effects. The author then assisted an effort led by Kalen Vos and Sylvia Lu to use volumetric efficiency benefits of dynamic charging via delayed IVC to translate into fuel efficiency benefits of up to 1.25% at elevated speed and load conditions. The results of this work are summarized in reference [57].

Evaluation of Miller Cycling for Improved Efficiency at Highway Cruise

The author co-led an effort with Mayura Halbe on an experimental investigation of Miller cycling to improve fuel efficiency through IVC modulation-enabled variation in effective compression ratio (ECR).

Charge Trapping Strategy Investigation

The author led an experimental investigation on the effects of different charge trapping strategies for CDA. This work also helped guide implementation of CDA used in a variety of other works in this research group, including the implementation of DCA. Results from this work are described in Chapter 4 and reference [58].

Dynamic Cylinder Activation Performance

The author assisted Dheeraj Gosala in the implementation and performance analysis of DCA in a diesel engine. This study demonstrated that DCA can enable greater control over torsional vibration of the engine while achieving similar fuel consumption and aftertreatment thermal management benefits as fixed CDA. This effort is published in reference [54].

NVH Characterization of Advanced VVA Strategies

The author co-led an effort with Dheeraj Gosala and Eaton collaborators to characterize the torsional and linear vibrations of various VVA strategies. These strategies include fixed CDA and DCA, the results of which are discussed in Chapter 5 of this document. The chapter also includes a separate acoustic study led by the author. Additional VVA strategies tested during NVH experiments include cylinder cutout, reverse breathing, and ventilated cylinder cutout. The results of these are not included in this dissertation.

1.4.2 NEXTCAR

The goal of the Purdue-led project for the DOE ARPA-E NEXTCAR program is to develop algorithms and technology that takes advantage of emerging connectivity infrastructure to enable efficiency improvements for on-highway class 8 trucks. The project is a collaboration between Purdue University, Peloton Technology, Cummins, ZF, PACCAR, and NREL. Some of the author's contributions to NEXTCAR are described below.

NEXTCAR Test Cell

The author led the development of a new engine test cell at Herrick Laboratories in support of the ARPA-E NEXTCAR project. Assistance in this effort to transform

the empty bedplate into the testing setup in Figure 1.8 was given by Alexander Taylor, Miles Droege, Akash Desai, David Meyer, Robert Brown, Ryan Thayer, Jonathan Ore, and numerous other colleagues. The completed test cell then housed a Cummins X15 on the 670HP A/C regenerative dynamometer for the NEXTCAR project. Results from this test cell are not detailed in this dissertation.

Figure 1.8.   The developed NEXTCAR engine test cell.

Development of Model Predictive Controller for Truck Platooning

The author led the development of a following vehicle model predictive controller (MPC) aimed at improving platooning performance in line-haul class 8 trucks. The control framework can utilize vehicle connectivity and look-ahead information to enable improved tracking and/or reduced fuel consumption. The results from this effort are not detailed in this dissertation.

1.4.3   Agricultural Vehicle Automation

The author served as the lead for an on-going multidisciplinary industry-funded project focused on developing agricultural machinery automation features and systems through model-based engineering. Results from this effort are not detailed in this dissertation.

1.5   Outline of this Dissertation

Chapter 1 begins by motivating the importance of clean and efficient diesel engines now and in the future. The current state of the art for diesel engine and aftertreatment is briefly discussed, followed by a literature review of relevant works. Finally, the contributions of the author to various projects are described.

Chapter 2 presents the experimental setup, including engine, aftertreatment, and variable valve actuation system, used for the results in this dissertation.

Chapter 3 details experimental studies on cylinder deactivation (CDA) fuel efficiency and thermal management performance. Steady-state performance at unloaded idle is assessed via experimental optimization. This calibration is extended to loaded idle for further performance assessment. Results of CDA implemented during HD-FTP and low-load drive cycles are then presented.

Chapter 4 presents a study comparing different deactivation transition strategies during CDA transitions via characterization of in-cylinder effects.

Chapter 5 details various studies on the NVH performance of CDA. Characterizations of torsional vibration, linear vibration, and acoustic effects of CDA are presented. An alternate implementation of CDA referred to as dynamic cylinder activation (DCA) is then introduced as a means to control NVH effects of CDA.

Chapter 6 summarizes the efforts discussed in previous chapters and presents recommendations for future work.

2. EXPERIMENTAL SETUP

The experiments for this dissertation were conducted on a Cummins inline 6-cylinder direct-injection diesel engine equipped with a camless variable valve actuation (VVA) system. Dynamometer results were taken with the engine coupled to a 670 hp Power Test AC dynamometer. The dynamometer has access to the engine throttle, allowing closed-loop torque control. Figure 2.1 shows a schematic drawing of the unit under test. The engine architecture includes a VGT, high pressure cooled EGR, air-to-water charge air cooler (CAC), and a high pressure common rail fuel injection system. Care is taken to ensure that no mechanical limits of the engine, shown in Table 2.1 are exceeded during testing.

The exhaust gas of the engine routes through a modern aftertreatment illustrated in Figure 2.2. This system consists of a close-coupled diesel oxidation catalyst (DOC) and diesel particulate filter (DPF) system followed by a selective catalytic reduction device. The SCR system is operated passively, or without urea dosing, for this work. Single-wall, stainless steel exhaust pipe with 4in (101.6mm) diameter is used for the exhaust system. There is a 1.47m long section of exhaust pipe between the turbine outlet and DOC inlet. There is a 1.27m long section between the DPF outlet and SCR inlet consisting of the decomposition reactor and exhaust pipe. Temperatures are measured at a variety of locations throughout the system.

Data is acquired using a dSPACE system. A variety of measurements are taken throughout the system. Volumetric fresh air flow before the compressor is measured using a laminar flow element (LFE) and is converted to a mass flow rate using measurements of pressure, temperature, and humidity of the supply air. Fuel flow into the engine is measured gravimetrically using a Cybermetrix Cyrius Fuel Measurement System.
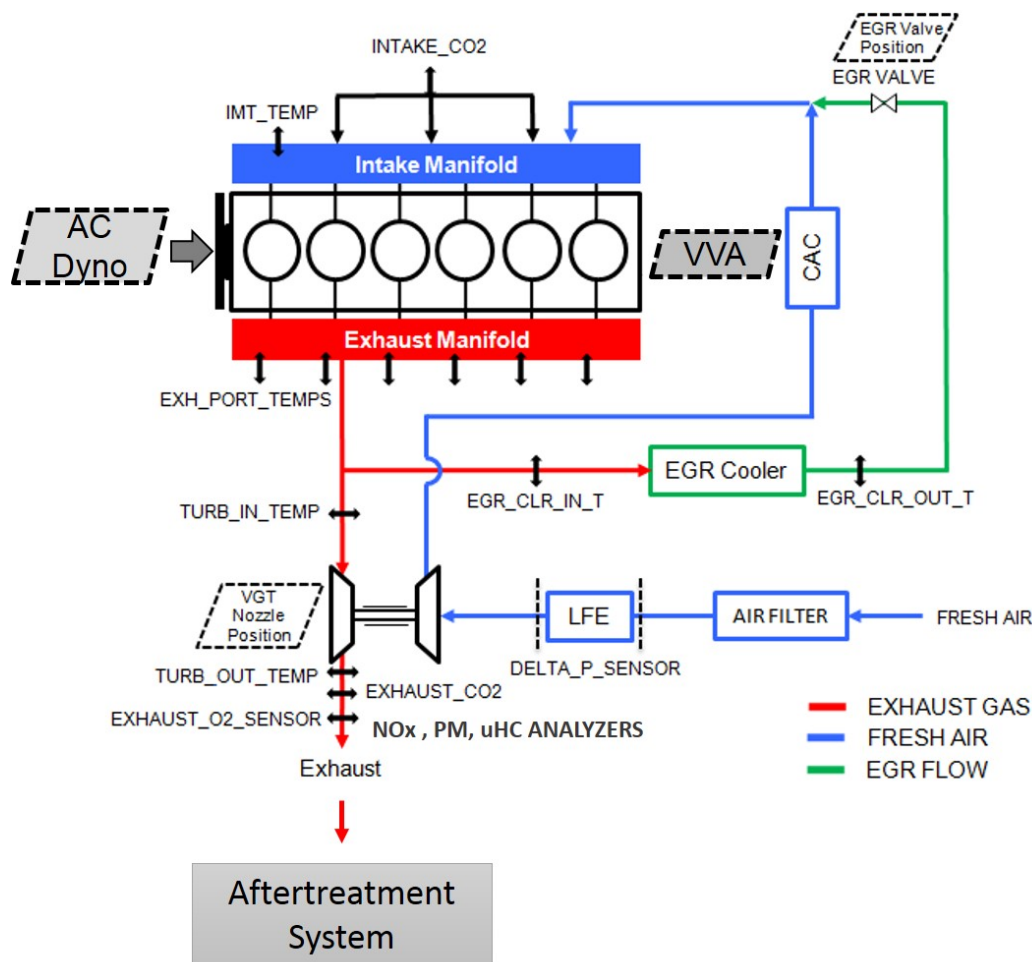
Figure 2.1. Schematic of the unit under test.

Kistler 6067C (cylinders 1 and 3) and AVL QC34C (cylinders 2, 4, 5, 6) cooled piezoelectric pressure transducers are installed in each of the six cylinders to measure in-cylinder pressure. The pressure signals are amplified by AVL MicroIFEM charge amplifiers and subsequently acquired by an AVL 621 IndiModul. Injector current for each cylinder is also acquired by this system for timing and fueling cutoff verification. The in-cylinder pressure and injector current measurements are synchronized with engine crank angle using the AVL 365C crankshaft position encoder.

Emissions are measured using a variety of gas analyzers located at the outlet of the turbine. UHC is measured using a CAI HFID 600. NOx is measured using the OEM

NOx sensor, with redundant measurements taken with a CAI HCLD 600 for verification of accuracy. Intake and exhaust CO_2 are measured using Cambustion NDIR 500 series analyzers, with redundant measurements via a CAI NDIR 600 analyzer. Simultaneous measurement of intake and exhaust CO_2 allows for the calculation of real-time EGR fraction. Soot levels are measured using an AVL 483 Micro Soot Sen-
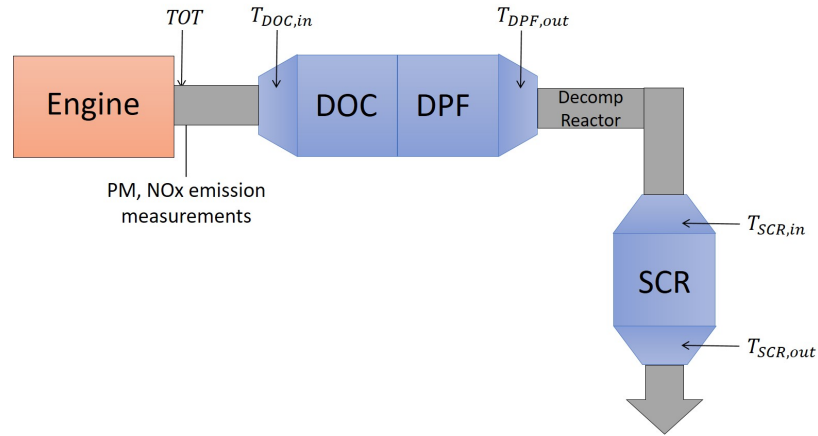
Figure 2.2. Aftertreatment component layout.

Table 2.1. Mechanical constraints.

Parameter	Maximum Constraint
Turbine In Temperature	760°C
Compressor Out Temperature	230°C
Turbo Speed	126 kRPM
Peak Cylinder Pressure	17.2 MPa
Exhaust Manifold Pressure	400 kPa (gauge)
Pressure Rise Rate	100 bar/sec

sor. Exhaust oxygen levels are measured using a universal exhaust gas oxygen sensor located after the turbine outlet. Emissions concentrations are translated to mass using exhaust flow rate, calculated from LFE measurements of fresh air flow and the instantaneous ECM fuel flow estimate.

The VVA system provides cylinder independent, cycle-to-cycle control of the valve events using the dSPACE hardware for control. Valve event characteristics of the intake and exhaust valves can be modified in real-time. Common profile variables are lift height, opening timing, closing timing, and ramp rates. An example of this type of event modification is shown in Figure 2.3. Another example of the flexible system is CDA, where the valve sequence before the deactivation dictates the type of residual gas remaining in the deactivated cylinder. The camless system is comprised of twelve electrohydraulic actuators that act on each intake and exhaust valve pair. The valves are actuated based on engine crank angle position obtained using an AVL 365C crankshaft position encoder. Position feedback for each valve pair is measured using linear variable differential transformers (LVDT). A schematic of the VVA system is shown in Figure 2.4. Accompanying the valve control is a generic serial interface (GSI) dSPACE module to coordinate cycle-to-cycle engine parameters, including fueling events, with the engine ECM. This allows for calibration of the engine at new valve settings and enables the full implementation of CDA on the engine.

It is important to maintain constant boundary conditions on the engine in order to have day-to-day repeatability. As such, fuel supply temperature is maintained via the fuel metering system at 41°C. Many of the boundary conditions on the intake and exhaust gas paths of the engine are also controlled in order to provide better repeatability of testing. Fresh air is supplied to the engine through a facility combustion air supply system. This air supply is maintained at 50% relative humidity and 25°C. Additionally, the temperature of the water-side supply of the CAC heat exchanger is controlled via an active heat exchanger at a constant 25°C. Repeatable conditions at the intake manifold are important due to the sensitivity of engine performance, particularly NOx creation, to intake manifold temperature. NOx has also been shown
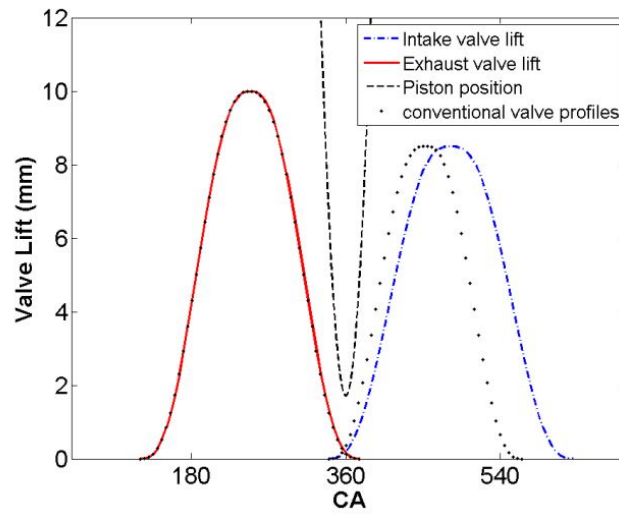
Figure 2.3. Example of late intake valve closure (LIVC).
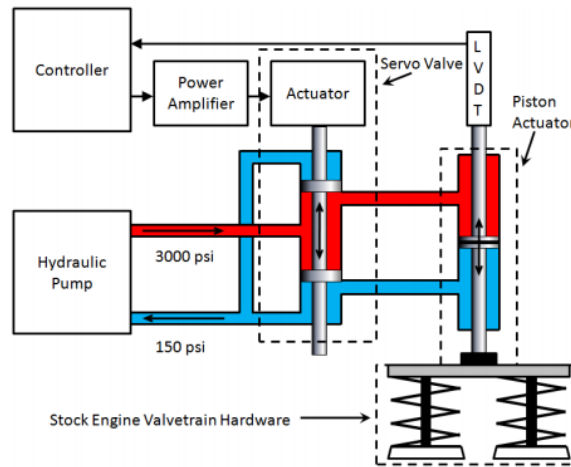
Figure 2.4. Schematic of the variable valve actuation setup used to implement CDA and other VVA strategies.

to vary with relative humidity of the supply air. Though the empirical relation described in [59] is used to correct for this NOx variation, maintaining the humidity levels better ensures accuracy. The supply pressure is maintained at atmospheric pressure via a weighted damper system that vents excess supply air to the test cell. This prevents an artificial supercharging effect of the turbocharger compressor.

The exhaust pressure boundary condition is maintained via one of two methods with the goal of representing the backpressure of an on-vehicle engine. If the aftertreatment system is attached during testing, this system provides the necessary backpressure because the setup represents an on-vehicle system. However, because many aftertreatment components are sensitive to the higher emission concentrations that may be produced during experimental testing, the aftertreatment system is often bypassed. In order to simulate the backpressure applied by the aftertreatment system in this scenario, a valve is installed in the bypass pipe that can be modulated to match the desired turbine outlet pressure levels based on the volumetric exhaust flow.

3. CYLINDER DEACTIVATION IMPLEMENTATION FOR FUEL EFFICIENT THERMAL MANAGEMENT

3.1 Motivation

Previous work indicates that CDA has merit for fuel consumption improvements at and around idle during steady-state operation [30]. Additional focus was determined necessary due to the common operation at idle and the high potential for CDA performance benefits at that condition. For instance, the certification drive cycle for on-road engines is the HD-FTP, which spends approximately 37% of the cycle time at idle. The significance of idle in real-world transportation applications is also well-documented. According to a study by Argonne National Laboratory, an average heavy-duty hauler spends 6 hours idling each day [60].

It was concluded that steady-state performance at unloaded idle (800 RPM, 0 bar BMEP) and curb idle (800 RPM, 1.3 bar BMEP), also referred to as loaded idle in this work, should be the focus of a steady-state study into the merits of CDA. Unloaded idle was chosen for thorough optimization because previous work indicated that lower load conditions have more potential for CDA fuel efficiency improvement, therefore the unloaded idle study gives some insight into the fuel efficiency ceiling for the technology. The 1.3 bar BMEP load for loaded idle was chosen based on its place as the indicated Curb-Idle Transmission Torque (CITT) during the HD-FTP for this project. The idle fuel efficiency studies are the focus of Sections 3.2 and 3.3.

Based on these steady-state idle results, CDA was experimentally implemented during the HD-FTP in Section 3.4 to explore fuel efficiency effects of CDA during this transient cycle.

Experiments utilizing a pair of auxiliary drivecyles were also conducted for a further focused analysis of low-load CDA operation. These cycles, referred to as

extended idle and creep operation and detailed in Section 3.5, allow for additional insight into the effects of CDA on the downstream aftertreatment component temperatures. These drive cycles also represent a variety of real-world driving scenarios, including last-mile freight hauling, refuse hauling, and drayage queuing at ports.

3.2 CDA Fuel Efficiency Optimizations at Unloaded Idle

3.2.1 Methodology and Optimization Predictions

Experimental fuel consumption optimizations were conducted for the unloaded idle operating condition (800 RPM, 0 bar BMEP) for 6 cylinders active (6CF), 3 cylinders active (CDA-3CF), and 2 cylinders active (CDA-2CF). Optimizing 6 cylinder operation using the same methodology as the CDA optimizations was necessary to accurately determine the effects of CDA, as the stock calibration on the engine has other design parameters, particularly at idle, that are difficult to account for in an academic setting. The unloaded idle operating condition was implemented in the tested setup by deactivating the dynamometer from the engine and allowing the low-speed governor to maintain the set speed of 800 RPM. This operating condition has relatively low fuel consumption which does create more uncertainty in the regression models, therefore this study was meant to provide a basis for calibration rather than explicitly optimal fuel consumption settings. Nevertheless, the following process is treated as an optimization.

A design of experiments (DOE) methodology was used to find the optimal fuel efficiency within predefined allowable emissions limits for conventional operation and each CDA mode. Constrained emissions were NOx, UHC, and soot. Parameters varied for the DOE design are main injection SOI, rail pressure, EGR valve position, and VGT nozzle position. These parameters were varied across the ranges given in Table 3.1 for the 6CF and CDA-3CF DOEs. The CDA-2CF DOE was performed last, and observations based on the first two in addition to limitations with respect to injection timing feasibility at this condition led to the parameters ranges in Table 3.2

for that DOE. Minitab, a statistical analysis software, was used to create the face-centered central composite DOE matrix. The DOE was chosen to be a face-centered central composite design with one center point per parameter. A central composite design was chosen instead of a factorial design in order to better capture the known non-linear interactions between parameters. The four control parameters in a face-centered central composite configuration create 25 unique test points for each cylinder configuration. More details on central composite design can be found in [61].

Center points of each DOE design were randomly mixed throughout the DOE in order to create a representative repeat point condition for each mode. This allowed for determination of statistical significance in the optimization through knowledge of experimental standard deviation. The engine was allowed to stabilize for 15 minutes between DOE points. Gravimetric fuel readings were taken for 8 minutes after stabilization. This relatively long fuel consumption measurement duration was due to the low fuel consumption at unloaded idle. Other measurements, including emissions, are also the result of an 8 minute average. In-cylinder pressure measurements were taken for 100 engine cycles. An intake event for each cylinder was commanded every 100 cycles during CDA in order to recharge the cylinder to minimize oil consumption during extended deactivation periods. Realistic aftertreatment backpressure was emulated through the modulation of a valve in the exhaust pipe according to volumetric exhaust flow rate.

After all DOE experiments were taken, Minitab was used to create a response surface for each design. The resulting optimization settings are shown in Table 3.3 with the corresponding predicted engine responses shown in Table 3.4. The predicted optimal settings were then run on the engine to validate the optimization results.

Observations can be made based on the predicted settings. The predicted optimal settings all have the lowest rail pressure allowed by the range. This indicates that any loss of combustion quality is overcome by the mechanical benefits of not compressing the fuel to as high of pressure. The parasitic losses of the high pressure pump are proportionally larger at idle. The VGT position is relatively open for the

Table 3.1. Unloaded idle optimization parameters and ranges for 6CF and CDA-3CF.

Parameter	Lower	Middle	Upper
Start of Main Injection (SOI) (normalized °BTDC)	-1	0	1
Rail Pressure (normalized bar)	-1	0	1
VGT Position (normalized % closed)	-1	0	1
EGR Position (normalized % open)	-1	0	1

Table 3.2. Unloaded idle optimization parameters and ranges for CDA-2CF.

Parameter	Lower	Middle	Upper
Start of Main Injection (SOI) (normalized °BTDC)	-0.6	0.2	1
Rail Pressure (normalized bar)	-1	-0.38	0.25
VGT Position (normalized % closed)	-1	0.17	0.67
EGR Position (normalized % open)	-1	0.125	1.25

6CF prediction even though the predictions are constrained by NOx rate. A more closed VGT position would allow for an increased EGR rate, decreasing the NOx. Instead, delayed SOI is predicted to be the NOx reduction strategy with less impact on fuel consumption at this condition. The limiting emission for CDA-3CF is soot. CDA-3CF has the maximum closure of VGT allowed for this study with a relatively open EGR valve. It is then logical that its NOx rate is predicted to be very low. This high level of EGR flow would then result in high soot. Therefore, the CDA-3CF optimization found that the most favorable fuel consumption for the NOx/soot trade-off is found at the maximum of the soot range for this operation, with the SOI allowed to be advanced to its predicted optimal setting. The larger combustion events occurring in the active cylinders place more importance on combustion efficiency than during 6CF operation. Finally, CDA-2CF is not predicted to be constrained by any emission, though soot is close to the defined limit. This means that these settings are predicted to represent the global optimal fuel consumption for this operating scenario.

Table 3.3. Predicted optimized parameter settings at unloaded idle (800 RPM, 0 bar BMEP).

Mode	SOI	Rail Pressure	VGT	EGR
-	norm °BTDC	norm bar	norm % closed	norm % open
6CF	-0.94	-1	-0.17	0.47
CDA-3CF	0.03	-1	0.93	0.35
CDA-2CF	0.176	-1	0.22	0.07

Table 3.4. Predicted optimized engine response at unloaded idle (800 RPM, 0 bar BMEP).

Mode	Normalized Fueling	Normalized NOx	Normalized UHC	Normalized Soot
6CF	1	1	0.31	0.37
CDA-3CF	0.76	0.18	0.1	1
CDA-2CF	0.75	0.38	0.38	0.91

3.2.2 Results and Experimental Validation

The predicted optimal settings for each cylinder configuration were run on-engine to validate the results at unloaded idle. All settings matched those in Table 3.3 except the 4-cylinder CDA rail pressure, which had to be increased by a minimal amount to maintain stable combustion. Table 3.5 shows a summary of the engine responses for each mode. Uncertainties are expressed as one standard deviation from the mean value of the repeated center points in each DOE, as described previously. Figure 3.1 shows a graphical depiction of the results. CDA-3CF results in 15% reduction in fuel consumption and CDA-2CF results in 23% reduction in fuel consumption over the improved 6CF settings.

Cycle efficiency analysis metrics are useful tools to examine the efficiency changes via CDA. As described by Equation (3.1), the brake thermal efficiency (BTE) of the engine can be depicted as the product of closed cycle efficiency (CCE), open cycle efficiency (OCE), and mechanical efficiency (ME). Though BTE is, by definition, null at the unloaded idle operating condition due to the 0 bar BMEP load, OCE and

Table 3.5. Engine response for the optimized settings at unloaded idle (800 RPM, 0 bar BMEP).

Mode	Normalized Fueling	Normalized NOx	Normalized UHC	Normalized Soot
Limits	-	1	1	1
6CF	1 ±0.04	0.88 ±0.05	0.19 ±0.04	0.50 ±0.08
CDA-3CF	0.85 ±0.06	0.17 ±0.02	0.35 ±0.01	0.77±0.02
CDA-2CF	0.77 ±0.01	0.43 ±0.05	0.76 ±0.04	0.99 ±0.03
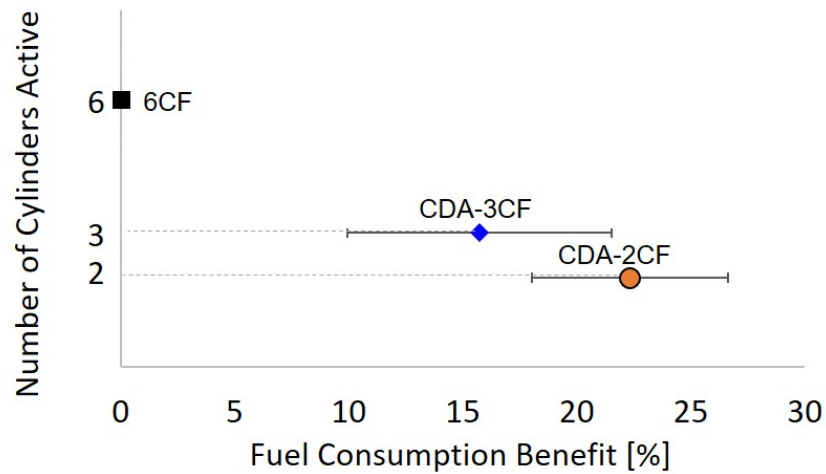
Figure 3.1. Fuel consumption benefits of CDA at unloaded idle (800 RPM, 0 bar BMEP).

CCE can still be calculated based on their definitions. The absolute ME at unloaded idle is, by definition, zero. The details of this analysis are described in greater detail in Appendix A.

$$BTE = CCE \cdot OCE \cdot ME \tag{3.1}$$

The efficiency gains from CDA are due to increases in OCE, shown in Figure 3.2, and CCE, shown in Figure 3.3. There is a large quantity of excess air flow at un-loaded idle. Deactivating cylinders results in a reduction in charge flow, as shown in Figure 3.4, which reduces the total pumping work of the cylinders compared to the net output. This increases the OCE.
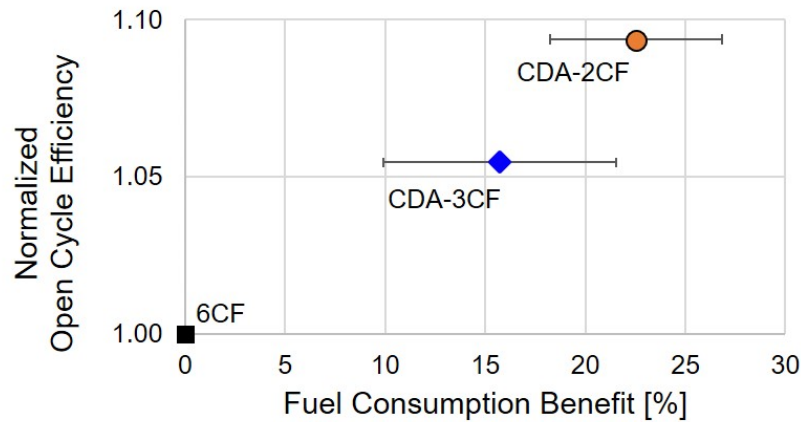
Figure 3.2. Normalized open cycle efficiencies of the improved un-loaded idle points (800 RPM, 0 bar BMEP).

An increase in CCE is a result of reduced in-cylinder heat loss due to a combination of improved combustion timing and less total surface area for heat loss. In general, the optimum heat release centroid for engines is between 7 and 9 degrees after top dead center and varies with engine speed [11]. This is the location of heat release centroid that typically best balances the efficiency and heat losses from earlier combustion timing. This trend is demonstrated by the heat release centroid plot in Figure 3.5. The ability to inject more fuel per active cylinder for equivalent torque allows the combustions during CDA to be closer to TDC while still maintaining emissions at allowable levels. Another large source of CCE increase is a reduction of in-cylinder heat loss. Combustion occurring in fewer cylinders results in less surface area available
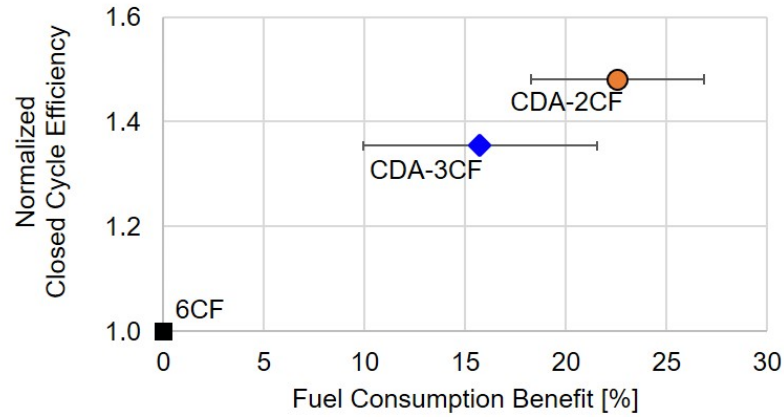
Figure 3.3. Normalized closed cycle efficiencies of the improved unloaded idle points (800 RPM, 0 bar BMEP).
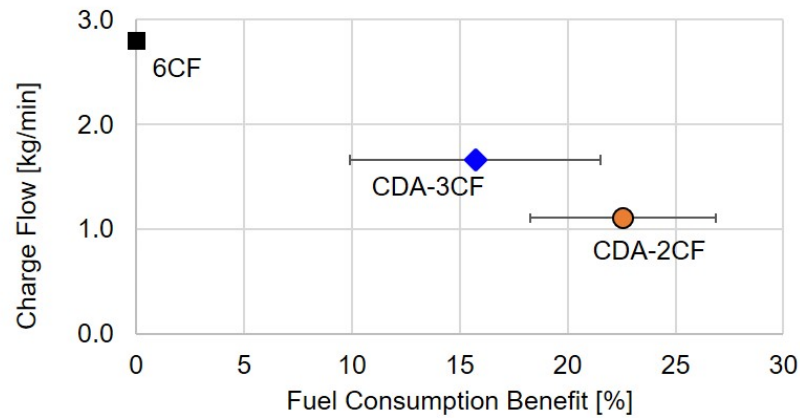
Figure 3.4. Charge flows of the improved unloaded idle points (800 RPM, 0 bar BMEP).

for in-cylinder heat losses. These heat losses can be calculated using the in-cylinder pressure measurements to determine indicated power. The in-cylinder heat loss effects on CCE are shown in Figure 3.6 for the unloaded idle points. Note that the in-cylinder heat loss reduces by 27% for CDA-3CF, while the closed cycle efficiency increases by 35%. Similarly, the in-cylinder heat loss reduces by 40.3% for CDA-2CF, while the closed cycle efficiency increases by 48%.
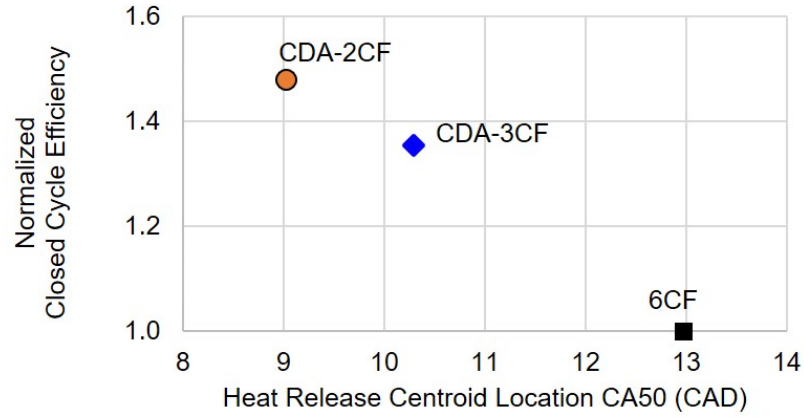
Figure 3.5. Normalized CCE vs heat release centroid locations for the unloaded idle points (800 RPM, 0 bar BMEP).
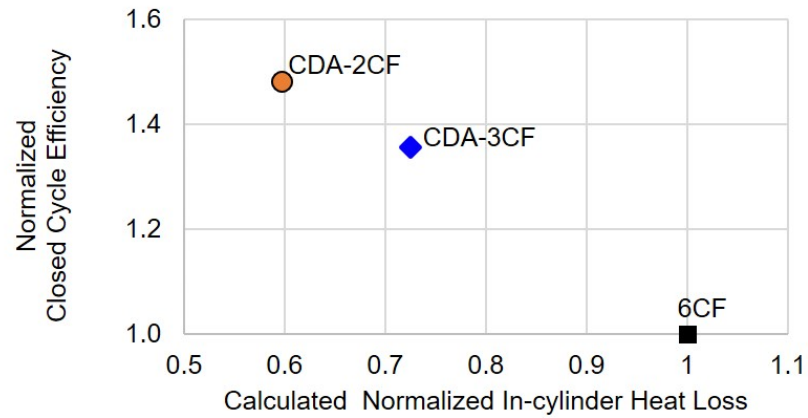
Figure 3.6. Normalized CCE vs the calculated normalized in-cylinder heat loss for the unloaded idle points (800 RPM, 0 bar BMEP).

Directly calculating ME at the unloaded idle condition is problematic by its mathematical definition shown in Equation (3.2). However, normalized mechanical efficiency can be compared using Equation (3.1) and assuming any change in BTE is a direct result of a change in fuel flow, giving Equation (3.3).

$$ME = \frac{BMEP}{NIMEP} \tag{3.2}$$

where NIMEP is the net indicated mean effective pressure.

$$\frac{ME_2}{ME_1} = \frac{OCE_1 \cdot CCE_1 \cdot (\%\Delta \dot{m}_{fuel} + 1)}{OCE_2 \cdot CCE_2} \tag{3.3}$$

The resulting normalized ME at unloaded idle is shown in Figure 3.7. Deactivating cylinders reduces ME. An engine operating with deactivated cylinders still has to move the inactive cylinders that are now contributing no positive work output. As discussed in detail in Chapter 4, these cylinders are an imperfect gas spring at best and still have friction and inertia. Since inactive cylinders have neither a closed cycle nor an open cycle, the losses caused by these cylinders are accounted for in the mechanical efficiency metric.
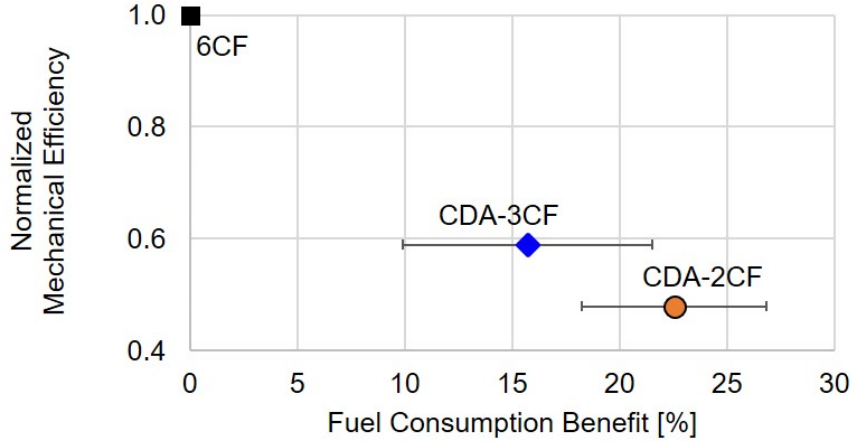
Figure 3.7. Normalized mechanical efficiencies of the improved unloaded idle points (800 RPM, 0 bar BMEP).

Thermal management effects, while not the focus of this study, are also observed when CDA is implemented. Figure 3.8 shows the exhaust temperatures, taken to be the turbine outlet temperatures (TOT), for each mode. CDA-3CF results in a TOT increase of 14°C over the baseline 6CF operation, and CDA-2CF results in a TOT

increase of 33°C. Increases in TOT for both CDA modes are results of decreased charge flows, shown in Figure 3.9, as excess charge through the cylinder acts as a thermal mass for the combustion heat. Exhaust temperature is a function of the air mass flowing through the engine and the combustion temperatures. Many times this function manifests as a trend between AFR and exhaust temperature, as more fuel at a given air flow means increased combustion temperatures at a given thermal mass. Similarly, lower air flow at a given fuel flow means lower thermal mass at a given combustion temperature. However, this AFR-exhaust temperature trend does not appear for this dataset, as shown in Figure 3.10. CDA-2CF has higher AFR than CDA-3CF but still has a higher exhaust temperature. It is the charge flow through the cylinder, however, that acts as the thermal sink. A modest increase in exhaust temperature likely also stems from combustion events for CDA-2CF being larger with a late enough timing to create higher gas temperature leaving the cylinder.
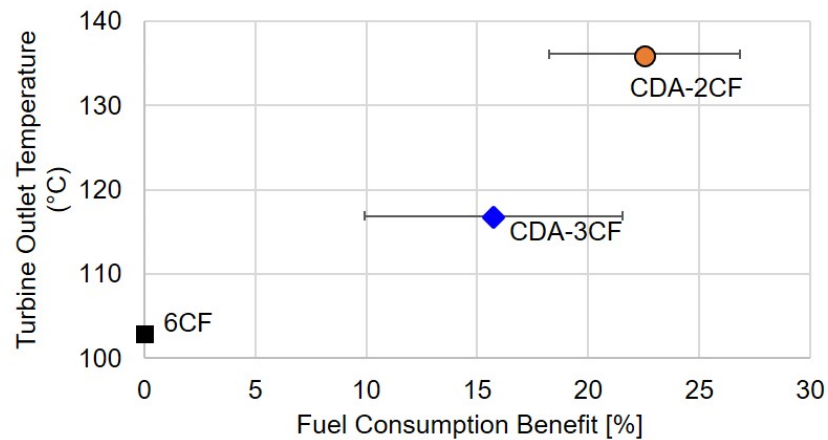
Figure 3.8.   Turbine outlet temperature for the improved unloaded idle points (800 RPM, 0 bar BMEP).

As mentioned above, this study was performed with periodic recharge events for the deactivated cylinders. Recharges were implemented by activating the intake valves of the deactivated cylinders every 100 cycles. Recharging the cylinder is thought to be necessary to prevent oil accumulation in the deactivated cylinders. However,
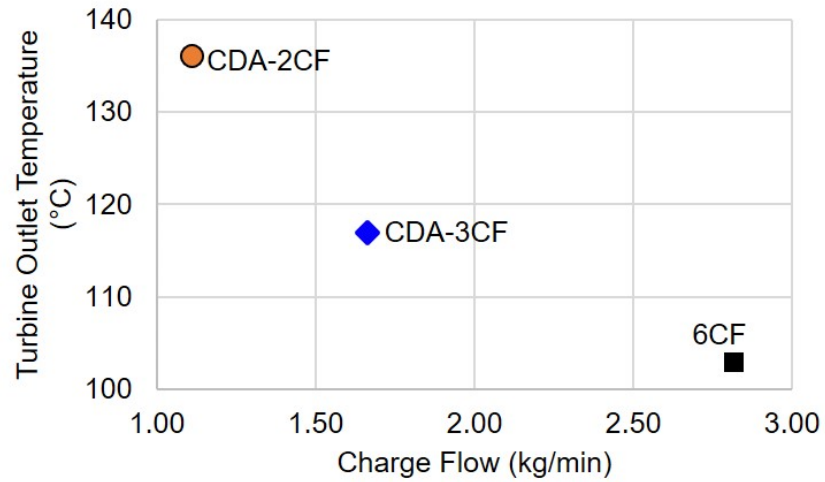
Figure 3.9. Turbine outlet temperature as a function of charge flow for the improved unloaded idle points (800 RPM, 0 bar BMEP).
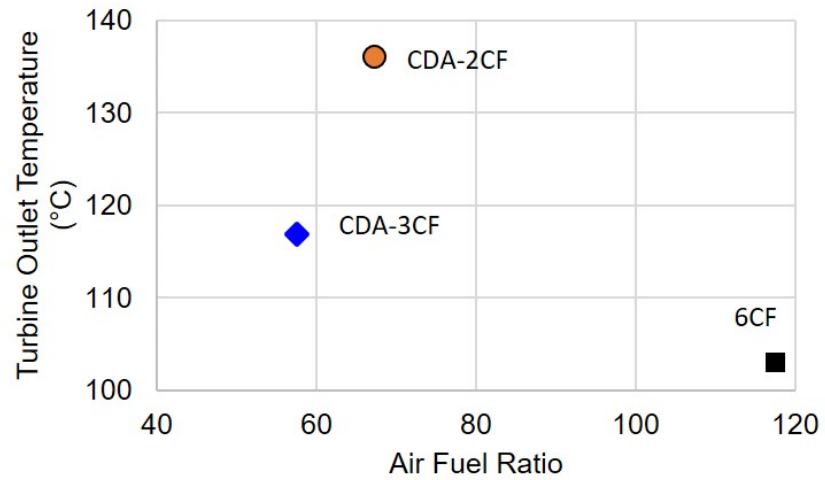
Figure 3.10. Turbine outlet temperature vs air fuel ratio for the improved unloaded idle points (800 RPM, 0 bar BMEP).

the recharging event is known to cause decreases in efficiency due to pumping work during the event and gas spring losses following the event, as pressure and mass losses after the recharge event continue to contribute parasitic losses until the pressure stabilizes. This effect is described in more detail in Chapter 4 of this document.

Therefore, the previously optimized settings were also run without the recharge events to explore possible additional efficiency benefits. The same engine calibrations were used. The resulting fuel efficiency changes are shown in Figure 3.11. Forgoing the recharge event gives CDA-2CF an additional 5% fuel consumption reduction over 6CF operation and gives CDA-3CF an additional 4% reduction. This results in CDA-2CF without recharging being 28±4% more efficient than 6CF operation, while CDA-3CF without recharging is 20±6% more efficient than 6CF operation. Air flow is mostly independent of the recharge event, therefore the reduction in fuel flow for each cylinder configuration slightly lowers exhaust temperatures.
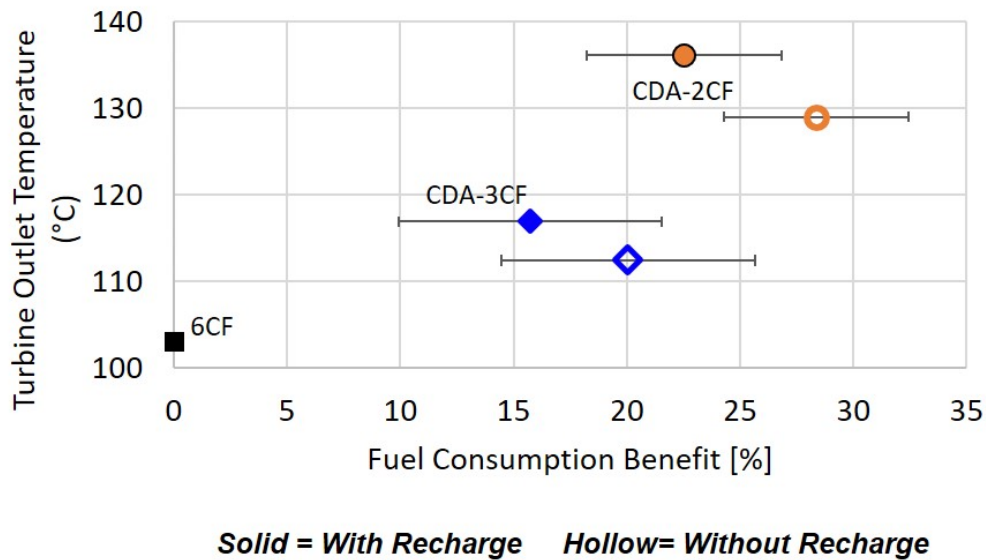
Figure 3.11. Fuel consumption and turbine outlet temperature for the improved unloaded idle points without cycle recharging (800 RPM, 0 bar BMEP).

3.2.3 Exploring Further Improvements via VVA

A supplementary brief study was conducted to determine if additional fuel efficiency benefits are possible via modulation of intake valve closing (IVC) timing in addition to CDA at unloaded idle. All calibration settings were maintained constant.

Only CDA-2CF was studied due to it having the lowest fuel consumption for the nominal IVC timing. An IVC sweep was conducted in 20°CA increments from -80°CA to 160°CA with respect to nominal timing, however only -70°CA could be reached while maintaining sufficient air flow. Three data points were taken at each IVC, with the results being the average of those data points.

The changes in fuel consumption from IVC modulation with respect to CDA-2CF were deemed statistically insignificant and are shown in Figure 3.12. However, a modest 8°C increase in exhaust temperatures are realized when using early intake valve closing (EIVC), as shown in Figure 3.13, due to the reduction in thermal mass via lower air flow shown in Figure 3.14.
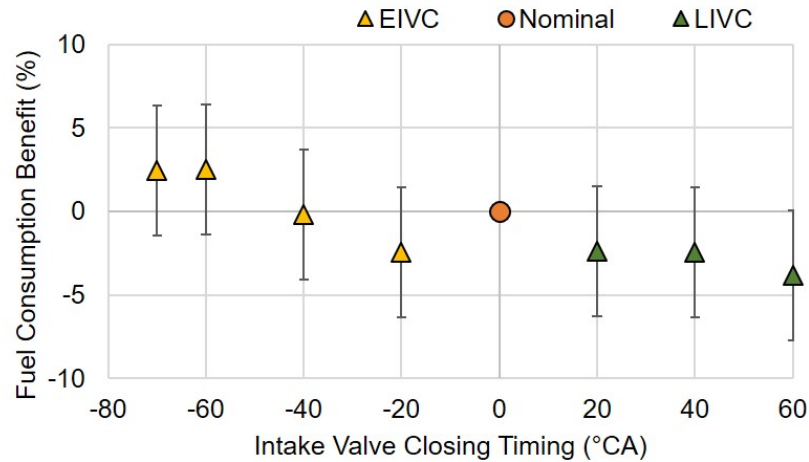
Figure 3.12. Fuel consumption benefits via IVC modulation at unloaded idle (800 RPM, 0 bar BMEP).

Additionally, as depicted in Figure 3.15, both EIVC and late intake valve closing (LIVC) provide a reduction in NOx emissions. The effective compression ratio (ECR) of the cylinder reduces when the IVC is advanced or retarded away from nominal, depicted in Figure 3.16. Ceteris paribus, a reduced ECR creates a lower maximum cylinder temperature due to the adiabatic compression result of Equations (3.4) and (3.5). Because NOx production is strongly correlated with temperature, the lower
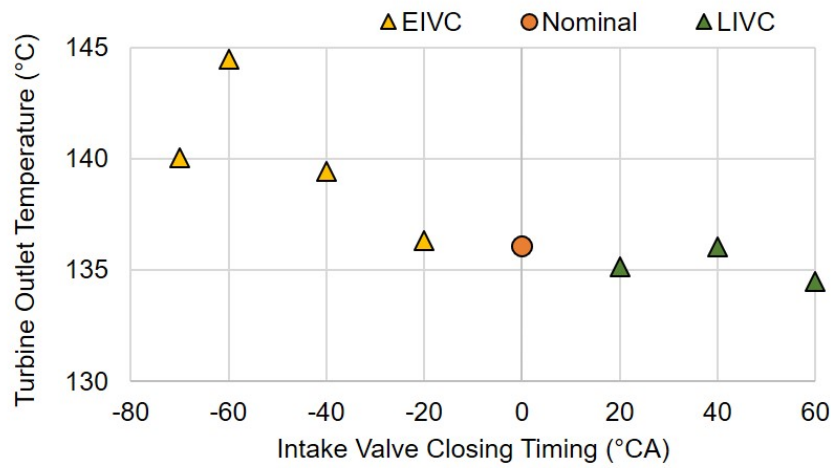
Figure 3.13.   Turbine outlet temperature over the IVC sweep at unloaded idle (800 RPM, 0 bar BMEP).
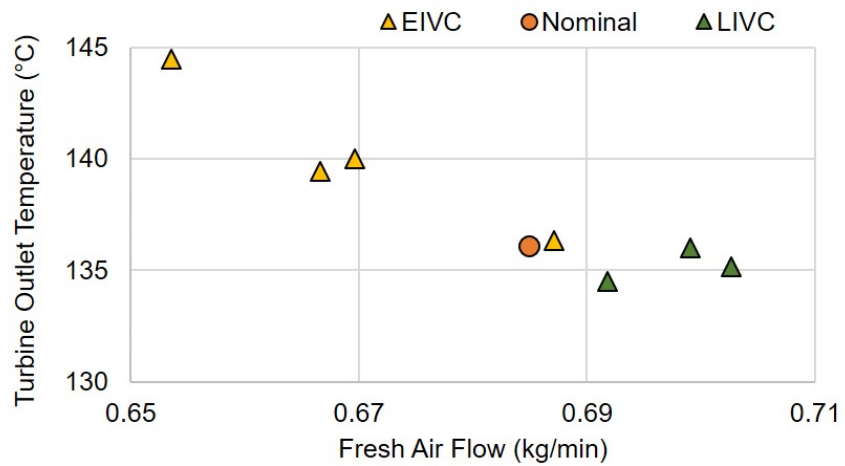
Figure 3.14.   Turbine outlet temperature is correlated with fresh air flow for the unloaded idle IVC modulation (800 RPM, 0 bar BMEP).

peak temperature reduces NOx. The monotonic relationship between ECR and NOx for this dataset is shown in Figure 3.17.

$$TV^{\gamma-1} = constant \tag{3.4}$$

$$T_{peak} \propto T_{intakemanifold}ECR^{\gamma-1} \tag{3.5}$$

where γ is the ratio of specific heats at constant pressure and at constant volume, T is the temperature at the indicated location, and ECR, effective compression ratio, is the ratio of the volume at the onset of compression to the clearance volume.
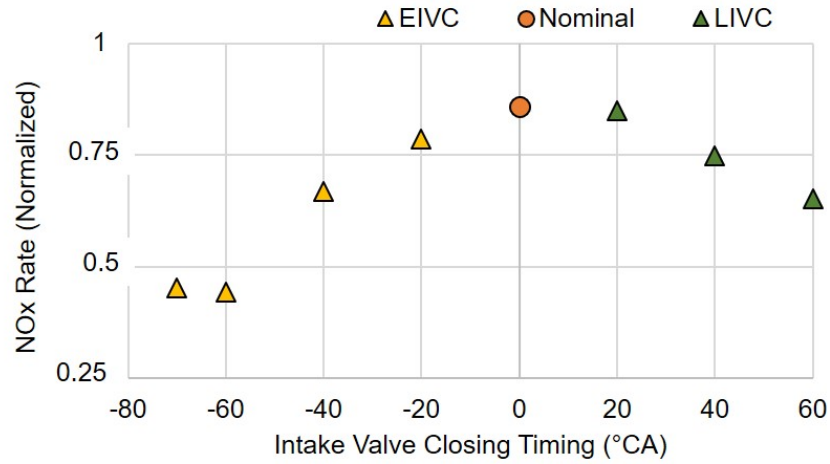
Figure 3.15. NOx rate for varying IVC timings at unloaded idle (800 RPM, 0 bar BMEP).
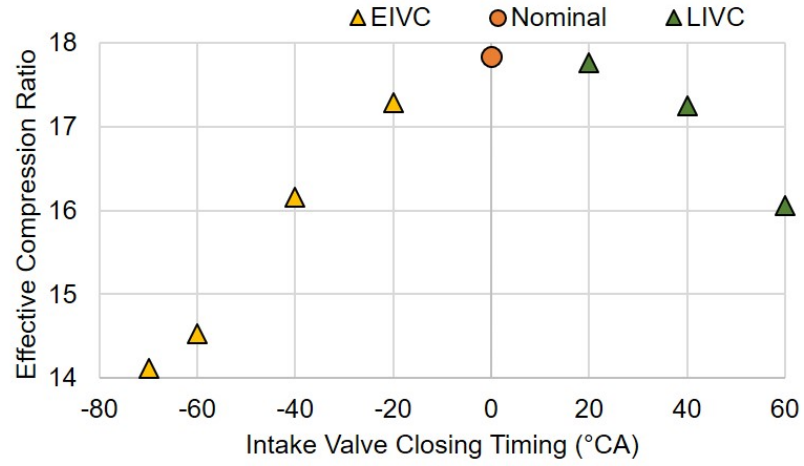
Figure 3.16. Effective compression ratio (cylinder 4 shown) for varying IVC timings at unloaded idle (800 RPM, 0 bar BMEP).
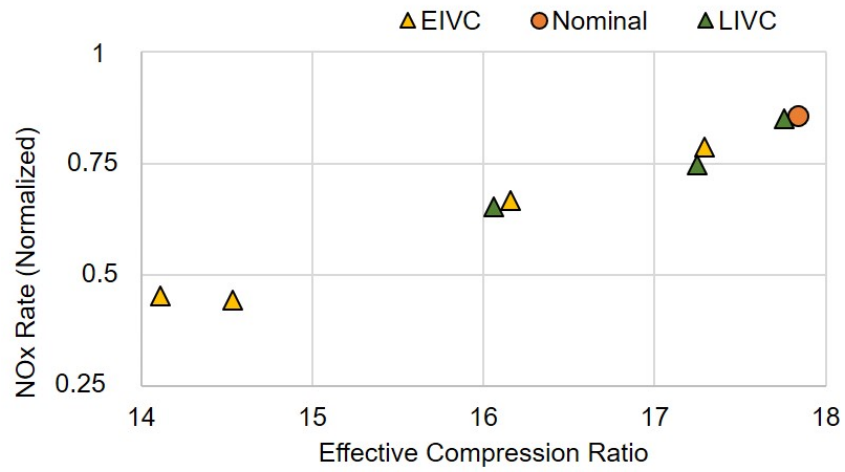
Figure 3.17. NOx rate as a function of effective compression ratio (cylinder 4 ECR shown) at unloaded idle (800 RPM, 0 bar BMEP).

3.2.4   Summary of Unloaded Idle Fuel Efficiency Optimizations

DOE-based emissions-constrained fuel efficiency optimizations at unloaded idle (800 RPM, 0 bar BMEP) for 6CF, CDA-3CF, and CDA-2CF operations resulted in fuel consumption improvements of 15% for CDA-3CF and 23% for CDA-2CF compared to optimized 6CF. All data is constrained to the predefined emissions limits. Removing cylinder recharging via intake events results in further improvements to fuel efficiency at this unloaded operating condition, with CDA-3Cf showing 20% and CDA-2CF showing 28% improvement compared to 6CF. Further improvements via intake valve modulation was not found.

3.3   CDA Calibration at Loaded Idle for Improved Fuel Efficiency

3.3.1   Methodology

The engine was calibrated for 6CF, CDA-3CF, and CDA-2CF operation at the curb/loaded idle operating condition for this engine (800 RPM, 1.3 bar BMEP) through experimental screenings centered on the unloaded idle (800 RPM, 0 bar BMEP) optimized settings discussed in the previous section. Specifically, lowering rail pressure to allow lower mechanical losses at these lightly loaded operating conditions, and using EGR for NOx reduction rather than injection timing were trends that were applied. The turbocharger was swapped between the unloaded idle and loaded idle testing for reasons not relevant to this work. However, since idle is an unboosted condition, the VGT primarily functions to control EGR and is mostly independent of sizing. 6CF screening was also conducted to create a fair comparison to CDA. However, unlike at the unloaded idle condition, a lower fuel consumption than the stock calibration was not found. Therefore, the lowest fuel consumption 6CF point is taken to be the stock calibration. NOx emissions for the final points are constrained to stock 6CF NOx levels, and predefined limits for UHC and soot.

The engine was allowed to stabilize between data points. Stability was determined based on exhaust temperature stabilization. A gravimetric fuel reading was then taken for 4 minutes. Other measurements, including emissions, are also the result of a 4 minute average. In-cylinder pressure measurements were taken for 100 engine cycles. Aftertreatment backpressure was emulated through the modulation of a valve in the exhaust pipe. Cylinder recharges were not performed during these tests, as the engine was taken to 6CF operation between CDA data points.

3.3.2 Results

The results of the emission-constrained fuel consumption screening at loaded idle are shown in Figure 3.18. The comparison is comprised of the stock 6CF operation, the best efficiency CDA-3CF operation found during screening, and the three best efficiency CDA-2CF points found during screening. The improvements in fuel efficiency are not on the same magnitude as unloaded idle, as expected, due to the lower proportional pumping losses at the loaded idle condition. CDA-3CF was found to be the most efficient loaded idle operation and is a 13% improvement over baseline 6CF operation at the same NOx levels. There are multiple CDA-2CF points on the plot to show that, unlike for the unloaded idle condition, CDA-2CF settings resulting in higher efficiency than CDA-3CF while still meeting NOx limits were not found. However, CDA-2CF is still approximately 6% more efficient than conventional operation at similar NOx outputs. The bounded emissions for all points are summarized in Table 3.6.

The fuel efficiency improvements from CDA can again primarily be attributed to an increase in OCE, as shown in Figures 3.19. CCE also improves, as discussed below, and ME is roughly equivalent for all tested points. Deactivating cylinders reduces the available cylinder volume to move air through the engine, which reduces the charge flow. This increases OCE, as shown in Figure 3.21, because there is an excessive amount of air flowing through this unthrottled engine at idle.
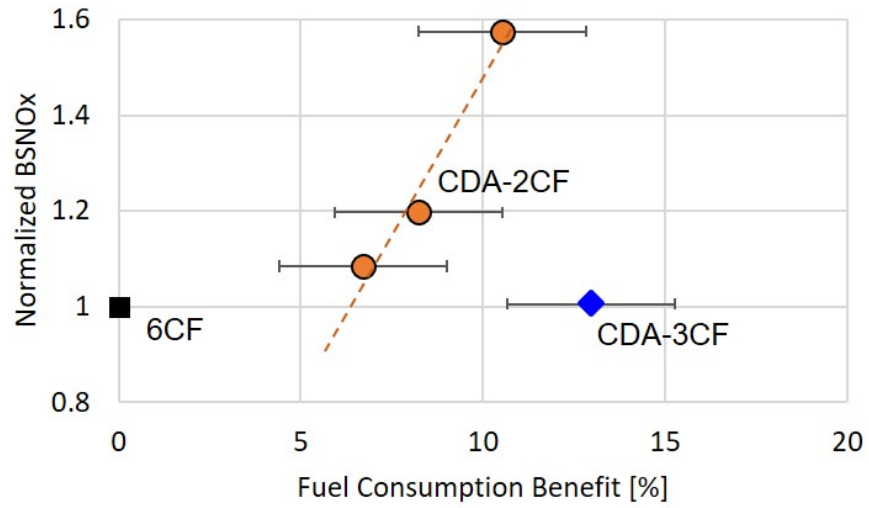
Figure 3.18. Normalized BSNOx vs fuel consumption improvement for the loaded idle points (800 RPM, 1.3 bar BMEP).

Table 3.6. Loaded idle emissions results (800 RPM, 1.3 bar BMEP).

Mode	Normalized Fueling	Normalized BSNOx	Normalized UHC	Normalized Soot
Limits	-	1	1	1
6CF	1	1	0.58	0.12
CDA-3CF	0.87 ±0.03	1.01	0.69	0.22
CDA-2CF	0.93 ±0.03	1.08	0.74	0.32
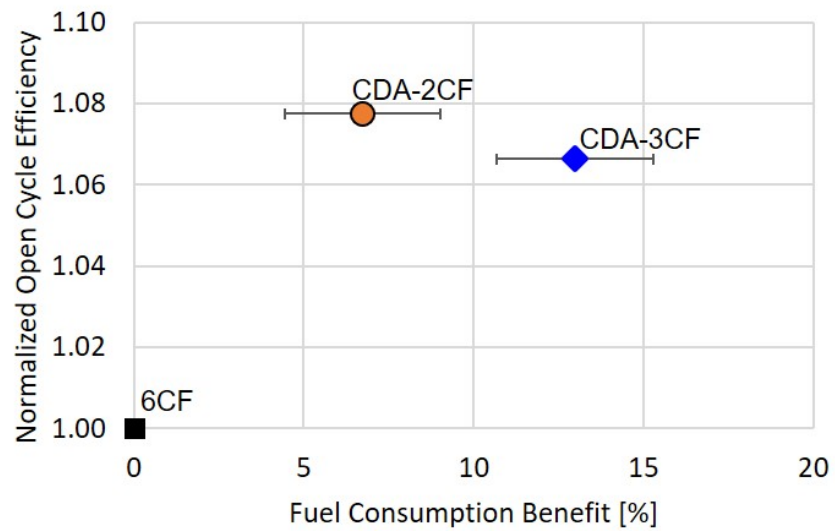
Figure 3.19. Normalized OCE vs fuel consumption improvement for the loaded idle points (800 RPM, 1.3 bar BMEP).
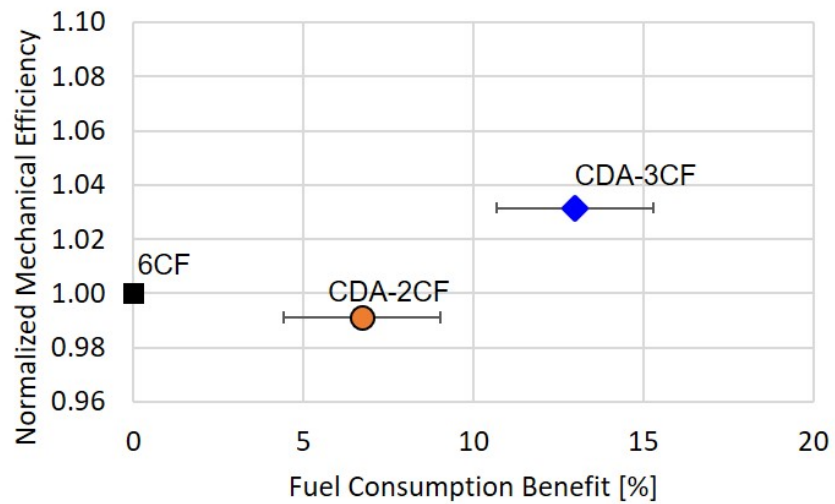
Figure 3.20. Normalized ME vs fuel consumption improvement for the loaded idle points (800 RPM, 1.3 bar BMEP).
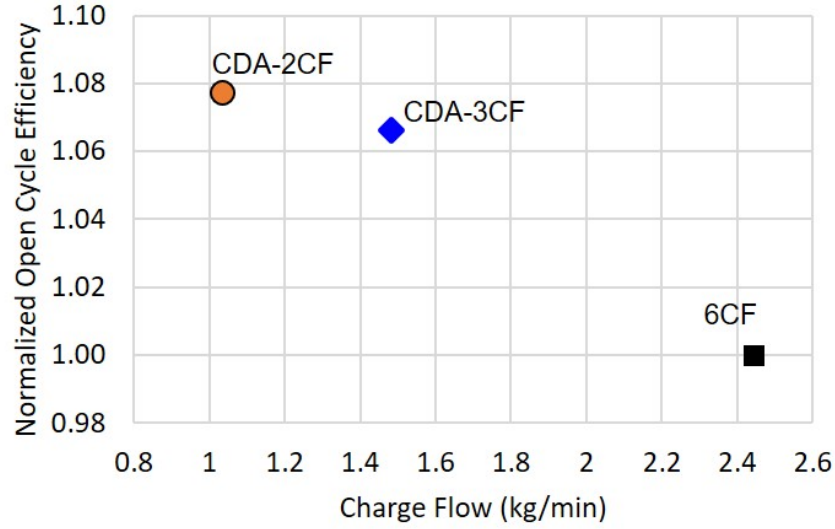
Figure 3.21. Normalized OCE as a function of charge flow at loaded idle (800 RPM, 1.3 bar BMEP).

Another way to describe the increase in OCE is through examining the pumping work of the engine. This can be visually inspected using the PV plots in Figure 3.22. Note the reduced pumping loop areas for the CDA operations compared to the 6CF operation. Moreover, the number of pumping loops are reduced during CDA operation due to reduced number of active cylinders. The pumping work of each cycle can be calculated directly from the pressure measurements. The reduction of pumping work directly correlates with increased OCE, as shown in Figure 3.23. Similar to unloaded idle, CDA-2CF has the highest OCE due to the least amount of pumping work.
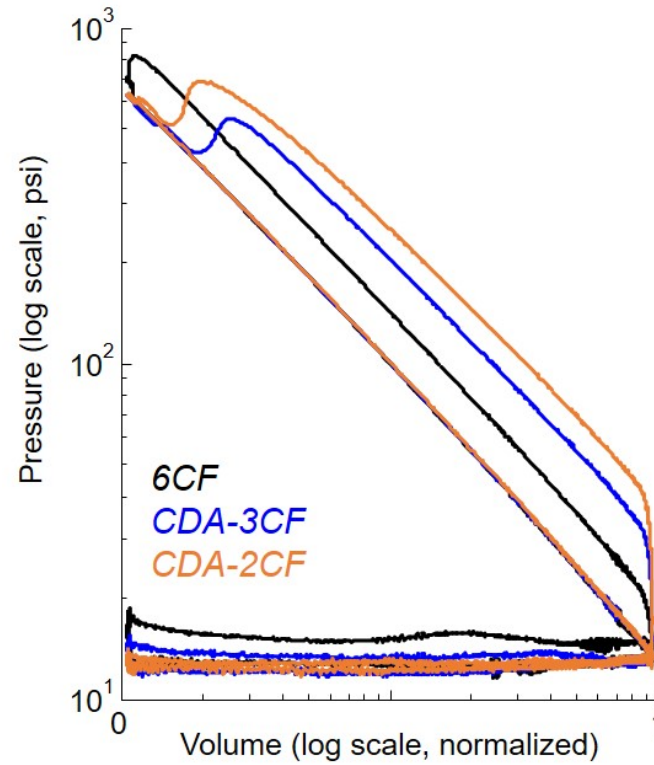
Figure 3.22. PV diagram for the CDA and 6CF operations at loaded idle (800 RPM, 1.3 bar BMEP).
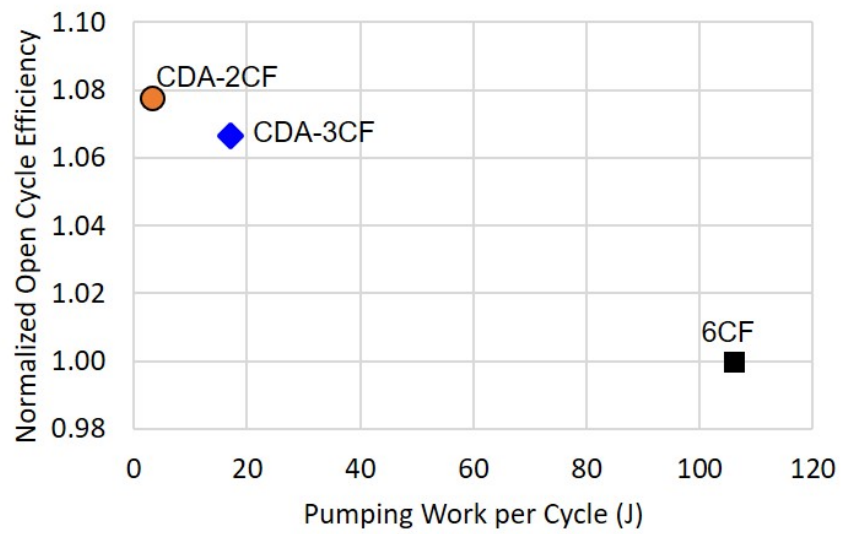
Figure 3.23. Normalized OCE as a function of cycle pumping work at loaded idle (800 RPM, 1.3 bar BMEP).

CCE also contributes to the fuel efficiency benefits of CDA over 6CF operation at loaded idle, as shown in Figure 3.24. Both CDA modes have higher CCE than 6CF operation due to lower in-cylinder heat loss. This relationship is shown in Figure 3.25. By firing on a fewer number of cylinders, the surface area for in-cylinder heat loss is proportionately decreased. This means that less fuel is needed to produce the same amount of brake work. However, CCE is also the driver for the reduced relative benefit for CDA-2CF compared to the unloaded idle case. The divergence between the CDA-2CF and CDA-3CF efficiency trends for unloaded idle and loaded idle occur primarily due to combustion timing. Having only two cylinders firing results in a heat release centroid that is more delayed than optimal, as shown in Figure 3.26. This is partly due to the necessary fueling per cylinder and partly due to the necessary delayed SOI in order to meet NOx limits. Nevertheless, the delayed heat release centroid results in reduced efficiency.

CDA also shows thermal management effects at loaded idle from the higher exhaust temperatures shown in Figure 3.27. CDA-2CF results in 107°C higher turbine outlet temperatures than 6CF operation, and CDA-3CF results in 41°C higher tur-
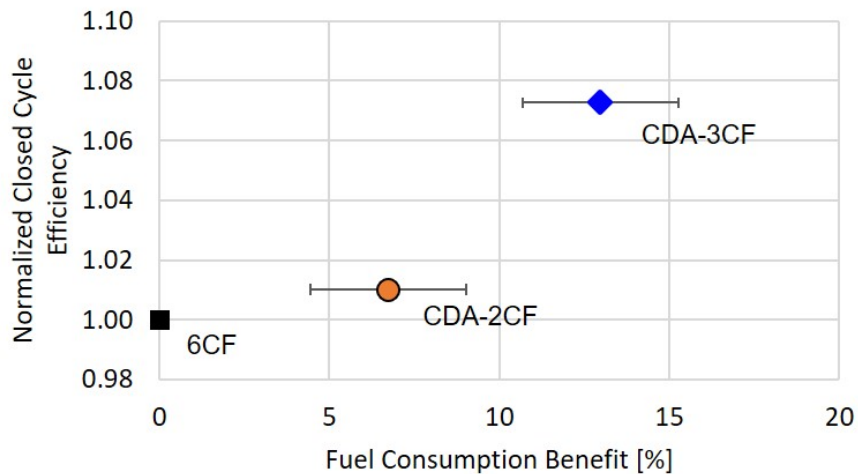
Figure 3.24. Normalized CCE vs fuel consumption improvement for the loaded idle points (800 RPM, 1.3 bar BMEP).
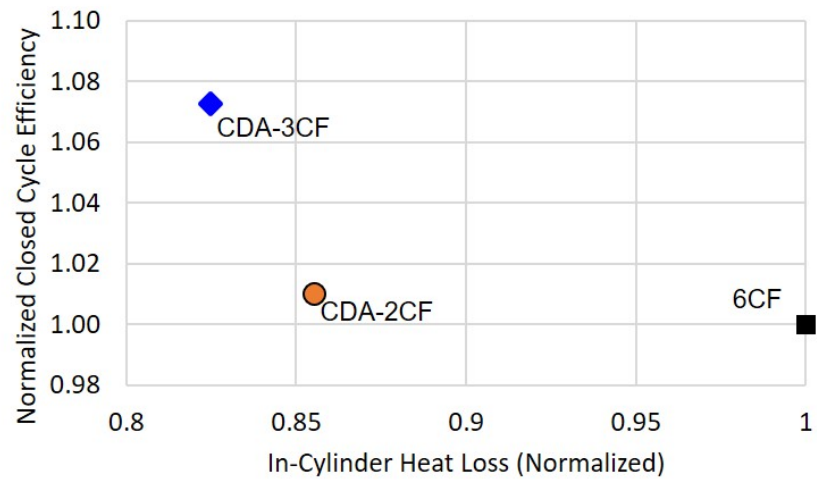
Figure 3.25. CCE correlates with in-cylinder heat loss at loaded idle (800 RPM, 1.3 bar BMEP).
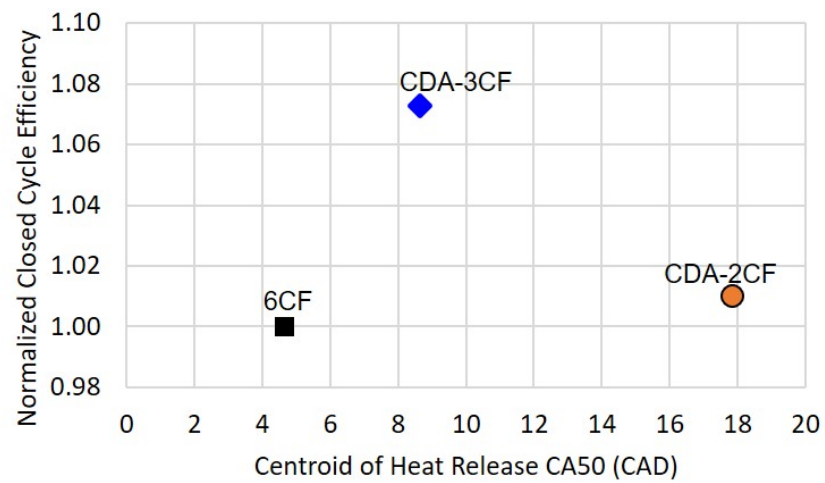
Figure 3.26. CCE vs heat release centroid location for the loaded idle points (800 RPM, 1.3 bar BMEP).
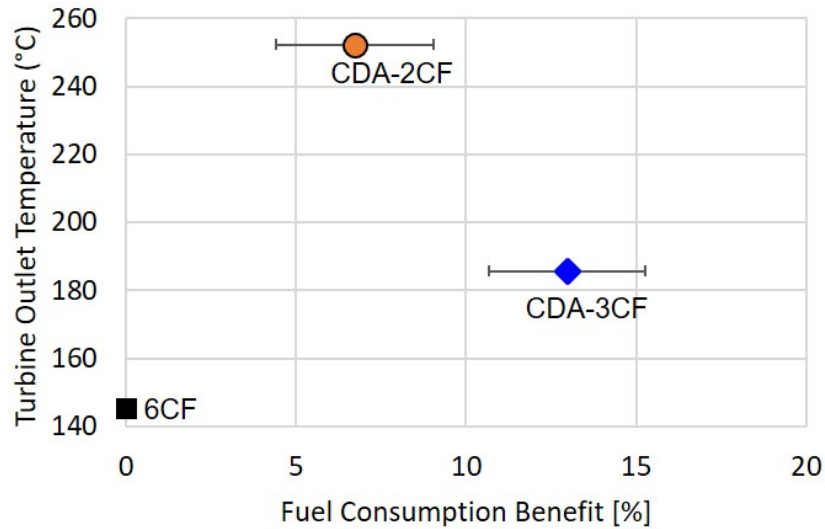
Figure 3.27. Turbine outlet temperature increases combine with fuel consumption improvements via CDA at loaded idle (800 RPM, 1.3 bar BMEP).

bine outlet temperatures than the 6CF operation. This is primarily due to a decrease in charge flow and AFR during CDA, depicted in Figures 3.28 and 3.29, resulting in less thermal mass flowing through the cylinders. It should also be noted that no screening was done specifically for thermal management characterization, and the CDA turbine outlet temperatures and heat transfer rates could likely be improved upon with some sacrifice in fuel efficiency for both CDA and 6CF operations.

Heat transfer to the aftertreatment components is a function of both temperature and mass flow rate out of the engine. While the higher exhaust temperature of CDA should be able to help maintain temperatures once the aftertreatment components are warm, it is not immediately clear if the lower mass flow will combine to form a beneficial warm-up strategy. An estimation of heat transfer rate to the catalyst bed was developed by [30] to evaluate the mass flow and temperature combinations. The DOC, DPF, and SCR are treated as lumped mass catalyst beds. The resulting equation, which was derived based on convectional heat transfer through a pipe,
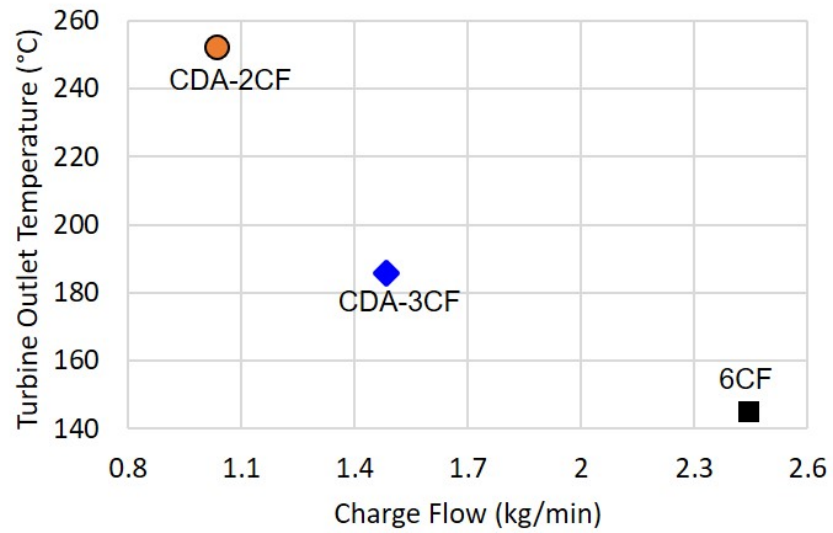
Figure 3.28. Reduced charge flow correlates with increased turbine outlet temperature at loaded idle (800 RPM, 1.3 bar BMEP).
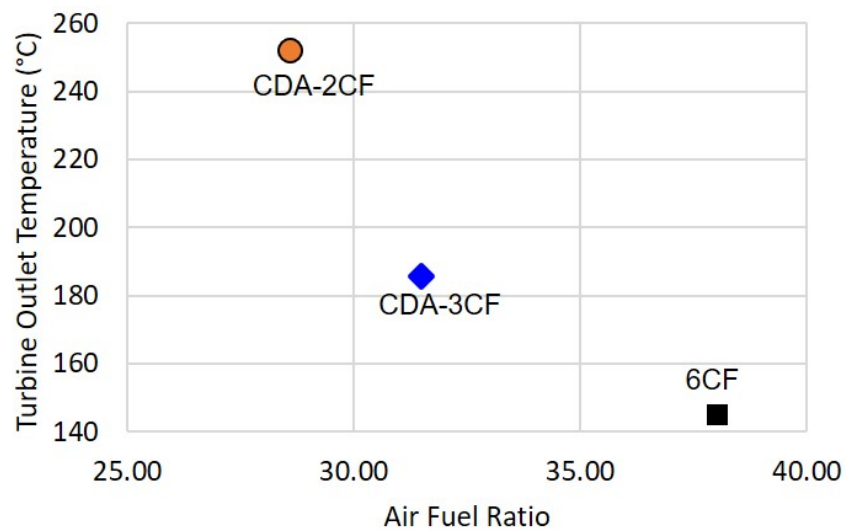
Figure 3.29. Reduced air-fuel ratio correlates with increased turbine outlet temperature at loaded idle (800 RPM, 1.3 bar BMEP).

calculates the heat transfer from the exhaust gas to the catalyst bed at the bed temperature and is given by

$$Q = C\dot{m}_{exh}^{\frac{4}{5}}(TOT - T_{cat}) \tag{3.6}$$

where Q is the heat transfer to the catalyst bed, C is a heat transfer coefficient depending on the geometry of the catalyst and flow characteristics, $\dot{m}$ is the exhaust mass flow rate, TOT is the turbine outlet temperature, and T_{cat} is the catalyst bed temperature.
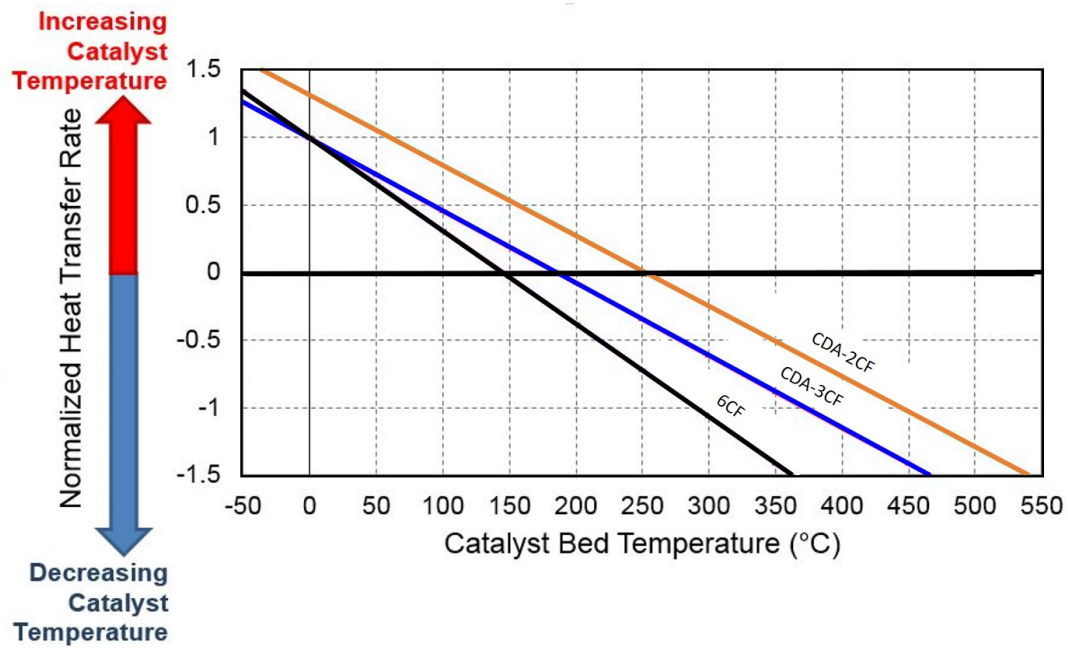
Figure 3.30. Normalized heat transfer at different catalyst bed temperatures for the loaded idle points (800 RPM, 1.3 bar BMEP).

The heat transfer coefficient C can be eliminated by normalizing the heat transfers of different flow scenarios, resulting in a comparative evaluation. The normalized heat transfer for the loaded idle 6CF, CDA-3CF, and CDA-2CF operating conditions is shown in Figure 3.30. This analysis indicates that it would be more beneficial to operate in CDA-2CF at any catalyst bed temperature, even though CDA-2CF has the lowest exhaust flow rate of the operations. CDA-3CF would also perform better

than this 6CF for catalyst bed temperatures greater than 0°C. That being said, explorations of thermal management calibrations for CDA and 6CF operations have shown that this trend is not universally valid [31].

3.3.3 Summary of CDA at Loaded Idle for Fuel Efficiency

Calibration screenings for fuel efficiency at loaded idle (800 RPM, 1.3 bar BMEP) were conducted for 6CF, CDA-3CF, and CDA-2CF operations. These calibrations were based on the optimized calibrations at unloaded idle and are emissions constrained. CDA-3CF at loaded idle demonstrates 13% improvement in fuel efficiency over 6CF operation. CDA-2CF at loaded idle demonstrates 6% improvement in fuel efficiency over 6CF operation. CDA-2CF is not as efficient as CDA-3CF at loaded idle due to the increased load causing less optimal heat release. This is in contrast to unloaded idle. CDA fuel efficiency improvements are accompanied by exhaust temperature increases of 41°C for CDA-3CF and 107°C for CDA-2CF over 6CF operation.

3.4 Implementation of CDA at Idle for HD-FTP Drive Cycle Fuel Efficiency Improvement

3.4.1 Methodology

The fuel consumption reduction of CDA over a transient drive cycle was realized by implementing half-engine CDA (CDA-3CF) over the HD-FTP. It is important to note that the HD-FTP was chosen as an arbitrary drive cycle and any fuel consumption benefits could be magnified or diminished for other drive cycles (as demonstrated in the next section). The HD-FTP is used by the EPA to certify emissions of heavy-duty on-road engines, therefore a clear procedure is mandated for its implementation in the 40 CFR 86 regulations. While emissions certification is out of the scope of this work, effort was made to follow the procedure in a manner such that the fuel consumption

results are comparable. The general procedure that was followed for the testing described here first consists of a 'cold' soak of the engine for at least 12 hours to allow the engine and aftertreatment temperatures to stabilize. The drive cycle shown in Figure 3.31 is then run in its entirety. This cycle represents the 'cold-start' test. The engine is then immediately turned off and a 20 minute timer is initiated. Once the 20 minutes have passed, the cycle in Figure 3.31 is run again. This cycle represents the 'hot-start' test. The end of the hot-start test concludes the HD-FTP. As per the HD-FTP guidelines, the fuel consumption is a weighted average of the cold-start test and hot-start test brake specific fuel consumptions (BSFC) shown in Equation (3.7), with the cold-start weighted at $\frac{1}{7}$ and the hot-start weighted at $\frac{6}{7}$ of the total fuel consumption [62].
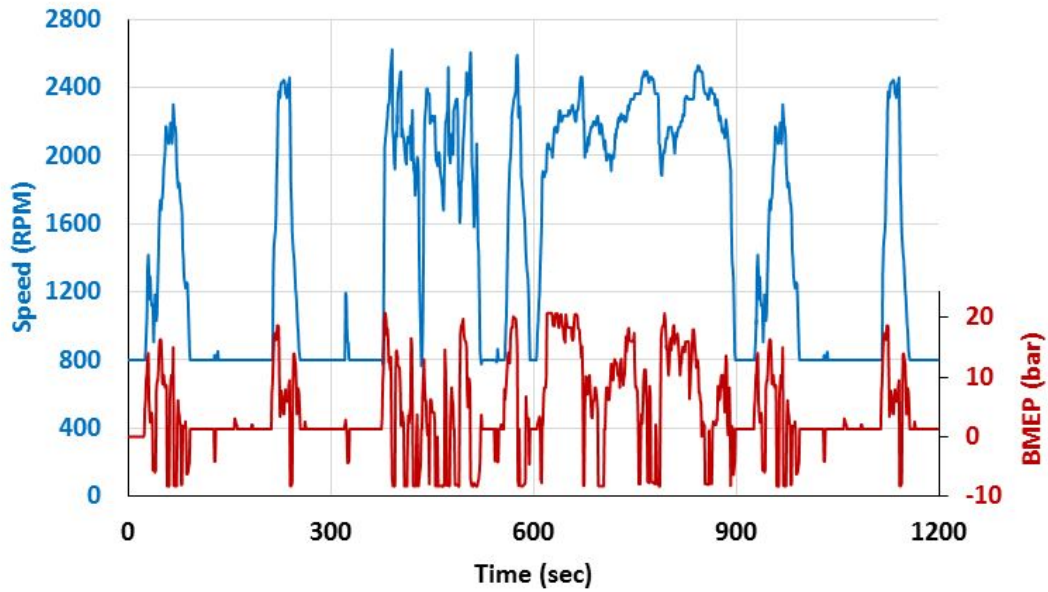
Figure 3.31. HD-FTP drive cycle for the tested engine.

$$BSFC_{net} = \frac{1}{7}BSFC_{coldstart} + \frac{6}{7}BSFC_{hotstart} \qquad (3.7)$$

The aftertreatment system consisting of a DOC, DPF, and SCR are attached for the tests described here. However, unlike during an actual certification procedure, DEF dosing for the SCR is disabled. Therefore, the function of the SCR for these tests is only to provide a thermal mass to obtain realistic exhaust temperatures. The inlet and outlet gas temperatures of the SCR can then be used in conjunction with an SCR efficiency curve to estimate the tailpipe-outlet NOx emissions based on the measured engine-outlet emissions. The SCR efficiency curve utilized for this study is shown in Figure 3.32. Due to the unknown temperatures within the catalyst, the tailpipe-out NOx values are calculated using both SCR inlet and SCR outlet temperatures as proxies. The actual SCR catalyst, however, can fall outside of these temperature bounds. Emissions are reported as a weighted sum of the two cycles with the cold-start weighted at $\frac{1}{7}$ and the hot-start weighted at $\frac{6}{7}$ [62].
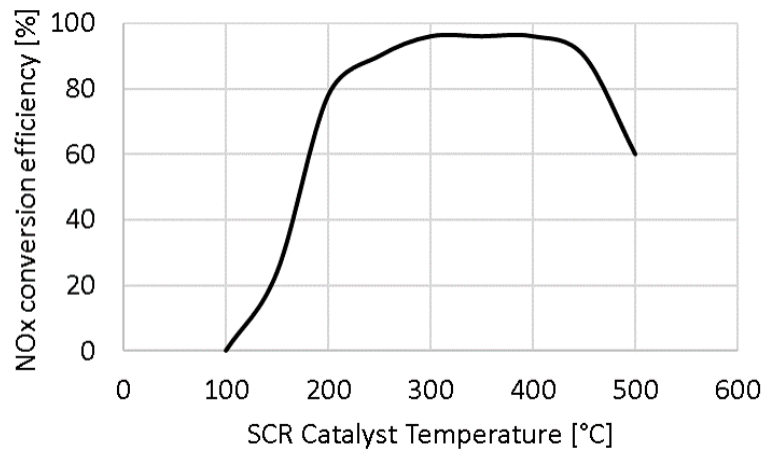
Figure 3.32. Assumed SCR NOx conversion efficiency as a function of catalyst temperature.

A full HD-FPT cycle was performed with stock ECM calibration. This represents the 6CF operation in the results below. On subsequent testing, two HD-FTP cycles with CDA-3CF at idle were run for comparison. All three cycle results are reported. CDA was implemented only after the aftertreatment had sufficiently warmed up, as previous transient testing had indicated inferior aftertreatment heating performance
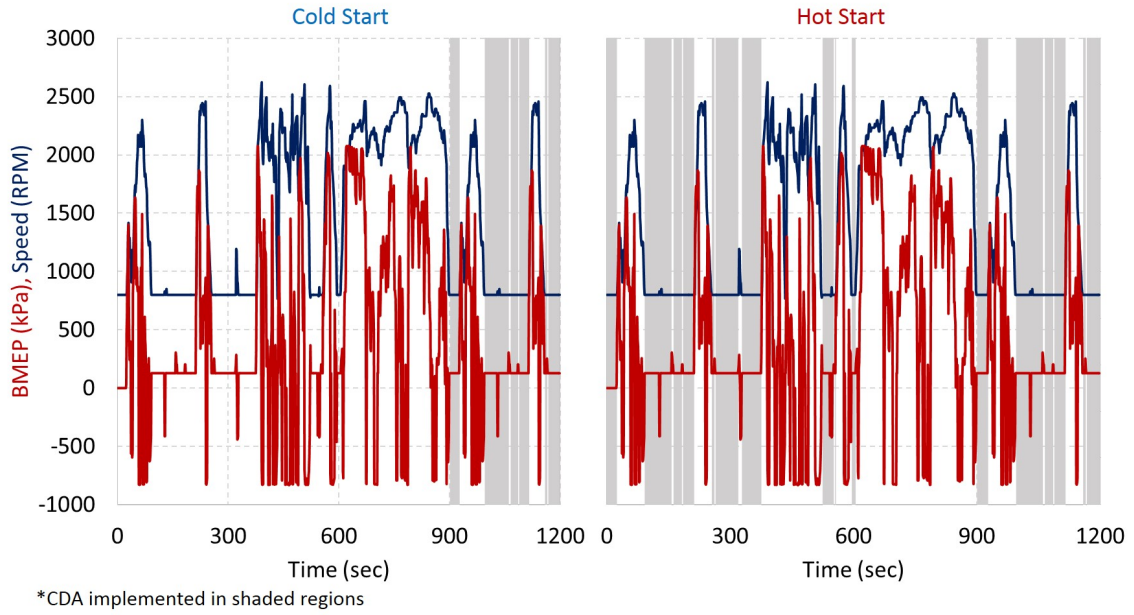
Figure 3.33. HD-FTP broken down into cold-start and hot-start cycles with shaded regions corresponding to CDA implementation.

for CDA compared to 6CF operation. Therefore, CDA was run during the shaded regions in Figure 3.33.

CDA-3CF was chosen over CDA-2CF to be the CDA mode for the drive cycle because CDA-3CF demonstrated better fuel efficiency than CDA-2CF at loaded idle. Since loaded idle comprises all idle conditions of the HD-FTP except the first 25 seconds, this means that CDA-2CF would have only run for 25 seconds during the very low fuel consumption unloaded idle period.

CDA was implemented using a look ahead strategy for these tests, where the transitions in and out of CDA are pre-programmed into the system. This simplified implementation was deemed acceptable for this study. Moreover, results from [34] demonstrate that CDA could be run during portions of the transient sections and still complete the cycle.

3.4.2 Results

Implementing CDA-3CF at idle in the manner described above results in an average of 0.7% improvement in fuel consumption over baseline 6CF operation at similar predicted tailpipe-out NOx levels. This result is shown in Figure 3.34. As a check, analysis indicates 5.8% of the HD-FTP fuel consumption is at idle conditions. Since CDA-3CF was shown to provide 13% fuel consumption improvement at steady-state idle, the predicted fuel consumption benefit then would be approximately 0.75%, which correlates well with the experimental result. The effect of the fueling weighting over the HD-FTP can be seen in Figure 3.35. The fueling in this plot represents the ECM estimated fueling, as it is less susceptible to measurement noise for integrating the instantaneous readings. Then, from Figure 3.36, it can be seen that the primary difference in drive cycles is in the hot start due to the weighting. This plot also shows the divergence happens at idle (shown by the shaded regions), as expected due to the implementation of CDA there.
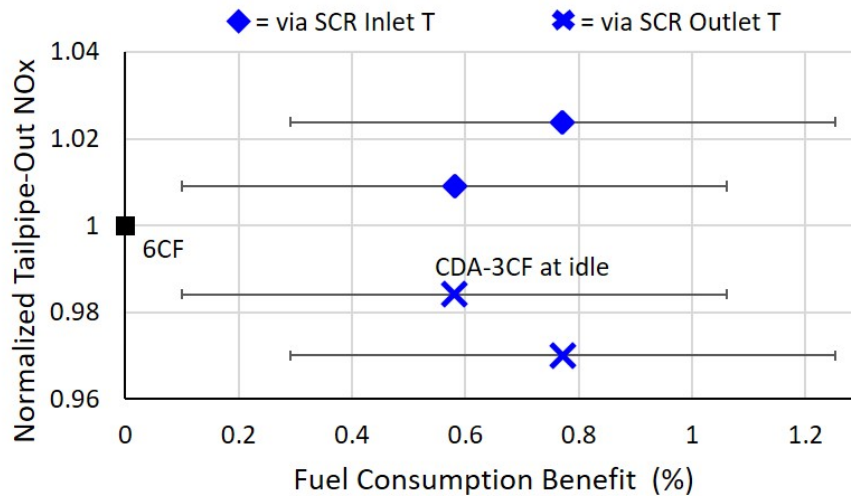
Figure 3.34. HD-FTP fuel consumption improvement via implementing CDA at unloaded and loaded idle conditions. Tailpipe NOx is relatively constant.
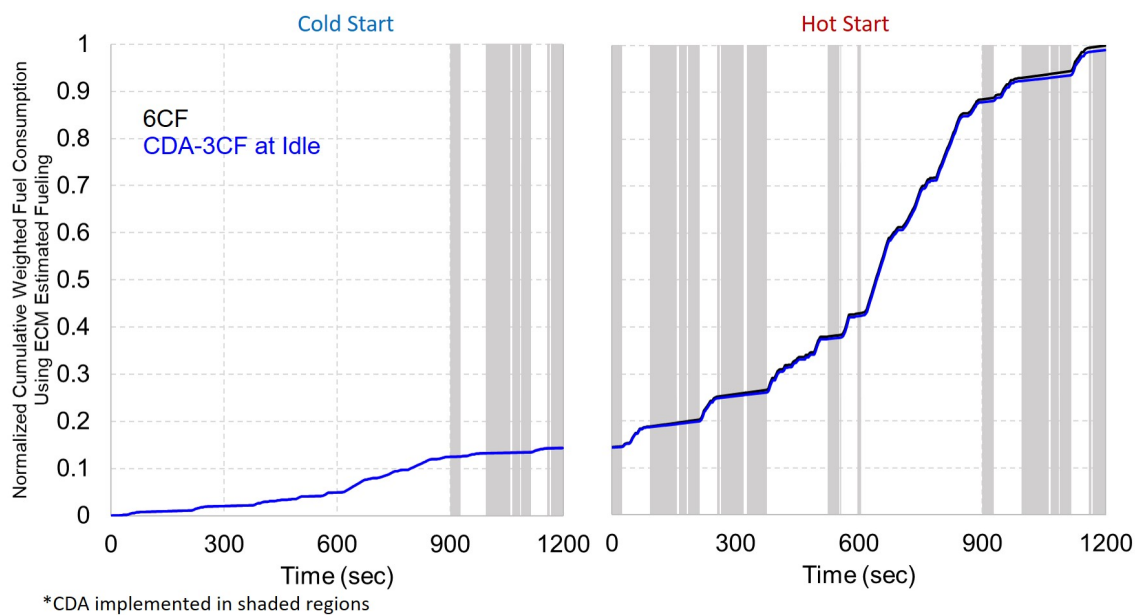
Figure 3.35. Weighted normalized cumulative HD-FTP fuel consumption.
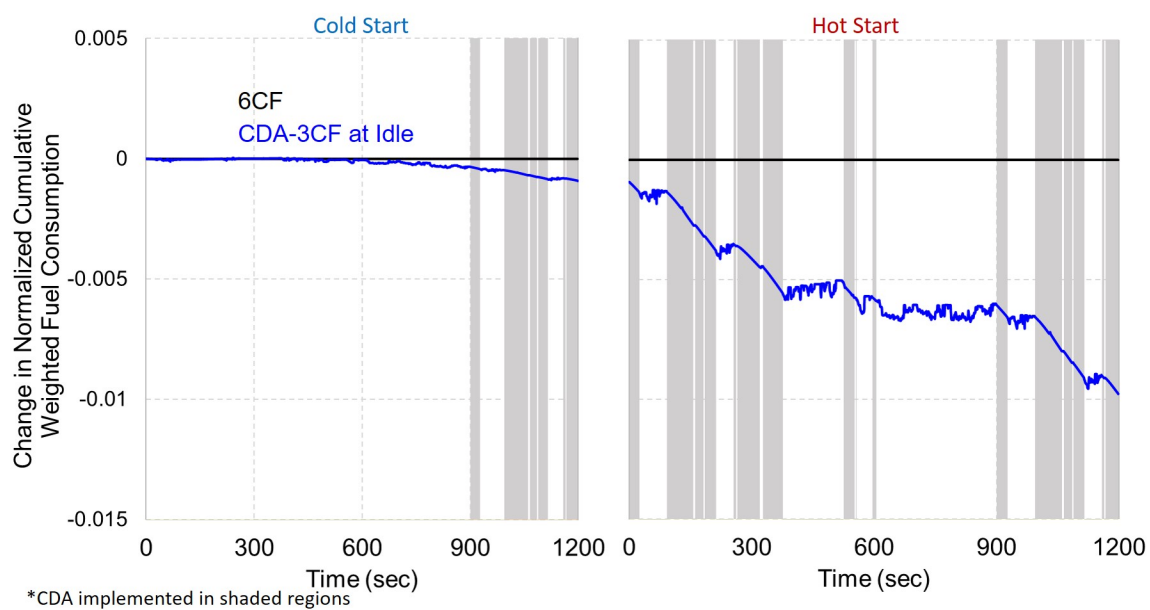
Figure 3.36. Change in the weighted normalized cumulative HD-FTP fuel consumption.

The thermal management effects of CDA at idle discussed in the above sections manifest in the turbine outlet temperature plot shown in Figure 3.37. CDA has a higher turbine outlet temperature when it is implemented. Additionally, due to the lower mass flow rate of CDA, the outlet gas temperatures cool off more slowly after acceleration hills. The temperatures are dampened, however, by the time the gas reaches the SCR. This is shown in Figures 3.38 and 3.39. The slight variation in the SCR inlet temperatures at the beginning of the cold cycle is due to any inconsistent start-up performance and reactions in the DOC/DPF. Nevertheless, the resulting SCR efficiencies shown in Figure 3.40 combined with the cumulative engine-out NOx shown in Figure 3.41 create almost equivalent predicted NOx levels for CDA-3CF. The resulting predicted cumulative weighted tailpipe-out NOx values are shown in Figures 3.42 and 3.43. Finally, there is a slight increase in measured engine-out soot over the 6CF drive cycle, shown in Figure 3.44. This is attributed to ECM-controlled engine variance because a large divergence occurs in the first 900 seconds when the calibrations should be the same. This is considered acceptable for this study.

Determining proper a proper 6CF baseline is a complex topic, so a final point of emphasis should be placed on the baseline for the above results being 6CF operation calibrated for fuel efficiency. Later studies contributed to by the author include comparisons of thermal management calibrations for 6CF and CDA operations over the HD-FTP. In that comparison, CDA was shown to provide 3% fuel savings when implemented at idle and 3.4% fuel savings when implemented at loads below 3 bar BMEP. This work is summarized in [31]. The following section discusses results against this 6CF thermal management calibration for other drive cycles meant to better represent real-world operating scenarios for CDA application.
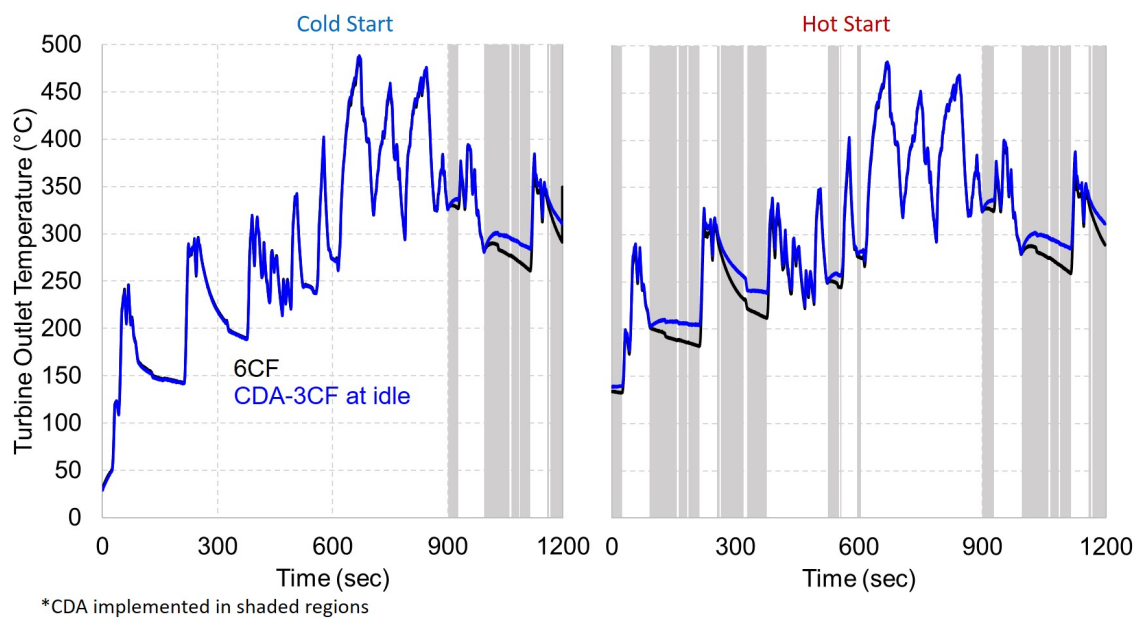
Figure 3.37. Turbine outlet temperatures during the HD-FTP drive cycle.
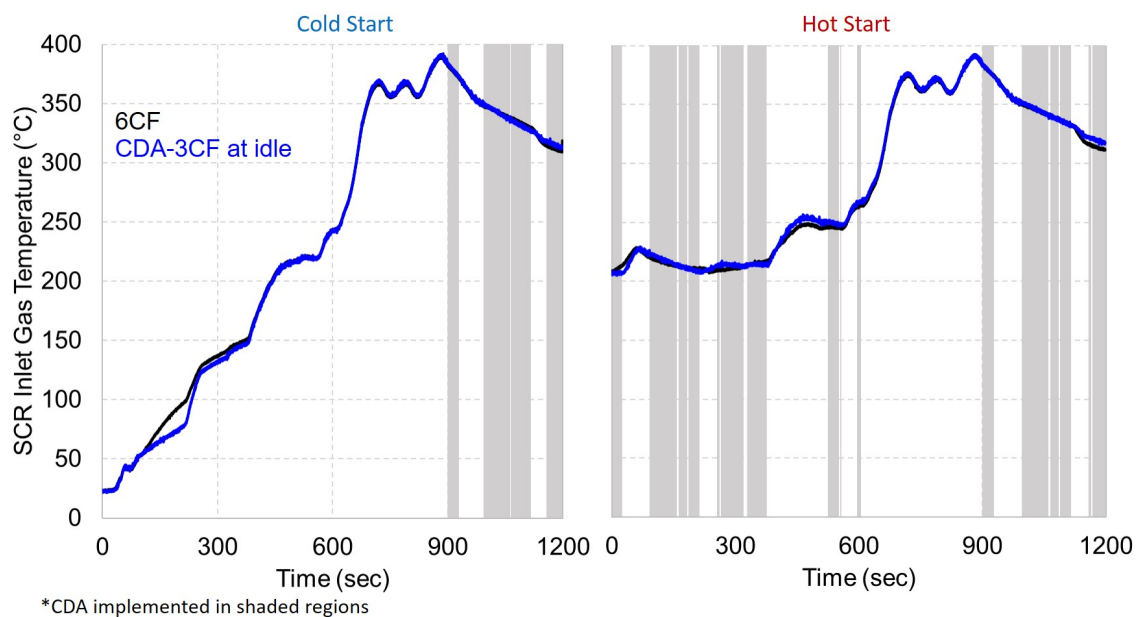
Figure 3.38. SCR inlet temperatures during the HD-FTP drive cycle.
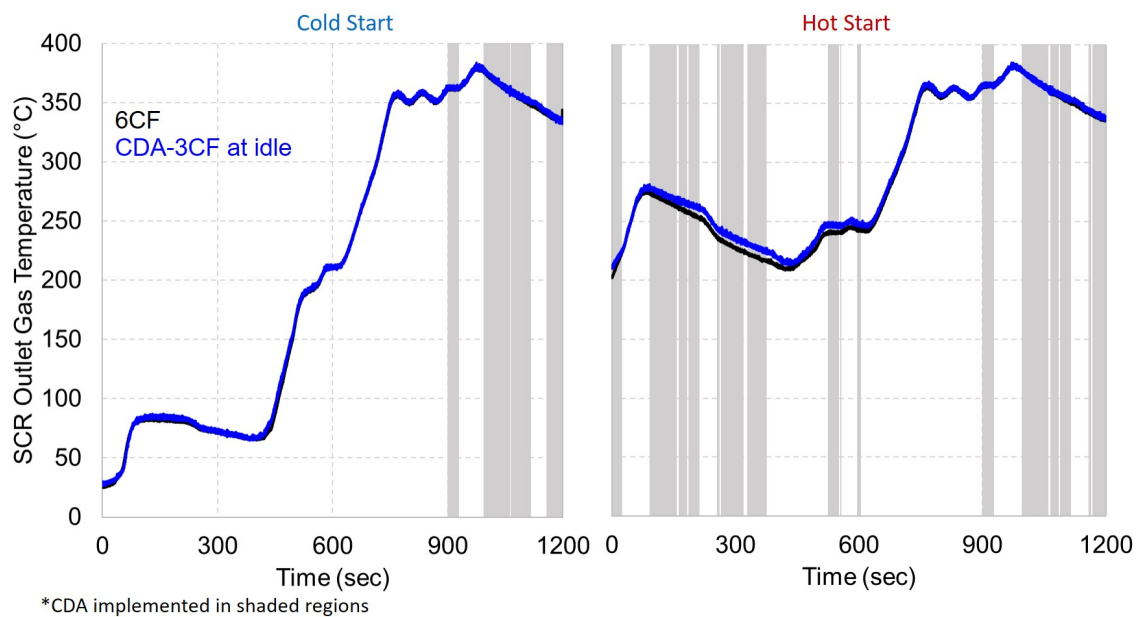
Figure 3.39. SCR outlet temperatures during the HD-FTP drive cycle.
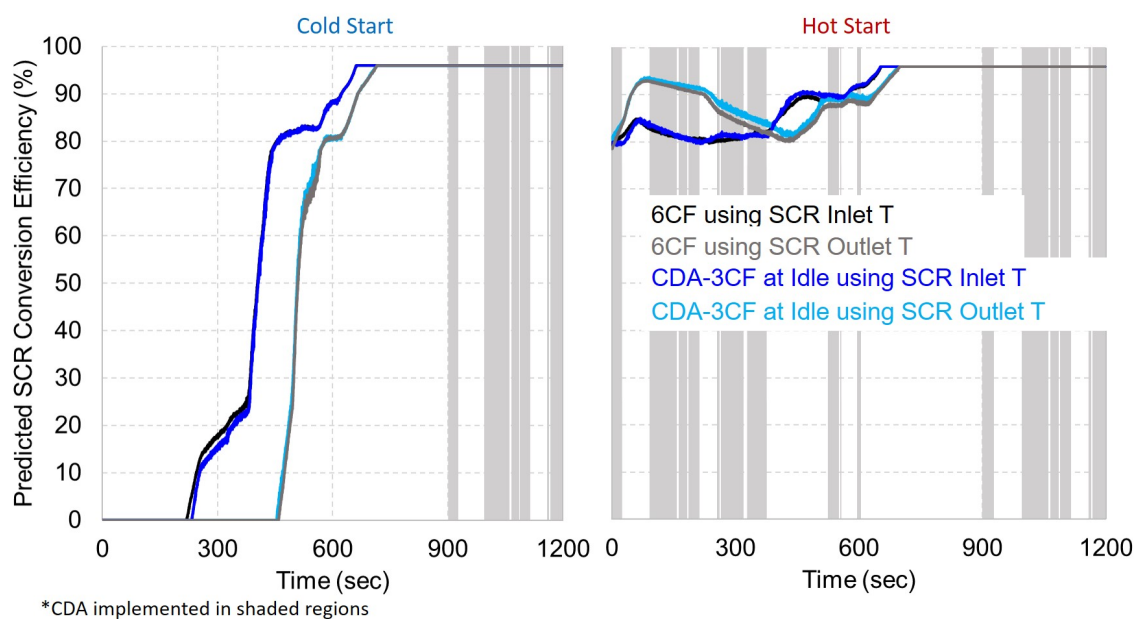
Figure 3.40. Predicted SCR efficiencies using both SCR inlet and outlet temperatures over the HD-FTP drive cycle.
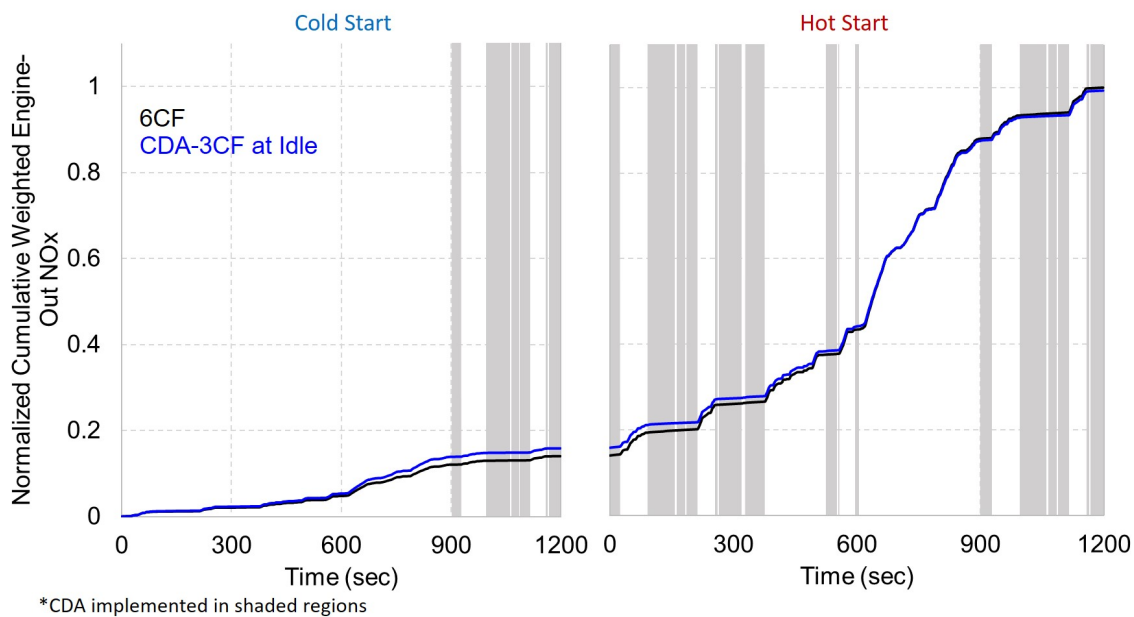
Figure 3.41. Engine-out NOx during the HD-FTP drive cycle.
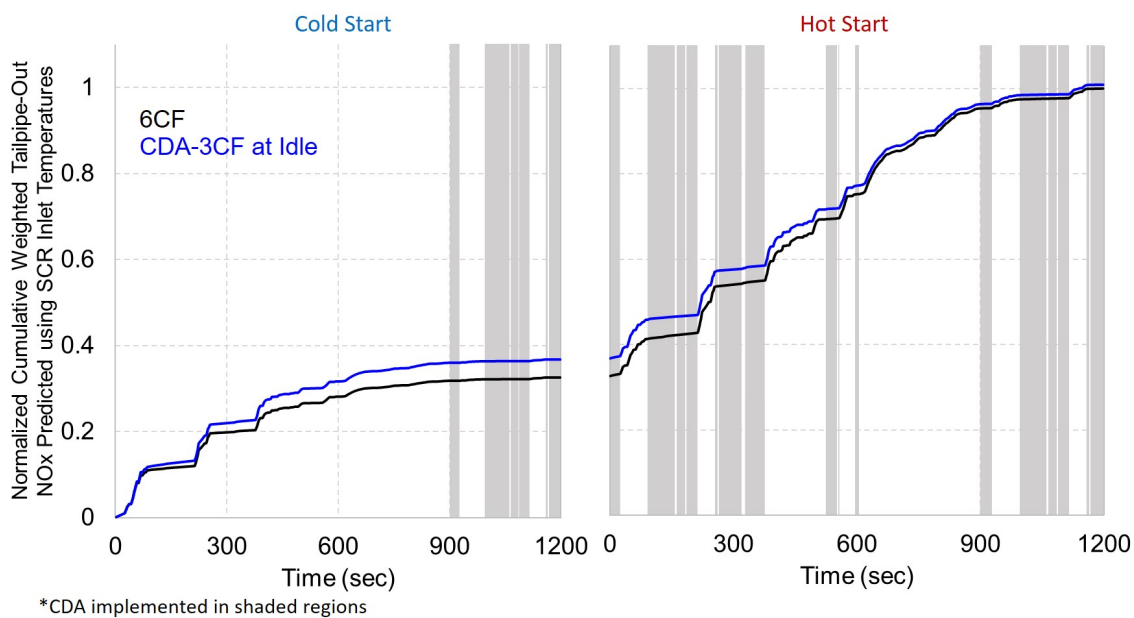
Figure 3.42. Predicted cumulative weighted tailpipe-out NOx during the HD-FTP drive cycle using SCR inlet temperature to estimate SCR conversion efficiency.
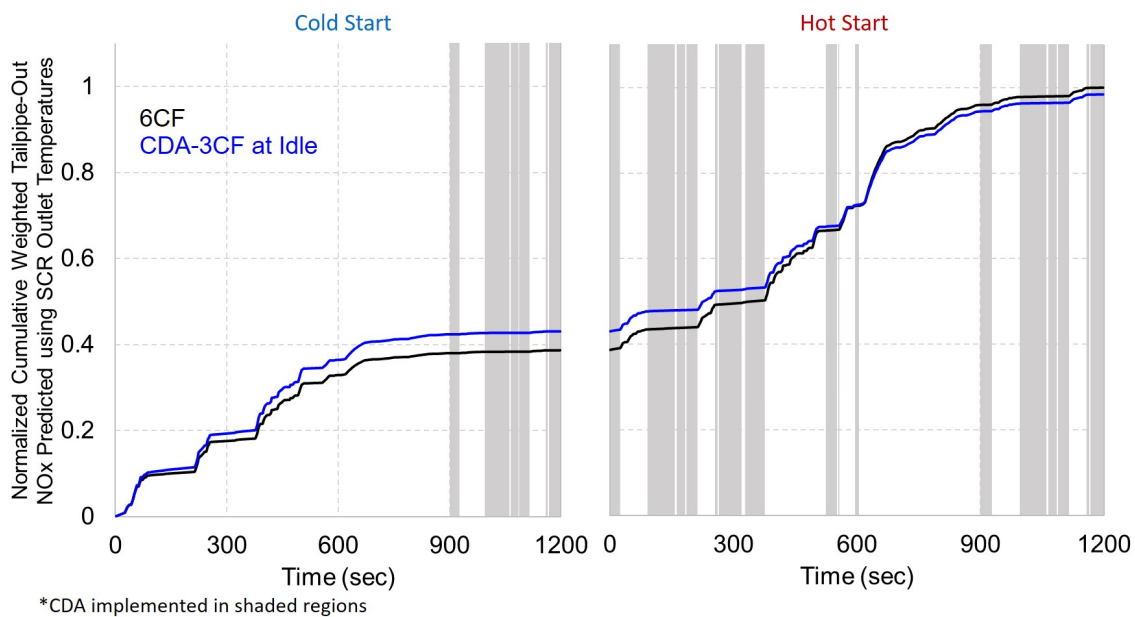
Figure 3.43. Predicted cumulative weighted tailpipe-out NOx during the HD-FTP drive cycle using SCR outlet temperature to estimate SCR conversion efficiency.
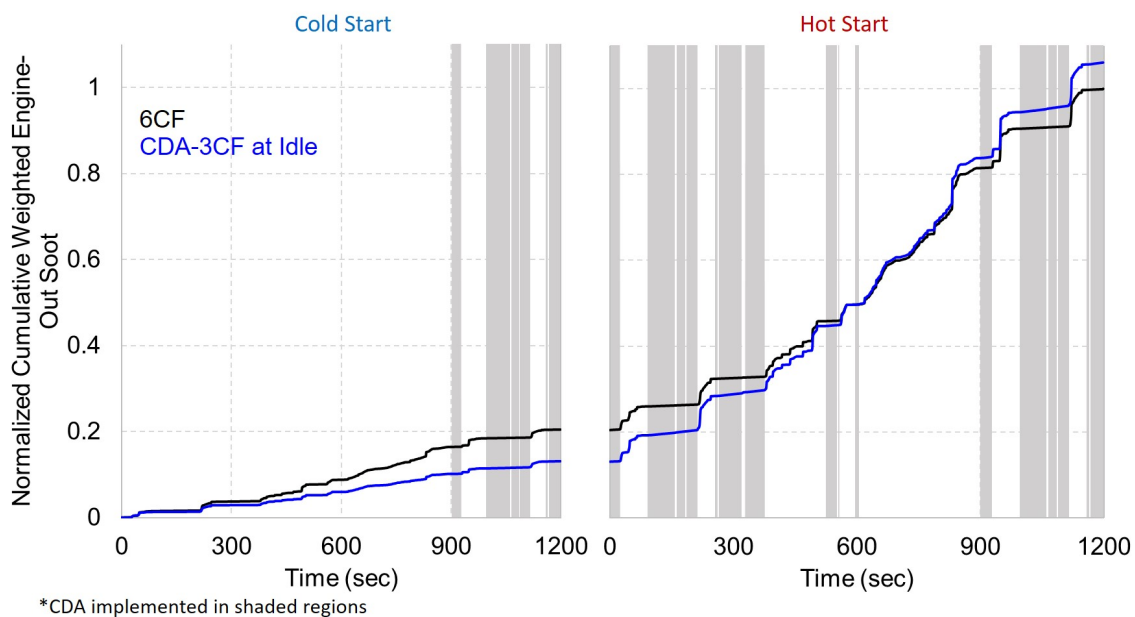
Figure 3.44. Cumulative engine-out soot during the HD-FTP drive cycle.

3.4.3   Summary of CDA HD-FTP Results

Implementing CDA-3CF at loaded idle over the HD-FTP results an average of 0.7% improvement in fuel consumption over baseline fuel-efficient 6CF operation at similar predicted tailpipe-out NOx levels. Thermal management performance is comparable to 6CF operation, although thermal management was not a primary consideration during these calibrations for 6CF nor CDA-3CF. In work where thermal management was further considered, CDA was shown to provide 3% fuel savings when implemented at idle and 3.4% fuel savings when implemented at loads below 3 bar BMEP [31].

3.5   Implementation of CDA for Low-Load Drive Cycle Fuel Efficiency and Thermal Management Improvement

3.5.1   Methodology

Assessment of CDA stay-warm thermal management and efficiency performance during low-load transient operation was conducted for: (1) extended idle operation and (2) creep operation. The inspiration for examining low-load operation effects on aftertreatment temperature in this manner is the cruise+creep portion of the study described in [63]. The initial conditions of both cycles were set by running at 1200 RPM, 7.6 bar BMEP to emulate a highway cruise condition [37] until the system, including the gas temperatures throughout the aftertreatment, reached steady-state. This warm-up takes approximately 40 minutes, as shown in Figure 3.45. The extended idle or creep cycle was then performed while temperatures, fuel consumption, and emissions were logged.

The idle condition for extended idle was set to be loaded idle (800 RPM, 1.3 bar BMEP). This represents a curb idle condition for the tested engine, and is therefore assumed to be representative of idle conditions during a queuing scenario. Data was collected for approximately 38 minutes, the equivalent length of nine HHDDT creep
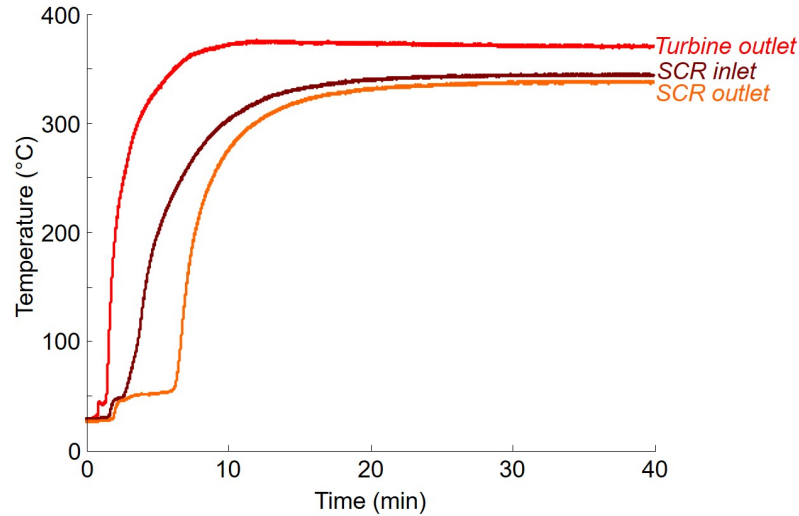
Figure 3.45. Turbine outlet and SCR inlet/outlet temperatures during the preconditioning warm-up at 1200 RPM, 7.6 bar BMEP.

cycles, during extended idle. The profile shown in Figure 3.46 represents the extended idle cycle. Four data sets of extended idle were obtained:

(FE-6CF) Conventional (6-cylinders active) fuel efficient operation throughout.

(TM-6CF) Conventional (6-cylinders active) thermal management operation throughout.

(CDA-3CF) 3-cylinders active operation calibrated for thermal management performance.

(CDA-2CF) 2-cylinders active operation calibrated for thermal management performance.

The creep cycle used for this study is the HHDDT Creep segment shown in Figure 3.47. The creep mode is used to represent low-speed truck operation [64]. This cycle is given as a chassis cycle, however CARB has available a normalized engine speed and torque profile that is used for this study [63]. This normalized profile was mapped to the experimental engine for this study to create the creep engine cycle.
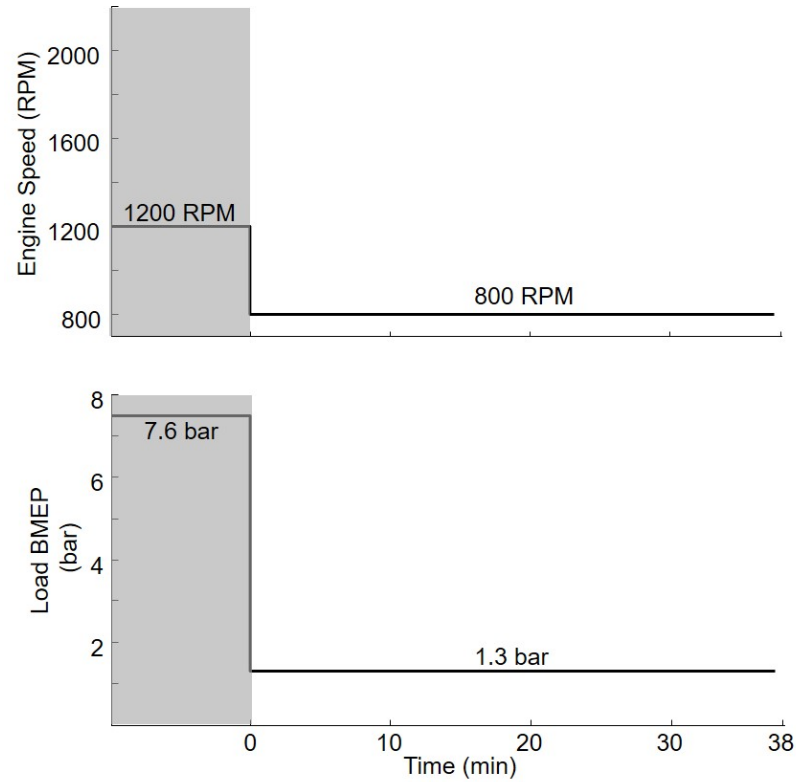
Figure 3.46. Reference engine speed and load for the extended idle cycle.

Nine concatenated HHDDT Creep cycles were used for the creep cycle of this study. The corresponding profile is shown in Figure 3.48. Because the creep cycle is transient and low-load, there are opportunities to explore CDA combinations to improve performance by separating idle from other low-load operation, as shown in Figure 3.49. This added two additional data set types to the set used for the extended idle study, namely (i) using 3 cylinders at idle and low-loads (below 3 bar BMEP) and (ii) using 2 cylinders at and below idle and 3 cylinders at other low-loads (below 3 bar BMEP). Thus, six data sets of creep operation were obtained:

(FE-6CF) Conventional (6-cylinders active) fuel efficient operation throughout

(TM-6CF) Conventional (6-cylinders active) thermal management operation throughout

(CDA-3CF idle) 3-cylinders active operation calibrated for thermal management performance at idle with conventional thermal management operation off-idle

(CDA-2CF idle) 2-cylinders active operation calibrated for thermal management performance at idle with conventional thermal management operation off-idle

(CDA-3CF low loads) 3-cylinder active operation calibrated for thermal management performance at idle, 3-cylinder active operation using stock calibration at off-idle loads below 3 bar BMEP, and with conventional thermal management operation at loads above 3 bar BMEP

(Combined CDA) 2-cylinder active operation calibrated for thermal management performance at idle, 3-cylinder active operation using stock calibration at off-idle loads below 3 bar BMEP, and conventional thermal management operation at loads above 3 bar BMEP.
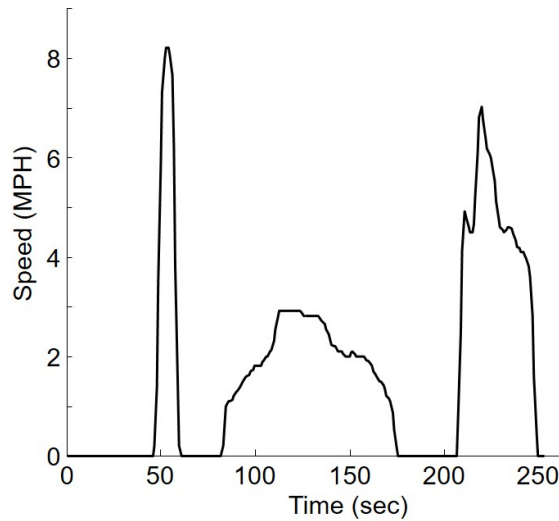
Figure 3.47. HHDDT Creep drive cycle [65].
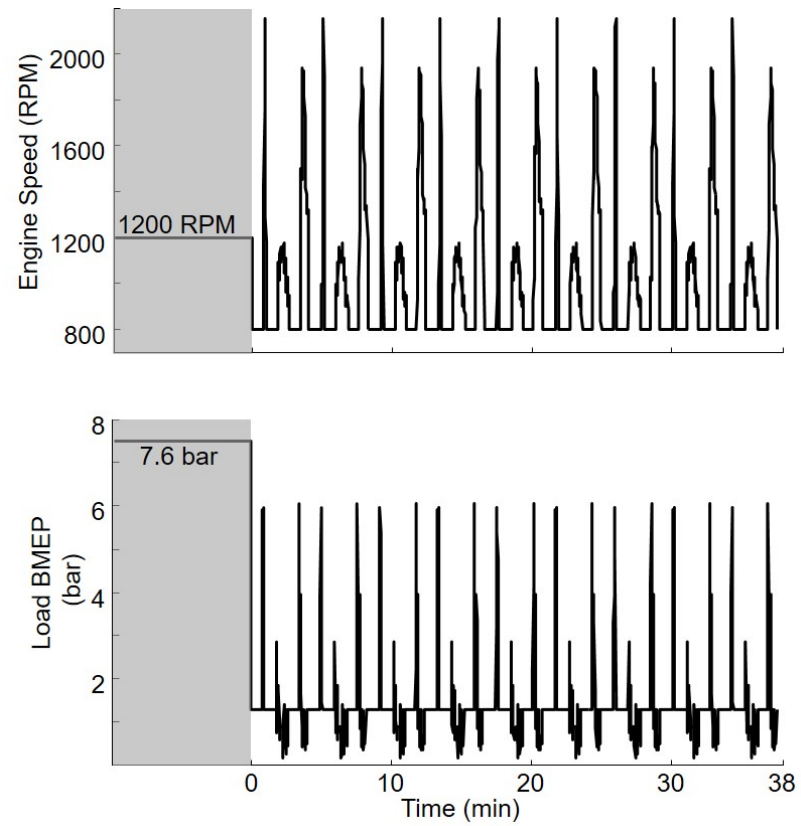
Figure 3.48.   Creep engine cycle for the tested engine. Nine creep cycles are repeated for the experiment.
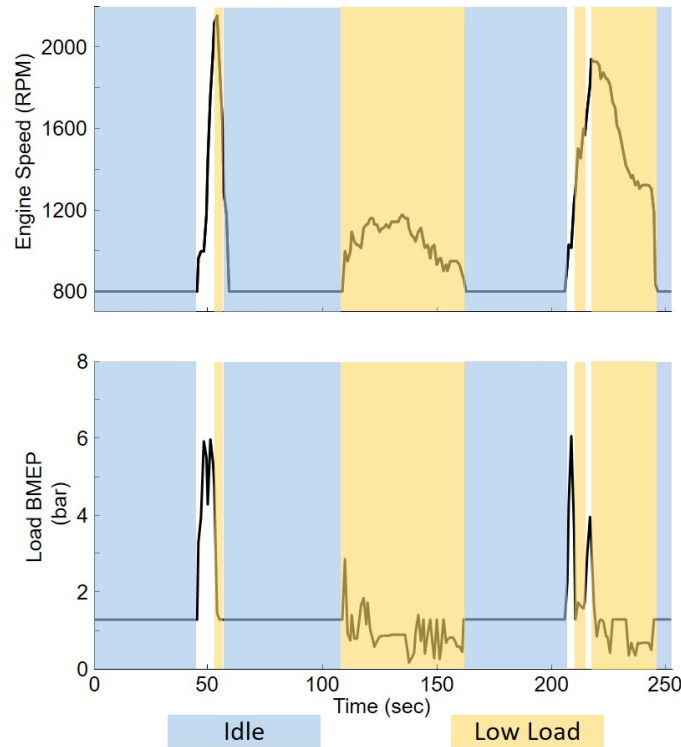
Figure 3.49. Identification of the idle and low-load regions of a creep cycle.

There are a variety of cylinder combinations that can be deactivated, and the deactivation combination affects the firing frequency of the engine [66]. This is studied in detail in Chapter 5. During this work, cylinders were deactivated in configurations that maintain the firing frequency of the engine as close to conventional operation as possible. This helps limit low-frequency torsional vibrations transmitted to the drivetrain. As an example, Figure 3.50(b) shows a possible 3-cylinder active configuration for an inline 6-cylinder engine. This configuration, which is used in this study, maintains a periodic firing sequence on the 1-5-3-6-2-4 firing order engine of *fire-inactive-fire-inactive-fire-inactive*. Similarly, Figure 3.50(c) shows the configuration for CDA-2CF operation used for this study with a firing sequence of *inactive-inactive-fire-inactive-inactive-fire*.

Fueling amount:

x   x   x   x   x   x

x = Conventional operation fueling per cylinder
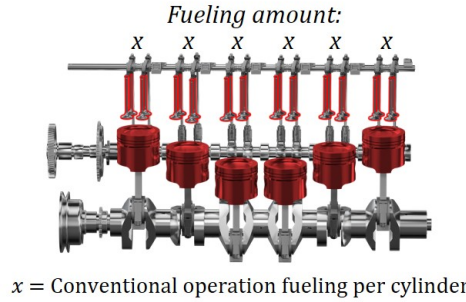
(a) Conventional operation with each cylinder receiving x fueling for a given load.

Fueling amount:

0   0   0   2x-Δ 2x-Δ 2x-Δ

x = Conventional operation fueling per cylinder
Δ = Fuel efficiency modifier
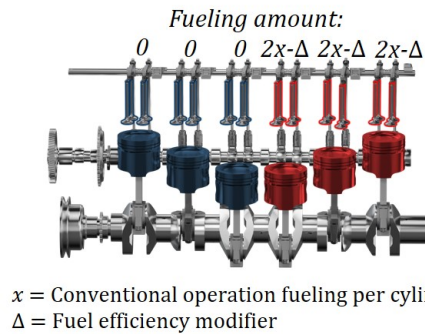
(b) CDA-3CF operation with each active cylinder receiving $2x - \Delta$ fueling to maintain torque, where Δ represents the change in efficiency during CDA operation.

Fueling amount:

0   0   3x-Δ 3x-Δ   0   0

x = Conventional operation fueling per cylinder
Δ = Fuel efficiency modifier
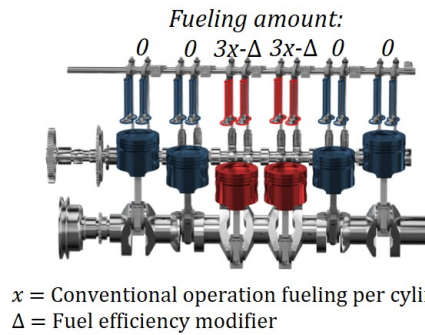
(c) CDA-2CF operation with each active cylinder receiving $3x - \Delta$ fueling to maintain torque, where Δ represents the change in efficiency during CDA operation.

Figure 3.50. Diagrams showing the CDA cylinder configurations.

3.5.2   Results: CDA during Extended Idle

Fuel Consumption and Emissions

It is important to establish the fuel consumption and emissions results for the extended idle and creep drive cycles so these characteristics can be considered together with thermal management performance. This is because there are essentially two conventional operations that serve as baselines for comparison. Specifically, TM-6CF has superior thermal management performance compared to FE-6CF, as shown by the cooling time to 250°C for the various aftertreatment locations in Table 3.7. However, the fuel consumption results in Table 3.8 show that the tested CDA operations give markedly lower fuel consumption than TM-6CF. CDA-2CF has 38% lower fuel consumption and CDA-3CF has 40% lower fuel consumption than TM-6CF over the extended idle cycle. As will be discussed in greater detail below, CDA has thermal management capability similar to the stock thermal management mode (TM-6CF) with fuel economy similar to the more fuel-efficient mode (FE-6CF).

Emissions for the tested CDA operations during extended idle are comparable or lower than the conventional operations for the tested calibrations. The NOx emissions for both CDA operations are lower than both conventional operations, with the CDA-3CF having 52% lower NOx than TM-6CF and 77% lower NOx than FE-6CF. The soot emissions for both CDA operations are lower than conventional thermal management operation and are comparable to the lower soot output of the conventional fuel efficient operation. Notably, CDA-3CF and CDA-2CF have 72% and 50%, respectively, lower soot than TM-6CF.

Table 3.7. Cooling times to 250°C during the extended idle (800 RPM, 1.3 bar BMEP) tests at the measured exhaust locations.

Run	TOT	DOC In	DOC Out	DPF Out	SCR In	SCR Out
TM-6CF	NA	844s	1130s	1268s	879s	1070s
FE-6CF	150s	192s	265s	454s	519s	894s
CDA-3CF	410s	402s	568s	885s	799s	1432s
CDA-2CF	NA	650s	829s	1237s	843s	1655s

Table 3.8. Normalized fuel consumption and engine emissions results for extended idle tests at 800 RPM, 1.3 bar BMEP.

Run	Cumulative Fuel	Cumulative Soot	Cumulative NOx
TM-6CF	1	1	1
FE-6CF	0.66	0.32	2.10
CDA-3CF	0.60	0.28	0.48
CDA-2CF	0.62	0.50	0.62

Thermal Management

As previously discussed, the turbine outlet temperatures and exhaust flow rates combine to determine thermal management performance of a given operation. During stay-warm operation, such as studied here, it is advantageous to reduce exhaust flow

whenever the gas temperature through the components is lower than the aftertreatment component temperature. The steady-state extended idle exhaust flows for each operating mode are shown in Figure 3.51. The reduced exhaust flow and increased temperatures of CDA operations change the aftertreatment cooling dynamics during the extended idle cycle.
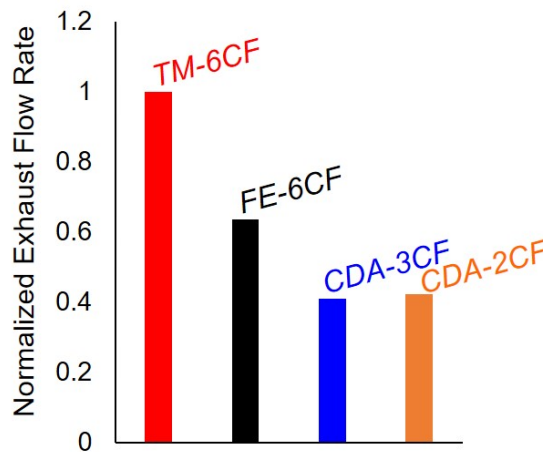
Figure 3.51. Normalized exhaust flow rates at steady-state during the extended idle tests at 800 RPM, 1.3 bar BMEP.

Figure 3.52 shows the turbine outlet temperature of the engine for CDA-2CF operation to be slightly superior to TM-6CF operation, maintaining 265°C at the end of the cycle. The CDA-3CF operation has lower final exhaust temperatures of 209°C. However, both CDA operations have greater than 50°C higher turbine outlet temperatures than FE-6CF operation, with CDA-2CF operation having greater than 100°C higher temperatures.

The turbine-out exhaust gas then traverses an intermediate section of single-walled exhaust pipe and enters the DOC. The temperature profiles at the DOC inlet are shown in Figure 3.53. The temperature advantage of CDA-2CF operation compared to conventional thermal management operation has dissipated at this point in the exhaust system. This is due to the lower exhaust flow of CDA having reduced space velocity and greater time for heat transfer to the ambient to occur through the in-

termediate exhaust piping. While this lower space velocity may be advantageous for other reasons, such as improved SCR performance [67], it does cause a larger temperature drop during the intermediate section of exhaust pipe. This temperature loss could likely be reduced through strategies such as exhaust insulation, double-walled piping, closer aftertreatment location, or close-coupled aftertreatment systems.

The outlet temperature of the DOC/DPF cannister, which is the DPF outlet, is shown in Figure 3.54. The heat transfer effects of the reduced exhaust flow of CDA becomes evident at this location in the aftertreatment system, as both CDA operations maintain higher temperatures than TM-6CF operation for a period of time. CDA-2CF operation maintains higher temperatures for over 20 minutes, even with the lower DOC inlet temperatures discussed above. However, the DPF outlet temperatures at the end of the extended idle cycle have the same magnitude order as the DOC inlet.

The exhaust gas travels through an intermediate section of pipe between the DPF outlet and SCR inlet. This section of pipe also includes the urea doser. The exhaust temperature at the inlet of the SCR catalyst is shown in Figure 3.55. The CDA operations again show a temperature drop between the aftertreatment components due to the lower flow rates. However, this reduced flow rate is beneficial to maintain elevated catalyst temperatures. This is demonstrated by the SCR outlet temperature in Figure 3.56, where CDA-2CF and CDA-3CF operations have greater exhaust temperatures than TM-6CF for 34 minutes and 28 minutes, respectively.

The exhaust temperatures of the CDA strategies during extended idle operation are more elevated throughout the aftertreatment system compared to the more fuel-neutral FE-6CF operation. The CDA strategies have comparable thermal performance to conventional thermal management operation, TM-6CF, while also showing 38%-40% fuel savings.
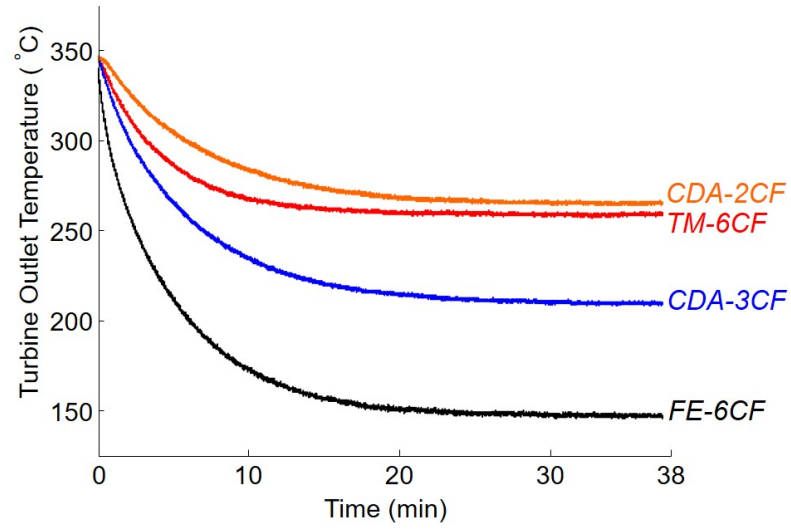
Figure 3.52. Turbine outlet temperatures during the extended idle tests at 800 RPM, 1.3 bar BMEP.
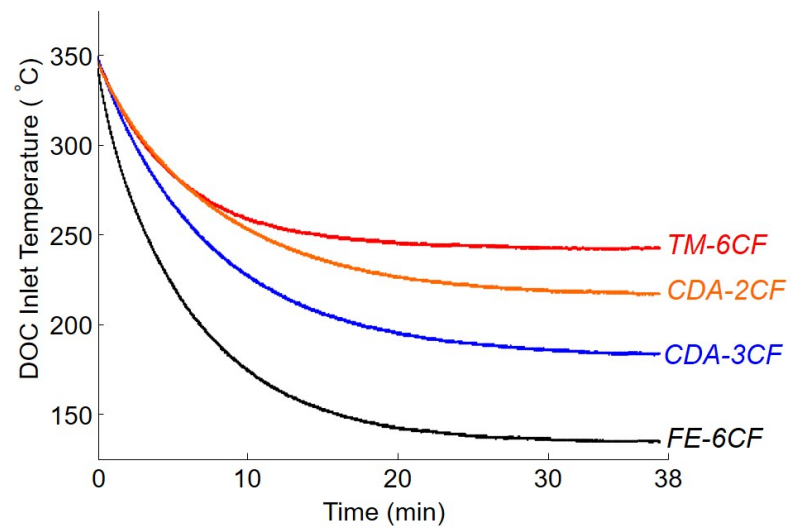
Figure 3.53. DOC inlet temperatures during the extended idle tests at 800 RPM, 1.3 bar BMEP.
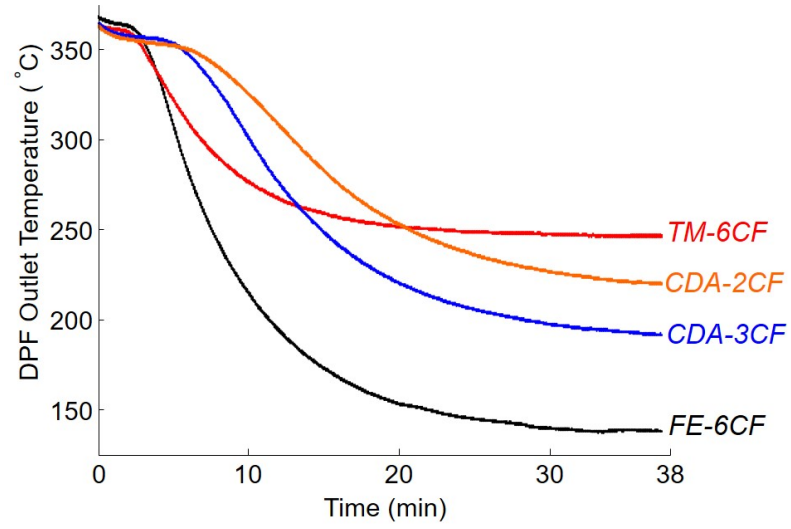
Figure 3.54. DPF outlet temperatures during the extended idle tests at 800 RPM, 1.3 bar BMEP.
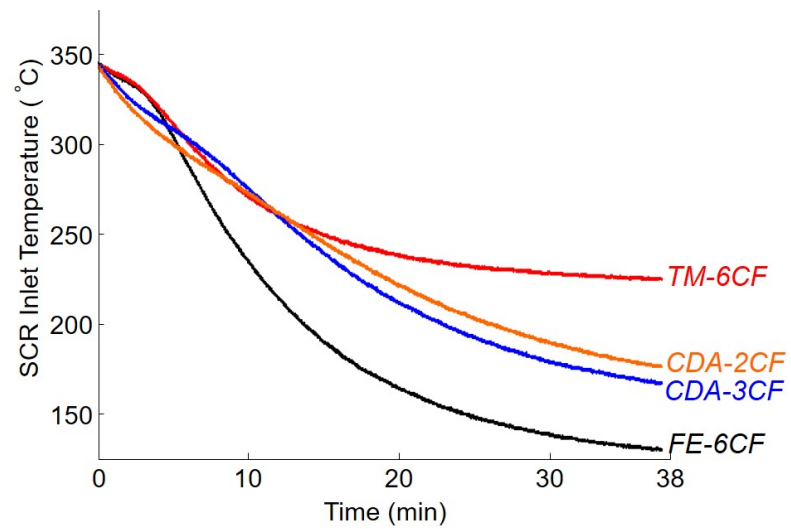
Figure 3.55. SCR inlet temperatures during the extended idle tests at 800 RPM, 1.3 bar BMEP.
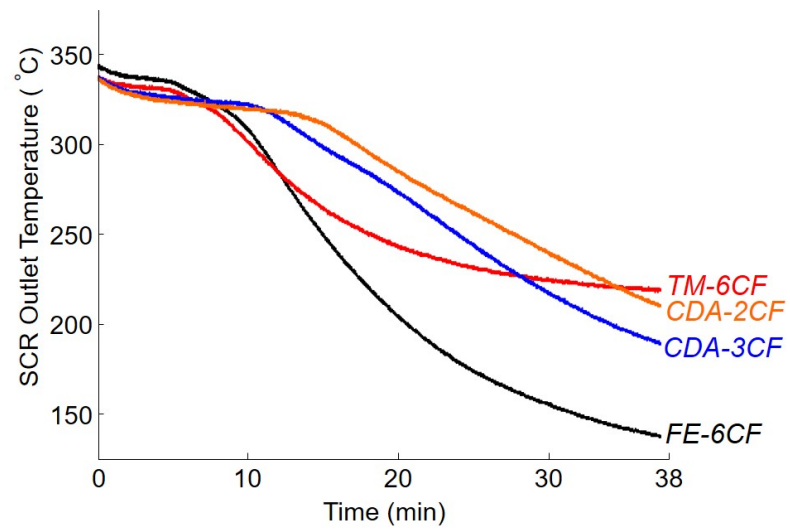
Figure 3.56. SCR outlet temperatures during the extended idle tests at 800 RPM, 1.3 bar BMEP.

3.5.3   Results: CDA during Creep Operation

Fuel Consumption and Emissions

CDA was implemented at curb idle, the same operating condition as the above extended idle tests, during the creep cycle (per Figure 3.48, as described earlier). The effects of CDA over creep operation are less predictable due to the more dynamic nature of the cycle requiring transitions in and out of CDA. CDA again enables comparable thermal management performance to TM-6CF, together with fuel savings. However, as shown by the cumulative fuel consumption and measured emissions for each creep test in Table 3.9, the idle-only implementations of CDA have reduced fuel consumption compared to conventional thermal management operation (TM-6CF) and comparable fuel consumption to conventional fuel efficient operation (FE-6CF), together with superior thermal management. Implementing CDA-3CF at idle over the creep cycle results in 15% lower fuel consumption compared to TM-6CF, while CDA-2CF at idle provides 16% fuel consumption reduction. Engine-out NOx and soot emissions for the CDA at idle operations are again lower or comparable to the conventional operations.

Extending CDA to other low-load (less than 3 bar BMEP) operating conditions further reduces the fuel consumption of the CDA cycles to lower than FE-6CF operation. CDA-3CF at low-load operations shows a 31% reduction in fuel consumption over the creep cycle compared to conventional thermal management operation, while the Combined CDA operation results in 25% fuel savings over the creep cycle. Soot and NOx concentration spikes occur during the deactivation and reactivation transitions from air handling actuator delays, increasing the cumulative emissions for the low-load CDA runs. It is expected that these spikes could be addressed in the future via additional calibration.

Table 3.9. Normalized fuel consumption and engine emissions results for creep cycles.

Run	Cumulative Fuel	Cumulative Soot	Cumulative NOx
TM-6CF	1	1	1
FE-6CF	0.77	0.59	1.76
CDA-3CF idle	0.85	0.62	0.86
CDA-2CF idle	0.84	0.82	1.04
CDA-3CF low load	0.69	3.24	1.25
Combined CDA	0.75	1.35	1.01

Thermal Management

CDA has a significant impact on the exhaust temperatures during the creep cycle. The turbine outlet temperatures, shown in Figure 3.57, are consistently elevated above both 6-cylinder operations for the Combined CDA run, primarily due to the elevated temperatures of CDA-2CF. This effect is sustained for the duration of the creep cycle. The other CDA operations have higher turbine outlet temperatures than conventional fuel efficient operation and comparable or slightly worse performance than conventional thermal management operation.

The temperature advantage of the Combined CDA operation is slightly diminished at the DOC inlet, shown in Figure 3.58, due to the reduced flow rate in the intermediate section of exhaust pipe, as discussed during the extended idle section. However, the temperatures remain elevated above conventional thermal management operation. This temperature advantage grows by the time the gas reaches the DPF

outlet of Figure 3.59 due to the reduced cooling of the component. A mixture of heat transfer to the exhaust gas from the DOC/DPF and DOC thermal effects contribute to slightly higher DPF outlet temperatures than DOC inlet temperatures for the Combined CDA operation. The other CDA modes have slightly reduced DPF outlet temperatures to conventional thermal management operation. All CDA operations show elevated DPF outlet temperatures compared to FE-6CF operation.

The SCR inlet and outlet temperatures for the system are shown in Figures 3.60 and 3.61. The Combined CDA cycle maintains higher SCR temperatures than conventional thermal management operation for greater than 20 minutes, keeping the SCR in the zone of high conversion efficiency for a prolonged duration. This effect is particularly notable at the SCR outlet location.
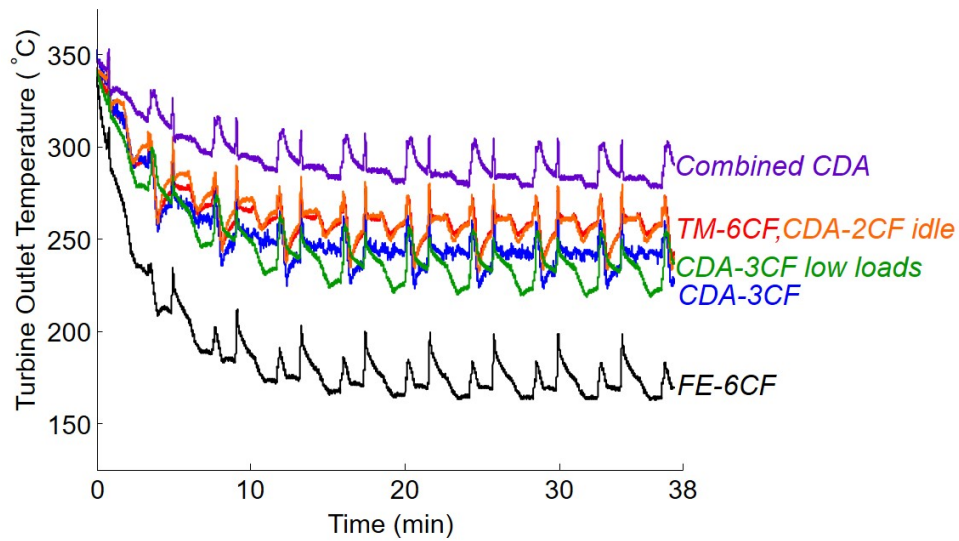
Figure 3.57. Turbine outlet temperatures during the creep tests.
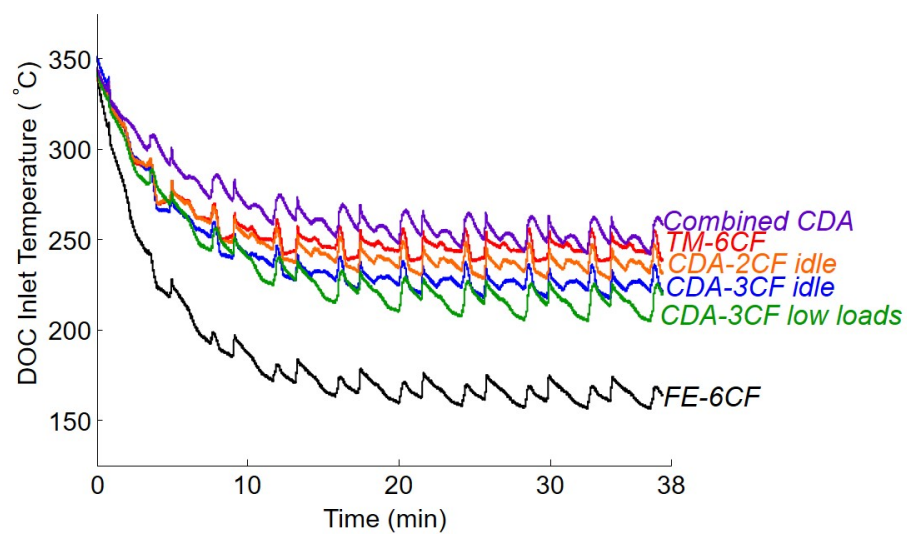
Figure 3.58. DOC inlet temperatures during the creep tests.
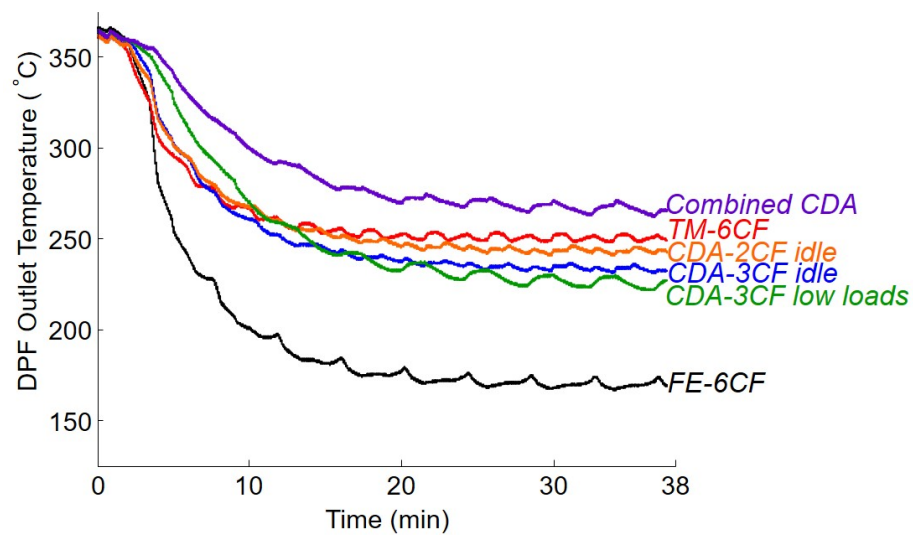
Figure 3.59. DPF outlet temperatures during the creep tests.
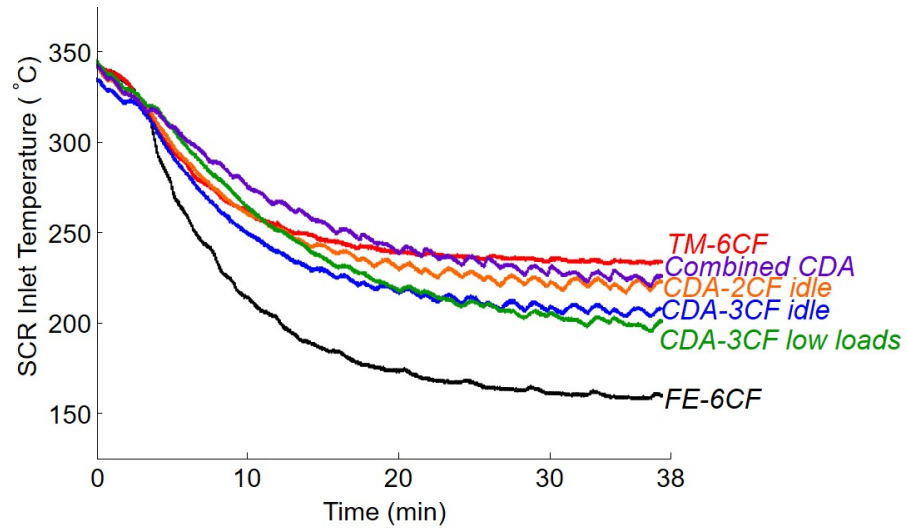
Figure 3.60. SCR inlet temperatures during the creep tests.
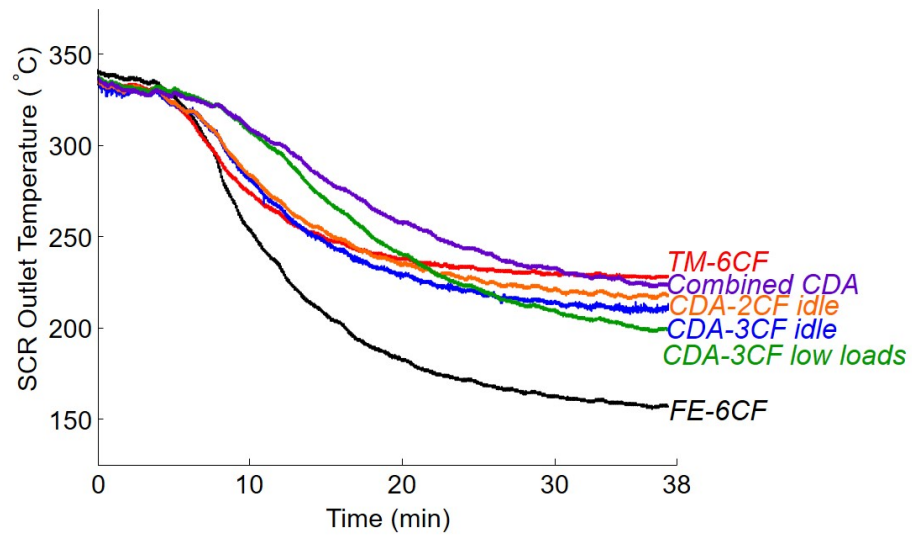
Figure 3.61. SCR outlet temperatures during the creep tests.

3.5.4 Summary of Low-Load Cycles

Aftertreatment thermal management in modern diesel engines is a difficult challenge during low-load operation. One of the most significant challenges is maintaining effective aftertreatment temperatures. Fuel efficiency is often sacrificed in order to slow the cooling of aftertreatment components during low-load operation. CDA has the ability to slow the cooling of aftertreatment components in a more fuel efficient manner through reduced exhaust flow and increased exhaust temperatures.

Two types of low-load operations following an elevated load scenario were examined: (i) extended idle operation at 800 RPM, 1.3 bar BMEP and (ii) creep operation. The aftertreatment temperatures during each of these drive cycles are presented. It was examined how the cooling rates of the aftertreatment varies depending on component location and CDA mode. The lower flow rate of CDA slowed the cooling of the aftertreatment components, however this lower flow rate also caused increased temperature drop between components from the uninsulated single-walled exhaust pipe. Ultimately, implementing CDA operations maintained higher SCR outlet temperatures than conventional thermal management operation for 34 minutes during extended idle for 2 cylinder active operation and is comparable during much of the creep operation. The thermal management for all components is notably improved for CDA operations compared to the more fuel neutral conventional fuel efficient operation. The fuel consumption reduction for CDA was up to 40% during extended idle and 31% during creep operation. This is achieved with typically comparable or improved engine-out emissions. Notably, CDA-3CF and CDA-2CF have 72% and 50%, respectively, lower soot than TM-6CF during extended idle. This coincides with 52% and 38% reductions in NOx for CDA-3CF and CDA-2CF, respectively.

4. COMPARISON OF CYLINDER DEACTIVATION TRAPPING STRATEGIES

4.1 Motivation

Cylinders can be deactivated through various combinations of valve and fuel deactivation events. The chosen combination ultimately dictates the type of residual charge gas trapped inside the cylinder. This can dictate performance characteristics both during CDA operation and after reactivation of the deactivated cylinders. Therefore, it is important to understand the effects of the charge trapping strategies. This work experimentally characterizes and compares two of the primary charge trapping options for CDA- fresh charge trapping and combusted charge trapping.

4.2 Methodology

The test plan for this study consisted of acquiring in-cylinder pressure data while transitioning into CDA with (1) fresh charge and (2) combusted charge trapped in cylinders 4, 5, 6. This cylinder combination represents a typical deactivation combination on an engine with a 1-5-3-6-2-4 firing order, as it maintains symmetry in the firing order. Valve profiles and injector currents were examined after deactivation to confirm the desired fresh or combusted charge trapping for the given cylinder.

Data was acquired while transitioning into CDA at two operating speeds at 1.3 bar BMEP: 2200 RPM and 800 RPM. This load is representative of a common curb idle load for this engine. The speeds were chosen based on the AVL 8-mode analysis for the tested engine. Categorizing the operating range of the engine into the eight modes based on the proximity of the given operating condition to a mode results in the allotment shown in Figure 4.1. This analysis divides the operating space into a high-speed range and low-speed range. 800 RPM was chosen to represent the low-

speed range for these tests due to its importance for idle operation. 2200 RPM was chosen as the representative mean for the higher speed range.

The minimum in-cylinder pressure values are sensitive to systematic measurement offset errors, including original transducer calibration, thermodynamic offset, and measurement noise, so the minimum cycle pressures are estimated based on the maximum cylinder pressure and the assumption of isentropic compression and expansion. This assumption should yield valid values for comparison of minimum cylinder pressures.
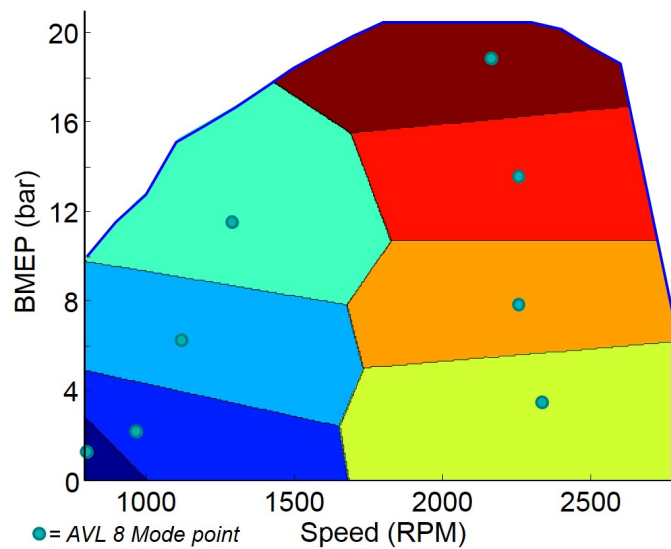
Figure 4.1. Engine torque-speed map divided into sections based on the AVL 8-mode.

4.3 Results

4.3.1 Transitioning into CDA

In this section, pressure-volume (PV) diagrams and crank angle-based pressures for the CDA transition at 2200 RPM and 800 RPM are used to illustrate the transition

for each charge trapping strategy. Figures 4.2(a) and 4.2(b) show the in-cylinder pressures for conventionally firing cylinders as baseline references.

The valves are deactivated after the induction stroke for each trapping strategy, as previously discussed and shown in Figure 1.7. Figures 4.3(a) and 4.3(b) depict the trapping of fresh charge during the deactivation at 2200 RPM and 800 RPM, respectively. The fresh charge trapping behavior is similar for both operating conditions. The fresh charge is inducted into the cylinder and compressed, however no fuel is injected following this compression event. The expansion line therefore closely traverses the traditional compression line on the PV diagram. Since the valves are now deactivated, the typical "exhaust" stroke now creates an additional compression event.

Each upward piston stroke now acts as a compression event and each downward stroke acts as an expansion event, creating a gas spring. An example of this gas spring effect is shown in Figure 4.4 for the cycle following the deactivation. This figure shows data for cylinders with fresh charge trapped, however the gas spring trend is consistent for both trapping strategies. The gas spring has irreversible losses from mass and heat losses. The gas is compressed to a slightly lower peak pressure during each subsequent compression due to charge mass leaked by the piston rings and heat transfer losses to the cylinder walls. The losses and ensuing pressure decay after deactivation, depicted in Figure 4.5, is examined in more detail in the next section.

Figures 4.6(a) and 4.6(b) show the trapping of combusted charge during the deactivation transition cycle at 2200 RPM and 800 RPM, respectively. Fresh charge is inducted into the cylinder and compressed. Fuel is then injected to create combustion during the deactivation at TDC (top dead center, taken to be 0°CA) that increases the cylinder pressure and adds energy to the gas. The expansion line on the PV diagram then resembles the traditional expansion line. Instead of then exhausting the combusted gas, the valve deactivation causes the typical "exhaust" stroke to become a second compression stroke with an increased initial pressure compared to the

first compression event. This is where the behavior of the combusted charge strategy can vary depending on the characteristics of the operating condition. The second compression event can cause greater cylinder pressures than during, or following, the combustion event when enough of the energy from the combustion event is released after the piston has reached TDC. A large fraction of the energy from the combustion event typically occurs after TDC in diesel engines. The analyzed dataset shows a measured pressure of 2.26 MPa greater than the combustion pressure. The "spike" in pressure occurs for the 2200 RPM, 1.3 bar BMEP condition, but not for the 800 RPM, 1.3 bar BMEP condition. This is due to a combination of greater heat loss at 800 RPM from slower piston motion and less heat release from combustion occurring after TDC, as discussed below. Nevertheless, the gas spring with losses then continues, as shown in Figures 4.5(a) and 4.5(b), similar to that of the fresh charge trapping case.

The elevated pressure caused by the recompression in combusted charge trapped CDA at 2200 RPM, 1.3 bar BMEP is shown again in the graphics of Figure 4.7. This effect is a direct result of the combustion at that condition resembling the constant pressure heat addition of the Diesel cycle. As shown in Figures 4.8a and 4.8b, an engine operating on the Otto cycle, or a diesel engine operating with a more advanced injection timing such as the 800 RPM, 1.3 bar BMEP condition, would not have the elevated pressure spike after deactivation. Conversely, as shown in Figures 4.8c and 4.8d, the theoretical Diesel cycle would have the largest possible pressure spike after deactivation due to the constant pressure heat addition. In practice, the pressure spike will occur when the combustion energy addition after TDC is greater than the heat losses that occur before the recompression TDC. The resulting abrupt torsional variation caused by the pressure spike could be problematic during cycle-to-cycle, dynamic CDA engine operation. It also creates unnecessary pumping losses due to the imperfect gas spring that follows deactivation.
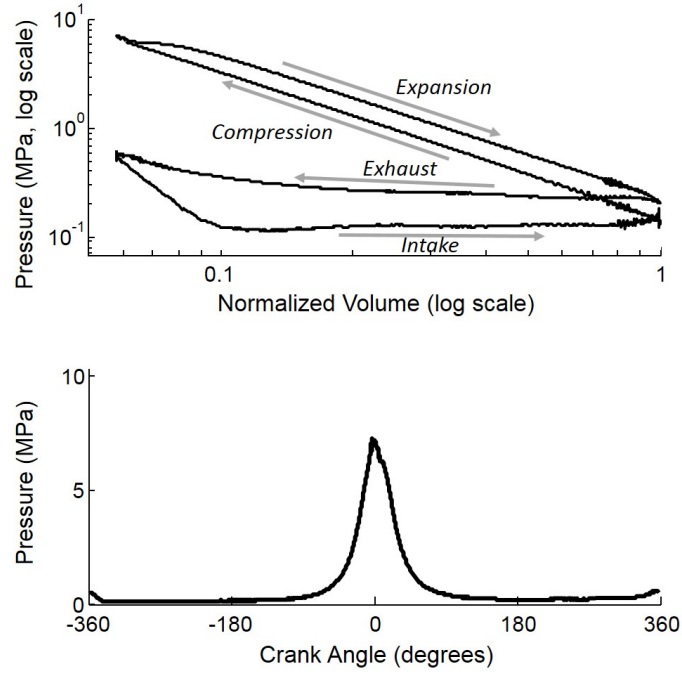
(a) Conventional operation at 2200 RPM, 1.3 bar BMEP
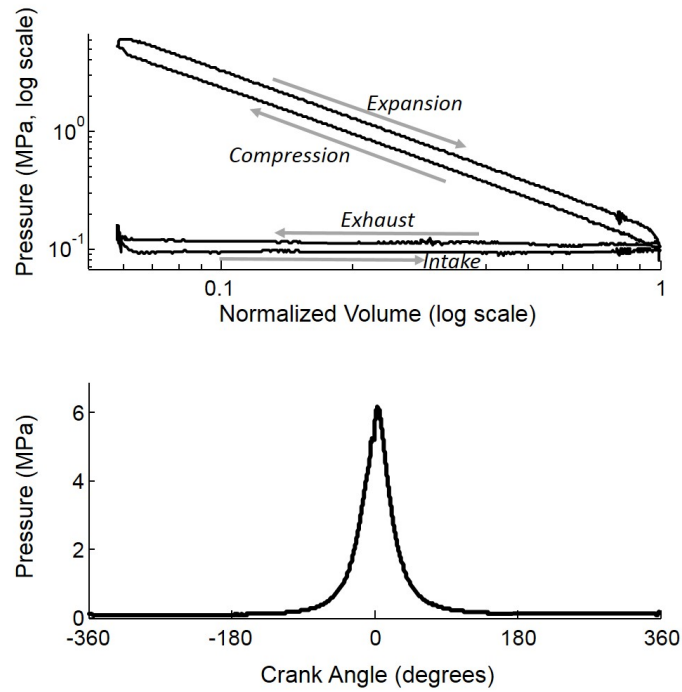
(b) Conventional operation at 800 RPM, 1.3 bar BMEP

Figure 4.2. LogP-LogV diagrams and crank angle-based pressures for conventional cylinder operation at the tested operating conditions.
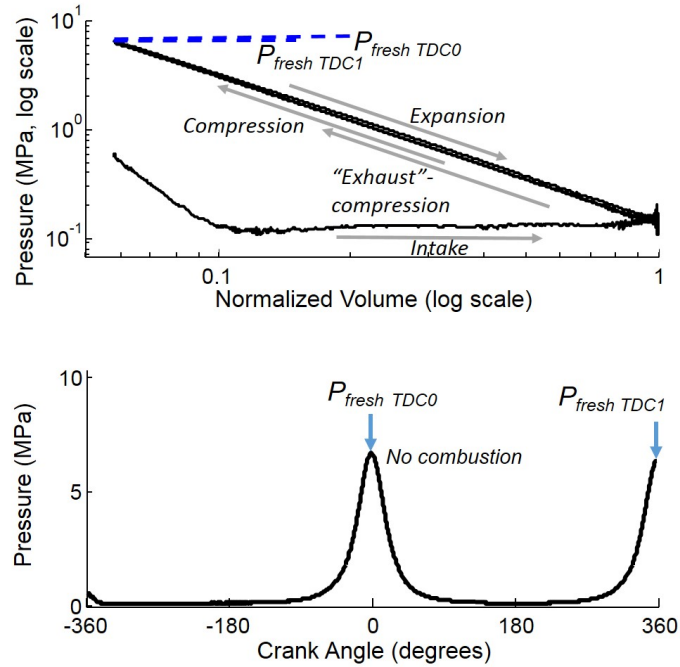
(a) Fresh charge trapping cycle at 2200 RPM, 1.3 bar BMEP
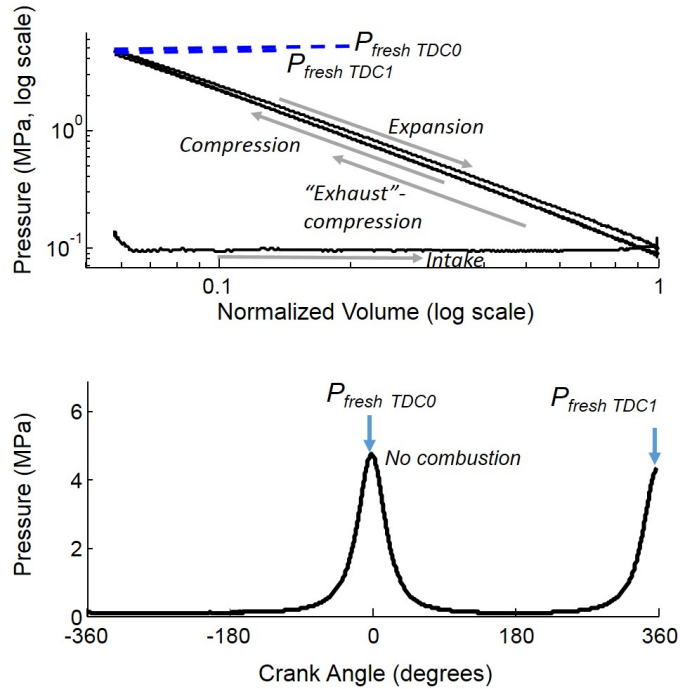
(b) Fresh charge trapping cycle at 800 RPM, 1.3 bar BMEP

Figure 4.3. LogP-LogV diagrams and crank angle-based pressures for the cycle trapping a fresh charge.
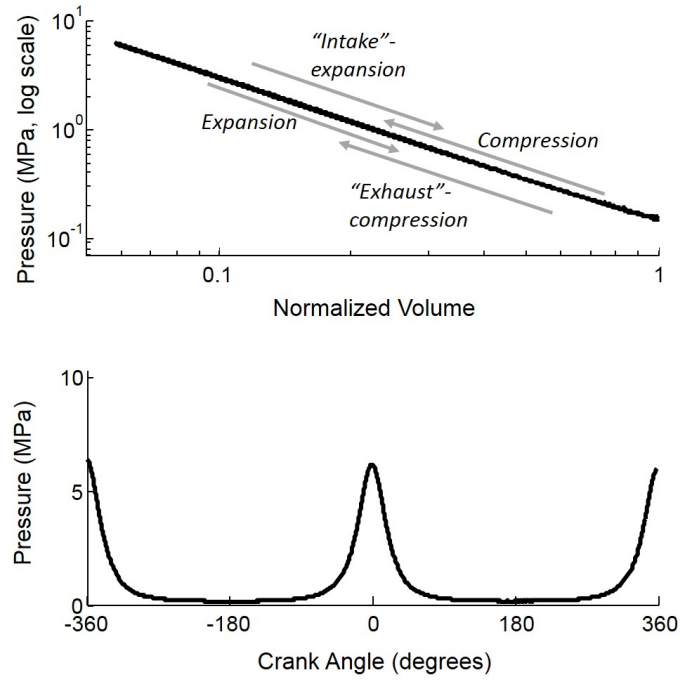
(a) Deactivated cylinder at 2200 RPM
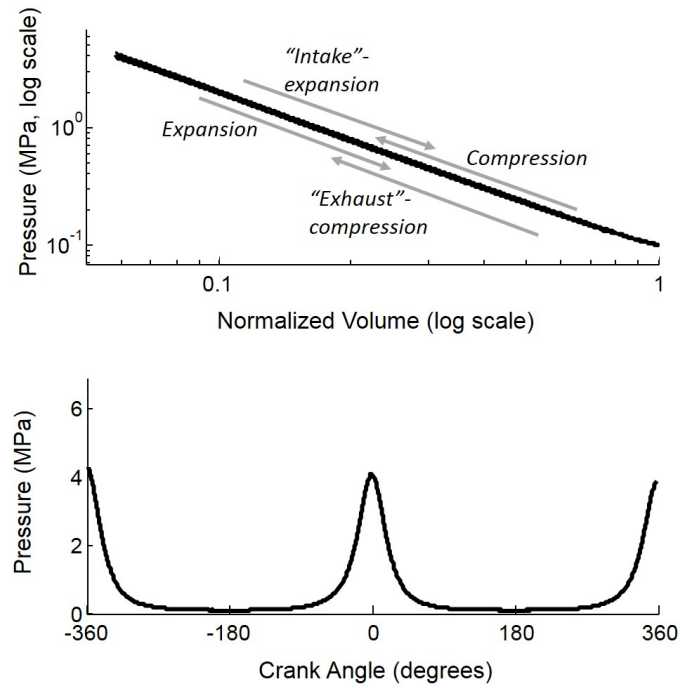
(b) Deactivated cylinder at 800 RPM

Figure 4.4. LogP-LogV diagrams and crank angle-based pressures of
a deactivated cylinder during the cycle after deactivation.
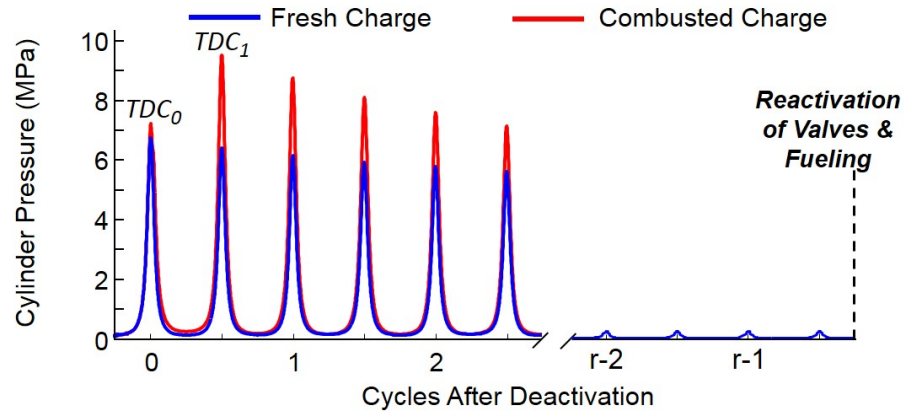
(a) Deactivated cylinder 6 at 2200 RPM, 1.3 bar BMEP
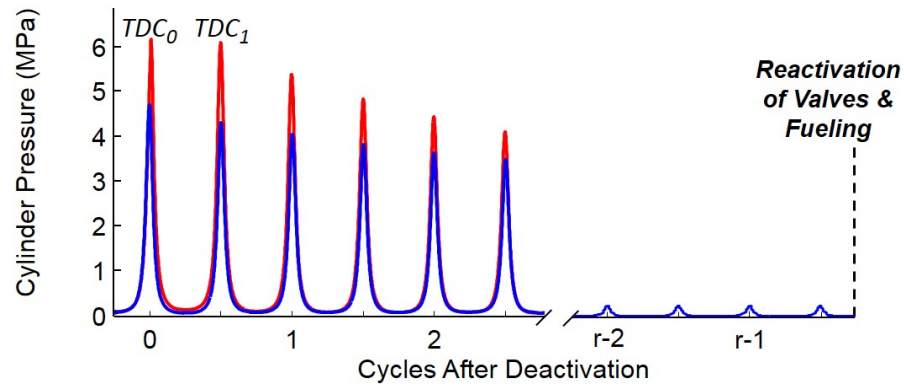
(b) Deactivated cylinder 6 at 800 RPM, 1.3 bar BMEP

Figure 4.5. In-cylinder pressure following the deactivations to demonstrate the gas spring effect and corresponding pressure losses after deactivation. TDC numbers correspond to the labels on Figures 4.3(a) and 4.6(a) for (a) and Figures 4.3(b) and 4.6(b) for (b).
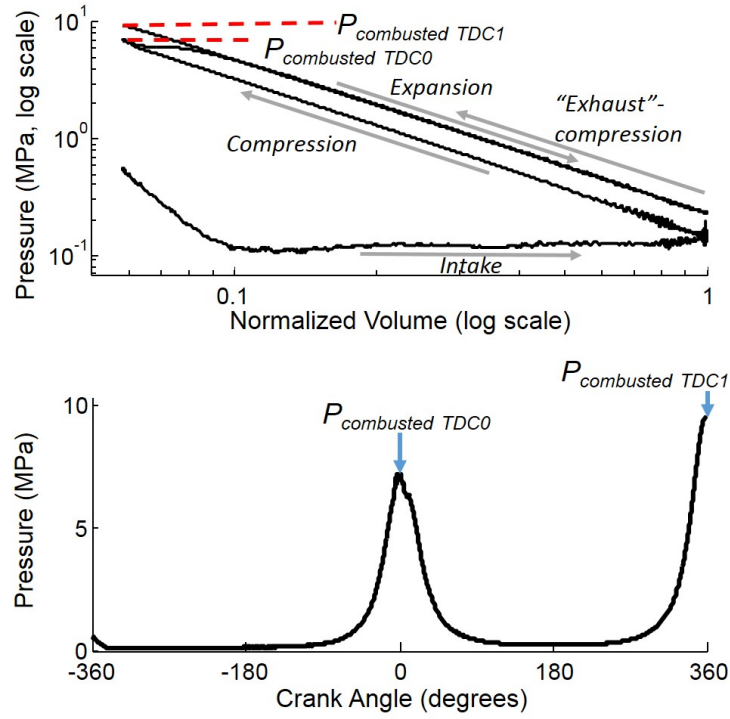
(a) Combusted charge trapping cycle at 2200 RPM, 1.3 bar BMEP
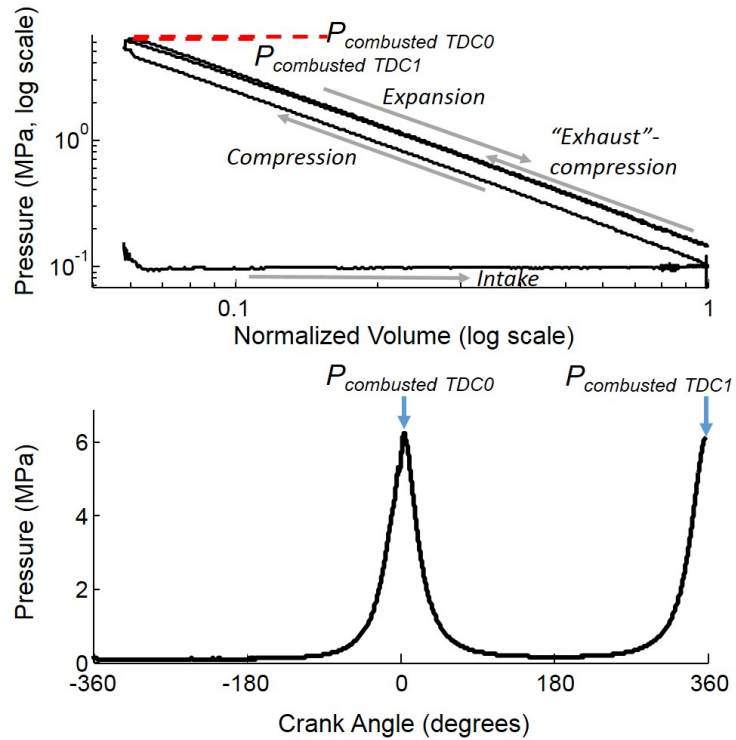
(b) Combusted charge trapping cycle at 800 RPM, 1.3 bar BMEP

Figure 4.6.   LogP-LogV diagrams and crank angle-based pressures for the cycle trapping a combusted charge.
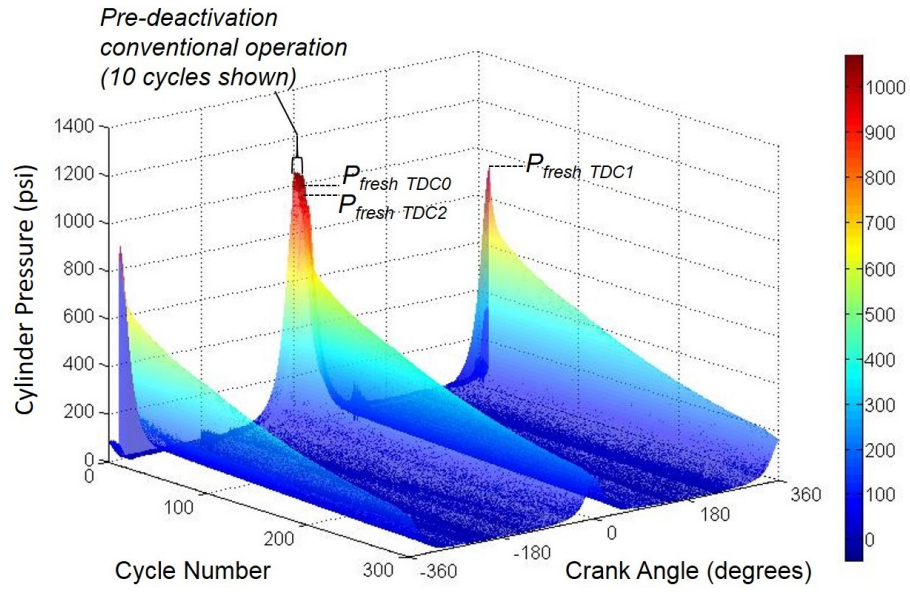
(a) In-cylinder pressures after fresh charge trapping at 2200 RPM, 1.3 bar BMEP
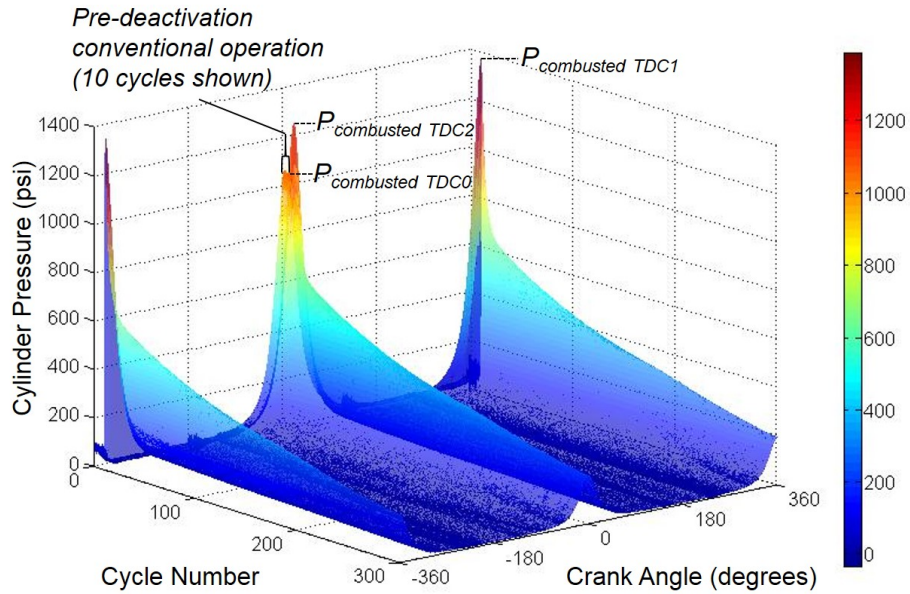
(b) In-cylinder pressures after combusted charge trapping at 2200 RPM, 1.3 bar BMEP

Figure 4.7. In-cylinder pressures following each type of tested charge trapping variants at 2200 RPM, 1.3 bar BMEP.
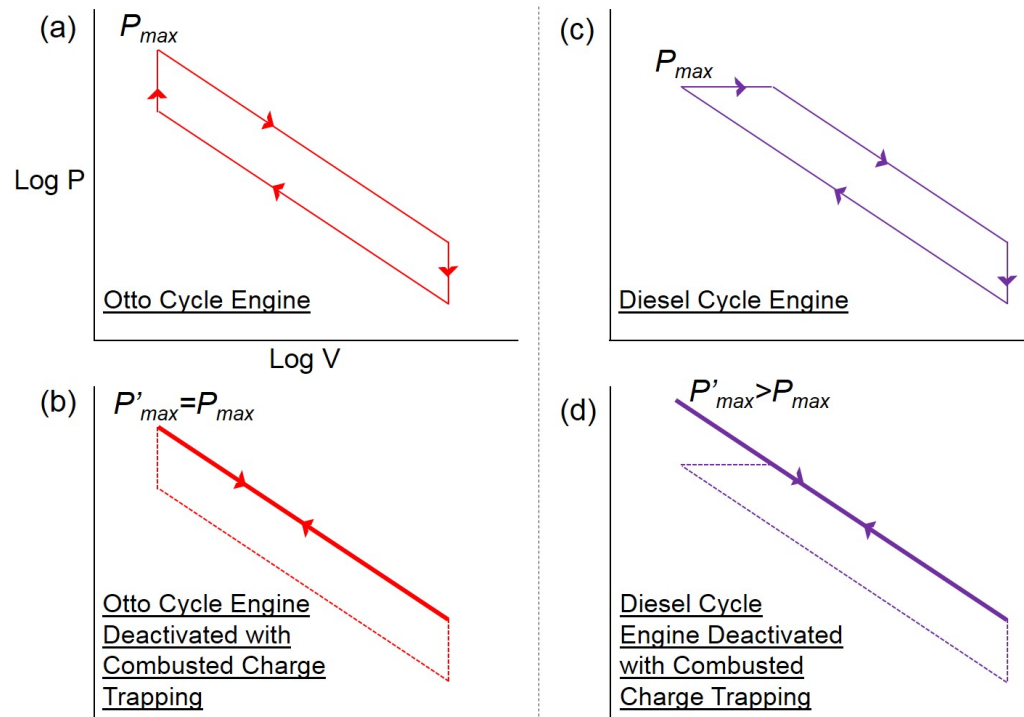
Figure 4.8. Ideal thermodynamic Otto cycles for conventional (a) and deactivated (b) operation are shown on the left. Ideal thermodynamic Diesel cycles for conventional (c) and deactivated (d) operation are shown on the right.

4.3.2   In-Cylinder Effects during Deactivation

The reciprocating piston of a deactivated cylinder acts as a gas spring after the valves are deactivated and the charge is trapped. This means there are no longer pumping losses for that cylinder because there is no gas exchange process. The gas spring trend will occur regardless of trapping strategy. An ideal gas spring would maintain in-cylinder mass and exhibit no heat loss, making fresh charge trapping and combusted charge trapping differ only via cylinder pressure magnitudes. A cylinder with a fresh charge trapped would have lower pressures, requiring less force to compress and consequently outputting less force during expansion than a cylinder with a combusted charge trapped. A combusted charge trapped cylinder would have elevated pressures which would result in higher temperatures in the deactivated cylinders. Higher temperatures in the deactivated cylinders correlates to a decreased temperature gradient to the active cylinders. This reduces heat transfer from the active cylinders to increase the efficiency of the engine. Higher temperatures in deactivated cylinders would also improve combustion quality upon reactivation due to elevated wall temperatures.

The assumption of an ideal gas spring in the deactivated cylinders is inaccurate. There will always be heat loss and blow-by around the piston rings that results in a decrease in trapped mass and, therefore, a reduced gas spring effect. However, the losses from the gas spring within a given cycle are small in magnitude relative to the power output of the engine. Figures 4.9 and 4.10 show this effect by examining the calculated work for a cylinder before deactivation, during the charge trapping cycle, and during deactivation. The gas spring does incur losses in each deactivated cycle, however these losses are small relative to the power output of the engine and the pumping losses that would have occurred during the gas exchange process. As expected for the reasons discussed above, combusted charge trapping initially requires greater forces to compress and consequently outputs greater forces during the gas

spring expansion. However, this effect diminishes quickly and the work converges to that of fresh charge trapping.

Also evident from Figures 4.9 and 4.10 are the losses due to the initial charge trapping. These losses are a result of the extra compression during the deactivation transition cycle. Once the pressure decays inside the cylinder, which is discussed below, the work of this extra compression becomes irreversible. Therefore, this creates a minimum deactivation duration before there are net efficiency benefits from CDA operation, as the efficiency benefits must overcome the initial deactivation losses. In practice, this occurs in short duration. However, the minimum duration is dependent on the magnitude of the efficiency benefit for the given condition.

The mass and heat losses in the deactivated cylinders manifest as pressure loss. There are negligible differences in the rates of pressure decrease between implementing CDA by trapping a fresh charge and implementing CDA by trapping a combusted charge. The temporal and stroke based maximum cylinder pressure decay in Figure 4.11 illustrates this observation at 800 RPM. The initial TDC=0 corresponds to the deactivation TDC, shown as 0°CA in Figure 4.3 and Figure 4.6. Both trapping strategies produce similar pressure decay profiles. The fresh and combusted charge maximum cycle pressures for a given cylinder converge to within 0.17 MPa of each other by 7 cycles, or approximately 1 second, after the deactivation at 800 RPM. The decay rates then continue along similar trends until reaching steady-state levels. This convergence time is small relative to the typical time an engine would be in CDA operation, therefore the impact of the trapping strategy on overall performance would be negligible.

The in-cylinder pressures, including pressure decay characteristics, are consistent for repeated deactivations (results not shown). Differences in decay profiles between cylinders is attributed to ring pack and per cylinder compression ratio variation. Additionally, pressure decay rates likely have some application dependency that is not accounted for in this study. For instance, it is hypothesized that higher geometric compression ratios would lead to increased pressure loss rates after deactivation.
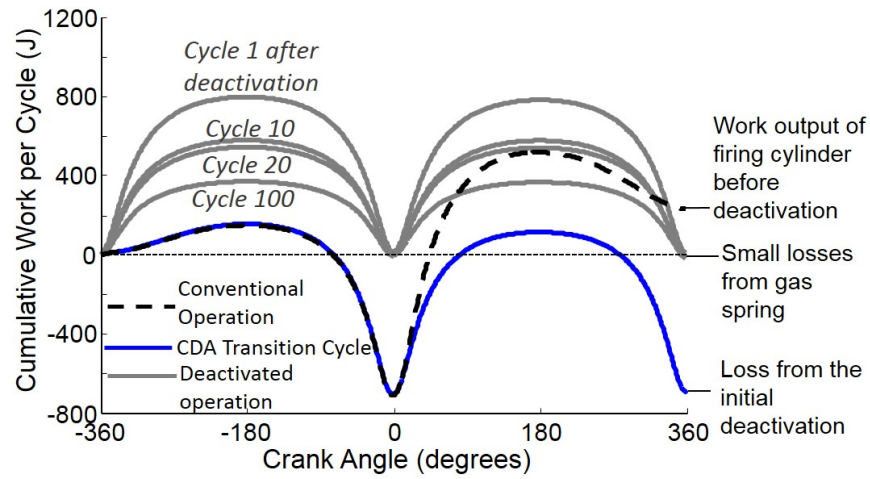
(a) Work for deactivated cylinder before and after deactivation with fresh charge trapping at 2200 RPM, 1.3 bar BMEP
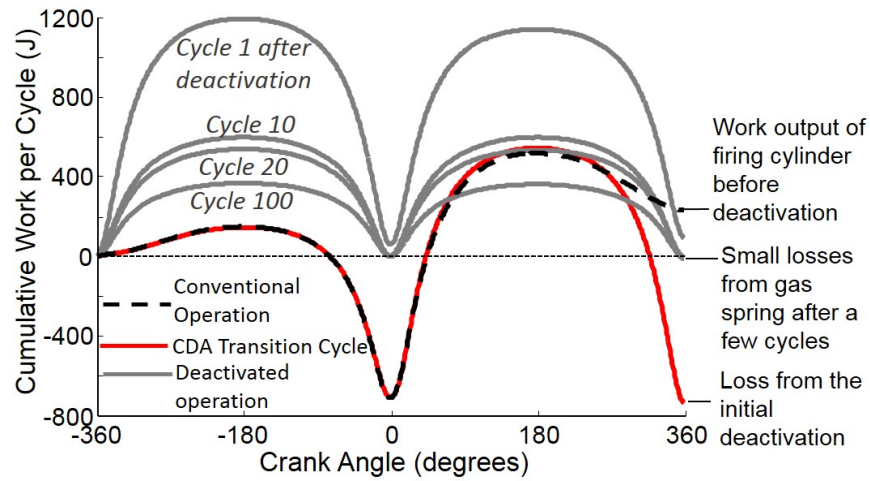
(b) Work for deactivated cylinder before and after deactivation with combusted charge trapping at 2200 RPM, 1.3 bar BMEP

Figure 4.9.   Cumulative work for a firing cycle before deactivation, the charge trapping cycle, and deactivated cycles at 2200 RPM, 1.3 bar BMEP.
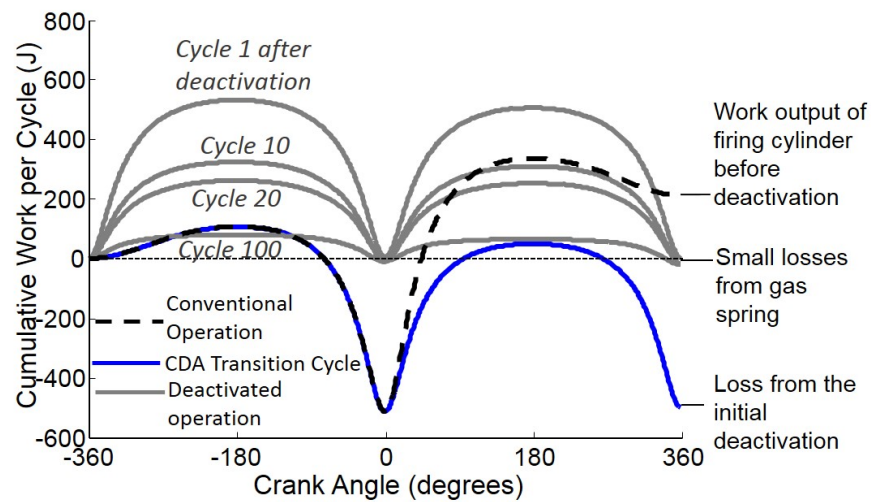
(a) Work for deactivated cylinder before and after deactivation with fresh charge trapping at 800 RPM, 1.3 bar BMEP
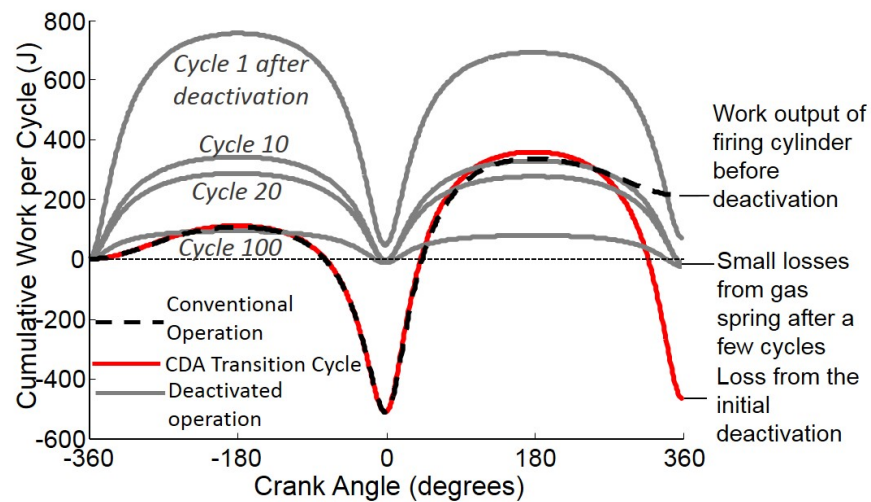
(b) Work for deactivated cylinder before and after deactivation with combusted charge trapping at 800 RPM, 1.3 bar BMEP

Figure 4.10. Cumulative work for a firing cycle before deactivation, the charge trapping cycle, and deactivated cycles at 800 RPM, 1.3 bar BMEP.
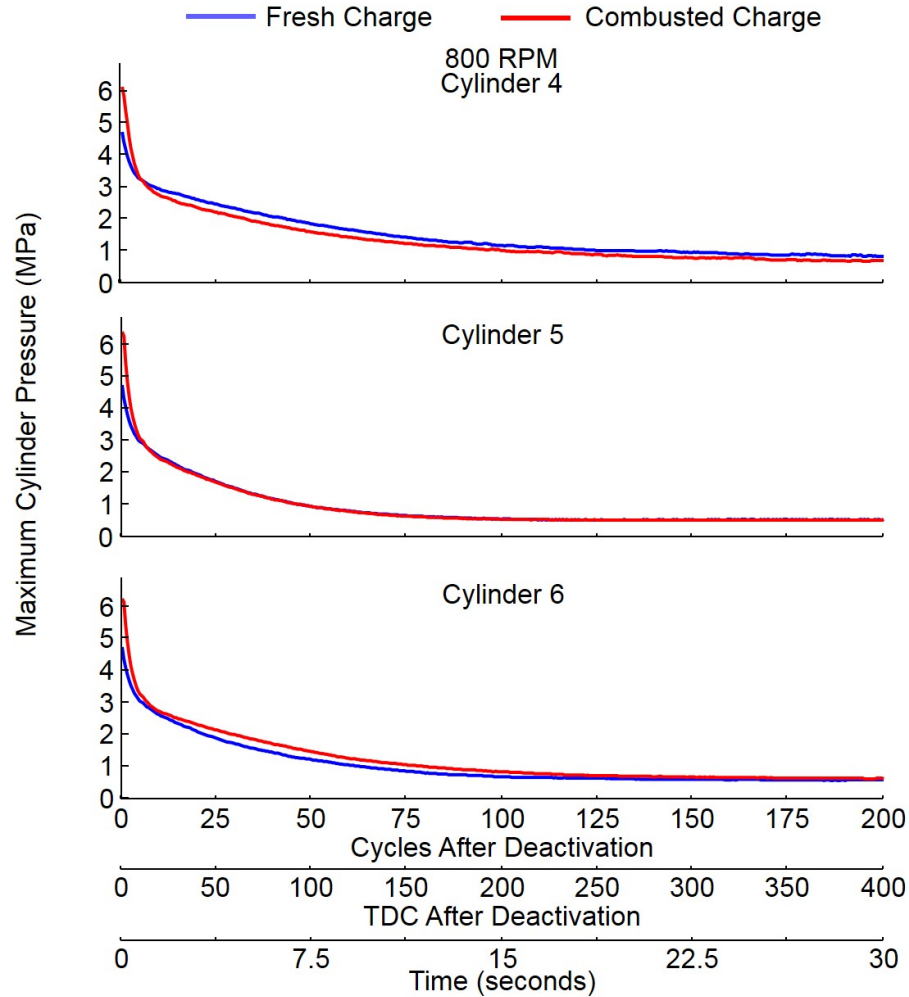
Figure 4.11. Maximum pressure for each deactivated cylinder at 800 RPM, 1.3 bar plotted on a TDC basis.

Figure 4.12 demonstrates a similar trend for the maximum pressure in a cylinder during CDA at 2200 RPM, 1.3 bar BMEP. A notable difference at this speed is the spike in pressure at TDC=1 for the combusted charge case. This characteristic was described in the previous section. The "spike" is not present for the 800 RPM case because the more advanced heat release locates the combustion closer to TDC at this operating condition. Moreover, the slower piston motion at 800 RPM allows more time for heat transfer to negate the pressure spike. It is hypothesized that heat transfer plays a large role in the pressure decay during the initial few cycles following

the deactivation due to the elevated temperatures. This initially rapid loss of cylinder pressure causes the fresh and combusted charge pressures to converge within 14 cycles, or less than 0.8 seconds, at this speed and load condition. Similar to the conclusion at 800 RPM, this convergence time is small relative to the typical time an engine is operating in CDA. This means that the impact of the trapping strategy on overall performance would be negligible.
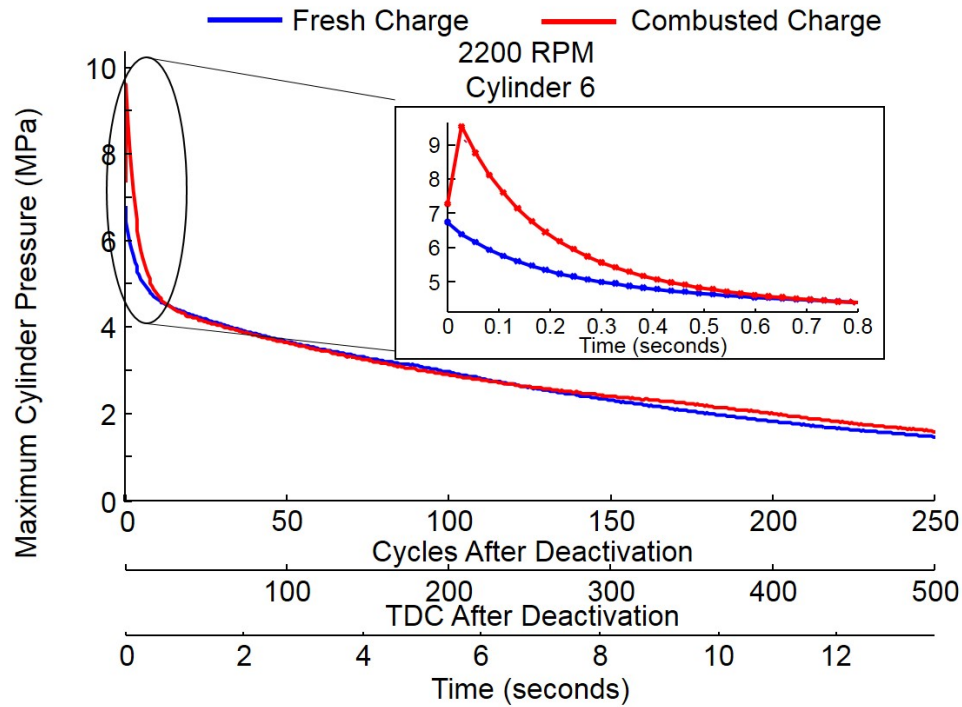
Figure 4.12. Maximum pressure for a deactivated cylinder 6 at 2200 RPM, 1.3 bar is plotted on a TDC basis.

Minimum cylinder pressure is important due to its role in oil accumulation during CDA [39, 41]. The accumulation of systematic measurement error leads to greater uncertainty in measured values of low cylinder pressures. For example, an error of 30 kPa would not significantly impact the conclusions regarding the maximum pressure values, where the magnitudes are in the MPa range. However, a 30 kPa measurement bias would distort conclusions with respect to minimum cylinder pressures given their smaller magnitudes. The minimum pressures are therefore estimated from the maxi-

mum cylinder pressures with the assumption of isentropic compression and expansion. This assumption should yield valid values for comparison of minimum cylinder pressures.

Figure 4.13 shows the calculated minimum pressure decay for the cylinders at both tested speeds after deactivation. The initial BDC=0 corresponds to the BDC at 180°CA in Figures 4.3 and 4.6. The pressure differential between the cylinder and crankcase at which oil starts to accumulate in the cylinder will vary based on ring design, however accumulation could theoretically begin once the cylinder drops below atmospheric pressure assuming the crankcase is vented to atmosphere. The fresh charge trapping strategy at 800 RPM, 1.3 bar BMEP could lead to oil accumulation from the onset of deactivation since the minimum in-cylinder pressure from the first deactivation cycle is below atmospheric pressure, as shown in Figure 4.13. The combusted charge trapped cylinders at 800 RPM, 1.3 bar BMEP drop below atmospheric pressure at the third BDC after deactivation, so there would be minimal difference in oil accumulation between the two trapping strategies. At the 2200 RPM, 1.3 bar BMEP condition, greater than atmospheric initial minimum pressures are a result of increased boost pressure at this operating condition.

The minimum pressures of both charge trapping strategies at the tested 2200 RPM condition first converge at 95 kPa less than 1 second after deactivation. Similarly, the minimum pressures of both charge trapping strategies at the 800 RPM condition reach and remain within a 7 kPa margin after 0.6 seconds of deactivation. As a result, there is minimal overall performance difference between strategies in terms of pressure decay after only a few cycles at both speeds. This indicates that the charge trapping strategy should not impact the amount of time a cylinder can be deactivated. [39] demonstrated that the engine is first fire ready after 20 minutes of CDA operation with negligible oil accumulation, therefore the viable deactivation time is on the order of minutes.
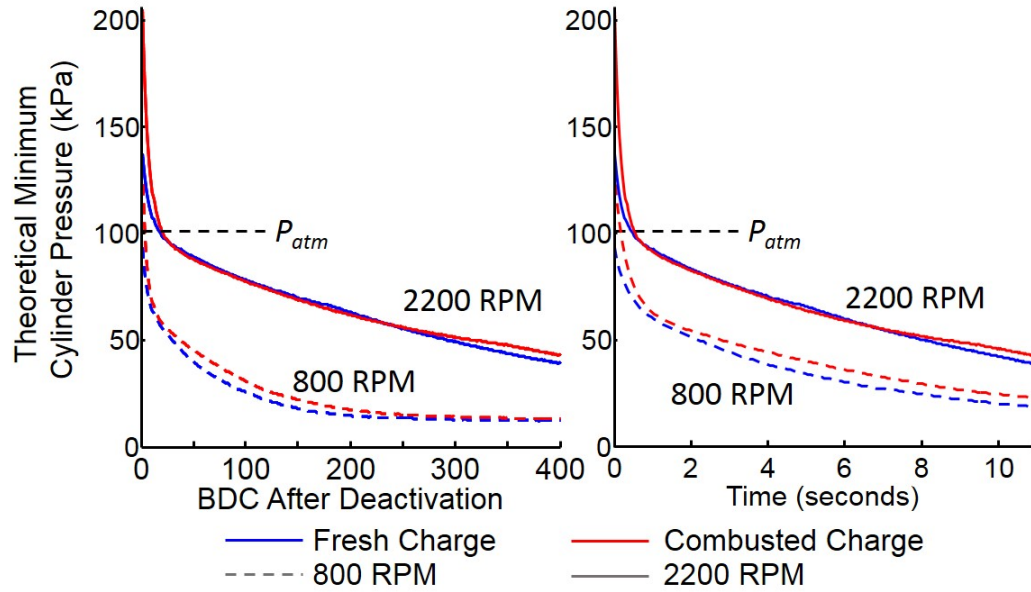
Figure 4.13. The calculated minimum cylinder pressures for a deactivated cylinder 6 at both tested speeds for each BDC and the corresponding times are shown.

4.4 Summary

Experiments were conducted to study the effects of CDA transition strategies on the in-cylinder pressures of a diesel engine. Two charge trapping strategies, fresh charge trapping and combusted charge trapping, were investigated. The implementations of the two charge trapping strategies were discussed in detail. Combusted charge trapping was demonstrated to have the potential for greater maximum cylinder pressures after the deactivation than during combustion. Conditions for this phenomenon were proposed- the recompression events after the deactivation can cause greater cylinder pressures than during, or following, the combustion event when the energy released after TDC from the final combustion event is greater than the mass and heat losses before the recompression. A pressure increase of up to 2.26 MPa was shown, however this increase could be more drastic with later heat release timings.

A deactivated cylinder acts as a gas spring during deactivation. The losses associated with this gas spring were shown to be small relative to the power output of the engine. Although the greater initial deactivation pressures associated with combusted charge trapping would theoretically prolong the loss of gas spring in the deactivated cylinder, the experimental results indicate this is not the reality. Blow-by around the piston rings and heat loss through the cylinder walls and pistons result in rapidly decaying in-cylinder pressures that cause the cylinder pressures for fresh and combusted charge trapping to converge as quickly as in 7 cycles, less than 1 second, after deactivation at the curb idle condition 800 RPM, 1.3 bar BMEP. The cylinder pressures converge as quickly as in 14 cycles, or less than 0.8 seconds, after deactivation at 2200 RPM, 1.3 bar BMEP. Hence, the charge trapping strategy should not impact the amount of time that a cylinder can be deactivated. Additionally, the time durations for pressure convergence are short relative to the typical time spent in CDA operation. Therefore, it can be concluded that the choice of charge trapping strategy will have negligible effect on overall engine performance during CDA.

5. CHARACTERIZATION OF NVH DURING CYLINDER DEACTIVATION

5.1 Motivation

NVH is an important consideration for any technology before it is deemed viable for the market, and the engine is a prominent NVH source in the vehicle. The NVH effects of CDA are of particular relevance because the engine is essentially transforming cylinder configurations in real-time. As discussed in Section 1.3.3, CDA has been in production gasoline engines with acceptable NVH for a number of years. However, the operating speeds of gasoline engines during CDA are higher than diesel engines during CDA, making diesel CDA a unique challenge that must be characterized.

Torsional vibrations refer to the axial rotational vibrations at the output of the engine. These vibrations get transmitted through the rest of the drivetrain systems. A concern is that implementing CDA will result in frequency content lower than previously seen with conventional operation because many drivetrains and vehicle bodies currently have resonance at lower frequencies. Lower frequency inputs to the drivetrain also result in more gear rattle than usual due to the gears becoming unmeshed between forcing inputs. This lower frequency content may prove acceptable, however, if the forcing magnitudes are small enough. Therefore, it is important to characterize the low-frequency effects of CDA from a torsional vibrations standpoint. These torsional vibration effects are discussed in Section 5.2.

While torsional vibrations are of great importance in engines, there are other significant axes of vibration as well. These are the vibrations from the translational movements of the engine block in the Cartesian directions caused by imbalances. These vibrations, often referred to as linear vibrations and sometimes longitudinal vibrations, are transmitted through the engine mounts and frame to the driver via the seat and steering wheel and to the other vehicle components. Since CDA dynamically

alters the geometric and firing balance of the engine, it is hypothesized that CDA will have effects on linear vibrations that must be characterized. Linear vibration effects of CDA are explored in Section 5.3.

Acoustic noise is another important NVH aspect due to consumer comfort and perceived product quality. Consumer comfort means not only to safe noise levels, but also lower annoyance levels. CDA must be safe and comfortable for the driver in order to be an accepted technology. However, even allowable noise levels can still harm a product reputation based on the perceived quality, as drivers are accustomed to a particular type of noise coming from their engines. Section 5.4 characterizes the noise content of CDA via its effects on frequency content and overall sound quality levels.

The NVH results discussed in this chapter are from an engine in an engine dynamometer test cell. Ultimately, in-vehicle NVH from the engine will depend not only on the engine output, but also on the rest of the vehicle. The drivetrain will attenuate or amplify the torsional vibrations depending on its dynamics. The mounting setup, vehicle frame, seat, and even driver geometry will affect the perceived linear vibrations from the driver. The hard-walled test cell will also produce different acoustic results than in a vehicle. All of these factors acknowledged, it is still useful to characterize the NVH in the engine test cell with the knowledge that, ultimately, an assessment needs to be done in-vehicle. The final section of this chapter describes an alternate CDA strategy, dynamic cylinder activation (DCA), that may provide a route to overcome restrictions of fixed CDA NVH.

5.2 Torsional Vibration Effects of CDA

5.2.1 Introduction and Methodology

Torsional vibrations result from rotational fluctuations along the crankshaft. Torsional vibrations are always present in reciprocating internal combustion engines. The torque/load of an engine fluctuates very rapidly between high (during expan-

sion strokes) and low (during compression stroke) through combustion and the basic piston-crank dynamic relationship [68]. The magnitudes of the peaks and mean torque vary with loads. An example of the torque fluctuations from the engine measured at a dynamometer is shown in Figure 5.1. During engine testing, a low-pass filter is applied to give a constant torque reading. Similarly, on a vehicle the driveline attenuates these torque deviations to finally output a seemingly constant torque at the wheels. However, the intermediate portions of the driveline still receive fluctuations, which can cause damage and undesired behavior if not considered. Because the torque transmitted through the driveline is equal to the product of component inertia and angular acceleration, torsional vibrations are characterized by examining the angular acceleration at the engine flywheel.
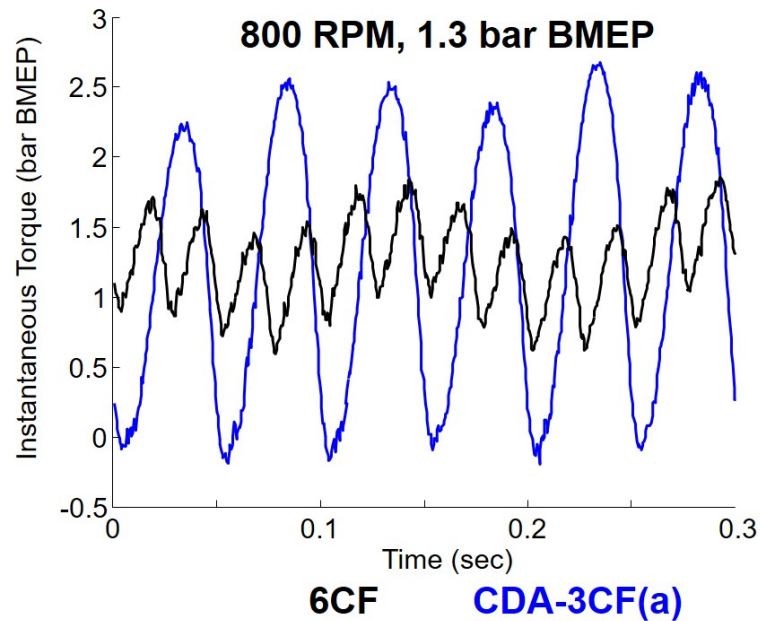
Figure 5.1. Instantaneous torque measured at the dynamometer for 6CF and CDA-3CF during curb idle at 800 RPM.

The firing frequency, the primary frequency at which the torque and angular acceleration fluctuations occur, is directly proportional to engine speed by Equation (5.1) for a periodically firing engine (this trend changes during some CDA operations, as

discussed below). For example, the firing frequency of a 6-cylinder, 4-stroke engine operating at 800 RPM should be 40 Hz. This can be verified by examining the experimentally-obtained angular acceleration spectrum of the engine shown in Figure 5.2. This plot type, which will be analyzed throughout this and the coming sections, represents the angular acceleration deviation from the mean at each frequency. The data is processed using the FFT function in Matlab with a Hanning window applied to reduce spectral leakage. Note that in this example, the peak angular acceleration deviation does appear at 40 Hz, with higher order harmonics at integer multiples of this frequency. It is also common to refer to the frequency content location normalized to engine speed using engine orders. Engine orders can be thought of as the number of times an event occurs during one engine revolution, or alternatively the nth order events are occurring n times per engine revolution. The first order corresponds to the rotational frequency of the engine. The increasing orders are then multiples of this rotational frequency. Additional information on this nomenclature can be found in [68]. For this 6-cylinder, 4-stroke engine, firing events occur three times every revolution. Therefore, the firing frequency is always third order during conventional operation. As will be discussed below, CDA changes the firing frequency to other engine orders.

$$Freq_{firing}(Hz) = \frac{N_{cylinders}RPM}{60(sec/min)C} \tag{5.1}$$

where $N_{cylinder}$ is the number of firing cylinders, RPM is the engine speed, and C is 1 for a two-stroke engine and 2 for a four-stroke engine (such as the one analyzed here).

An experimental characterization of torsional vibrations transmitted at the rear flywheel was conducted. Instantaneous velocity measurements at the rear flywheel are taken using a Cherry GS100502 Hall effect sensor positioned on the flywheel housing. Gear teeth on the outside of the flywheel create pulses as it rotates by the Hall effect sensor, which is acquired by a Rotec data acquisition system with a time stamp. The time differential between tooth crossing can then be used to calculate

the instantaneous rotational velocity of the flywheel. There are 173 gear teeth on the flywheel of the tested engine, making the resolution of this measurement 2.08 CAD. The additional measurement of time allows for instantaneous rotational velocity to be calculated. The forces transmitted to the drivetrain are proportional to the angular acceleration of the flywheel, so this velocity signal is differentiated to give the angular acceleration. This angular acceleration is used to characterize the torsional vibration content.

The test plan for the torsional characterization of CDA consists of loaded idle steady-state testing at various idle speeds, speed sweeps at constant loads, and load sweeps at constant speeds. Load was maintained at 1.3 bar BMEP for the load idle tests, representing curb idle torque for this engine. The idle speeds tested were 700 RPM and 800 RPM. Speed sweeps were performed by accelerating the engine from 700 RPM to 2200 RPM at 15 RPM/sec while maintaining constant loads of motoring, 0 bar, 1.3 bar, 2 bar, 3 bar, and 3.75 bar. Similarly, torque sweeps were performed by maintaining constant speeds of 800 RPM and 1200 RPM while increasing torque from motoring at a rate of 0.13 bar/sec BMEP. All tests were conducted in conventional 6 cylinder operation and the various CDA modes shown in Figure 5.3.
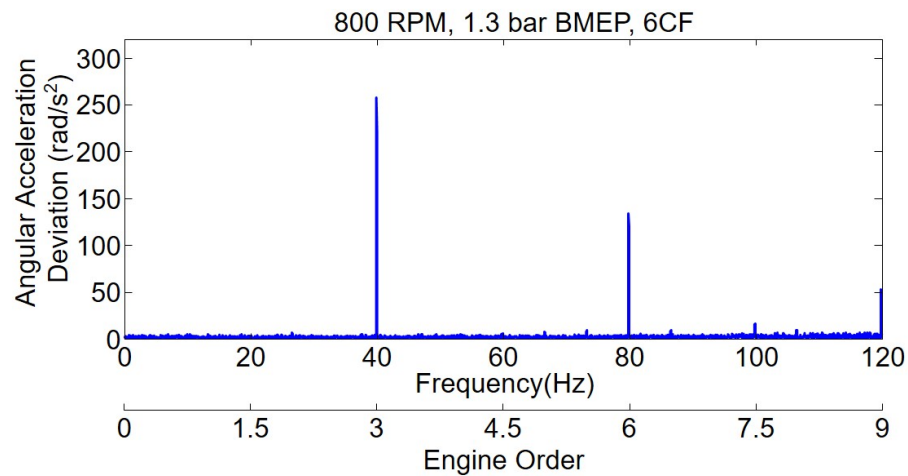
Figure 5.2. Angular acceleration variation from the mean shown as frequency spectrum for conventional operation at idle.
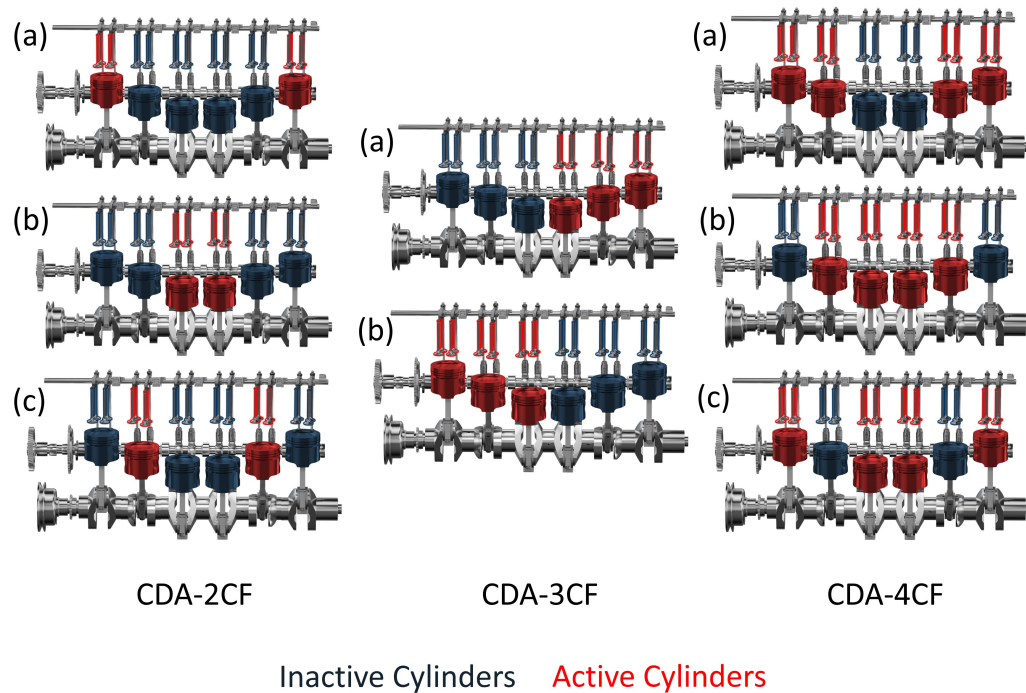
Figure 5.3. Fixed CDA configurations examined during the vibration study.

While it is notable that the torsional characteristics of conventional 6CF operation are considered acceptable, as this engine is currently in production, this is not equivalent to the threshold for acceptability. Torsional acceptability of the engine is ultimately dependent upon the frequency response of the given vehicle driveline.

5.2.2 Loaded Idle Results

Figure 5.4 shows the angular acceleration spectrums for conventional 6CF operation and various CDA modes. The firing frequency of each mode is indicated by the frequency location of the peak magnitudes in the plots. When cylinders are deactivated, the engine is firing less often. Therefore, it is somewhat intuitive that decreasing the number of active cylinders results in a decrease in firing frequency. For instance, this six cylinder engine operating in 6CF at 800 RPM will have a third order (40 Hz) firing frequency because combustion events occur three times per en-

gine revolution. If that engine deactivated half of its cylinders, the maximum firing frequency would now be 1.5 order (20 Hz), or half that of conventional operation. This is consistent with CDA-3CF and would be equivalent, with respect to frequency content, to conventional 6CF operation at 400 RPM. CDA modes also exhibit more torsional harmonics due to the lower primary firing frequency. This is important to consider because any harmonic could also excite a resonant frequency in the driveline.

Referencing Figure 5.4, CDA-4CF and CDA-2CF have the same firing frequency, though with varying magnitudes. This is because the firing orders for these modes are inverses of each other. CDA-4CF has the firing sequence *nonfire-fire-fire-nonfire-fire-fire* and CDA-2CF has the sequence *nonfire-nonfire-fire-nonfire-nonfire-fire*. Note that each of these patterns have a period equal to three events. Therefore, the firing frequency for both of these CDA modes is first engine order. While this correlates with the traditional formula in Equation (5.1) for CDA-2CF, it does not for CDA-4CF. This is because CDA-2CF has symmetry with respect to each firing cylinder event, an assumption of the original formula, where a firing occurs once per engine revolution. CDA-4CF does not have this symmetry. The fundamental firing period repeats itself every revolution for both CDA-2CF and CDA-4CF, giving the same frequency content locations.

The dynamometer driveline has a resonant frequency of 5.4 Hz, therefore all operations are well above resonance. This was a design parameter for the test cell. However, a non-standard CDA firing sequence would produce frequency content close to this limit. A non-standard CDA firing sequence in this context refers to any non-standard CDA firing configuration that will inherently be 0.5 engine order for the firing frequency, meaning that its firing order takes two full engine revolutions to repeat. At 800 RPM, a non-standard CDA operation would have a firing frequency of 6.67 Hz. Peak resonance would occur at 648 RPM. It is common to set a limit at $\sqrt{2}$ time the resonance frequency, meaning a lower limit for non-standard CDA operation would be 916 RPM for this system. Non-standard firing CDA is explored experimentally at higher engine speeds during the speed sweep section of this study.

Deactivating cylinders also requires the remaining firing cylinders to proportionally increase their fueling, and therefore combustion event magnitudes, in order to maintain torque. This results in larger torque-producing combustion events being transferred to the crankshaft, though less frequently. The magnitude of angular acceleration at the firing frequency increases with decreasing number of active cylinders due to load per firing cylinder being greater for CDA to maintain equal torque to 6CF operation. For instance, CDA-2CF and CDA-4CF have peaks at the first engine order, however CDA-2CF has a larger magnitude due to larger combustion events per firing cylinder.

Angular acceleration spectrums are included at 700 RPM in Figure 5.5 for reference, however more detailed effects of speed variation are located in the next section. The trends, however, are consistent with those described for the 800 RPM idle case above. The frequency content for all modes are still engine order-dependent. However, the actual frequency content is at slightly lower frequency due to the lower engine speed. For instance, third engine order at 700 RPM is 35 Hz, whereas third engine order at 800 RPM is 40 Hz. This is consistent with the shift in the third engine order peaks in Figure 5.5.

Magnitudes of the content are similar to 800 RPM with the exception of CDA-2CF, however this is due to experimental testing issues. CDA-2CF artificially excited the low-speed governor, even with a reduced low-speed governor setting. This caused an increase in torque at 700 RPM.
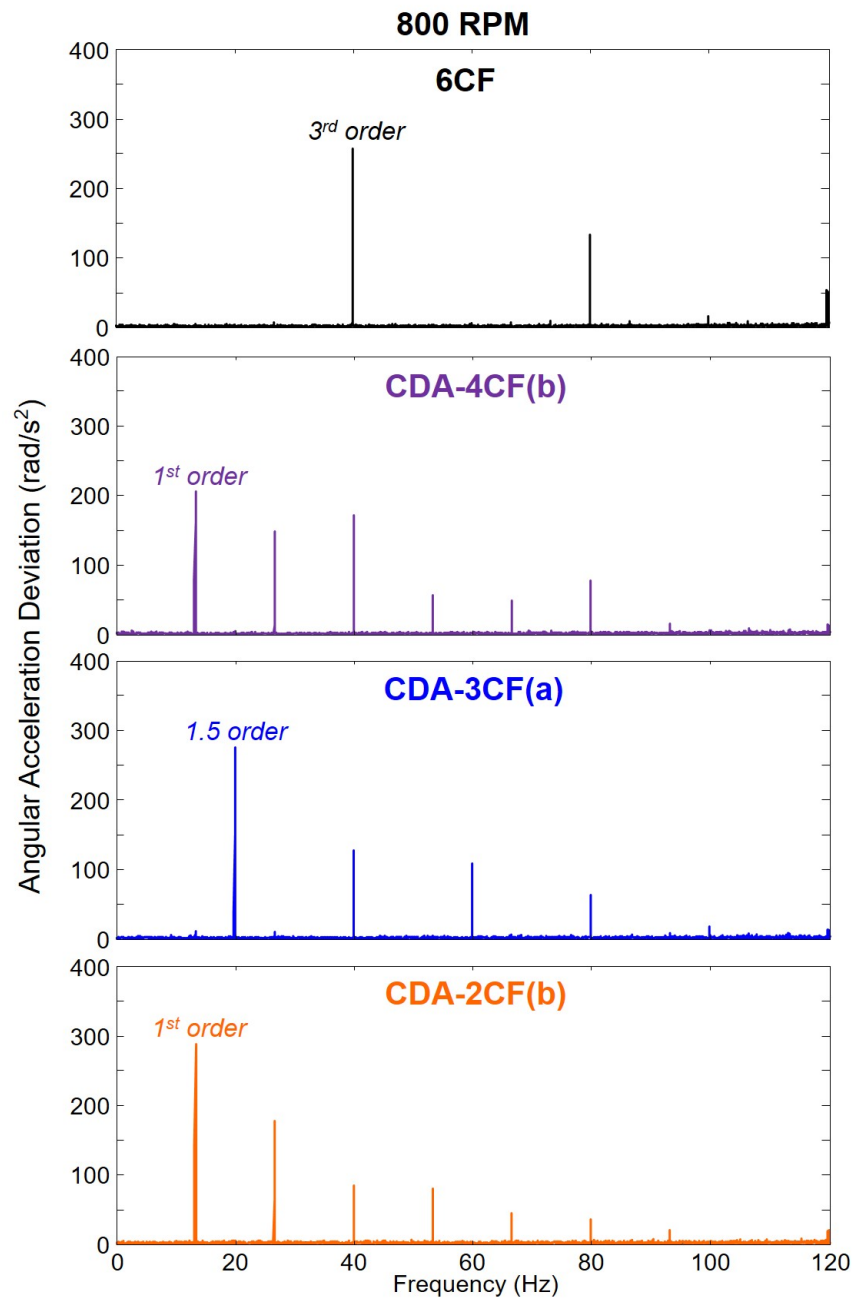
Figure 5.4. Angular acceleration frequency analysis for loaded idle at 800 RPM conventional and CDA operations.
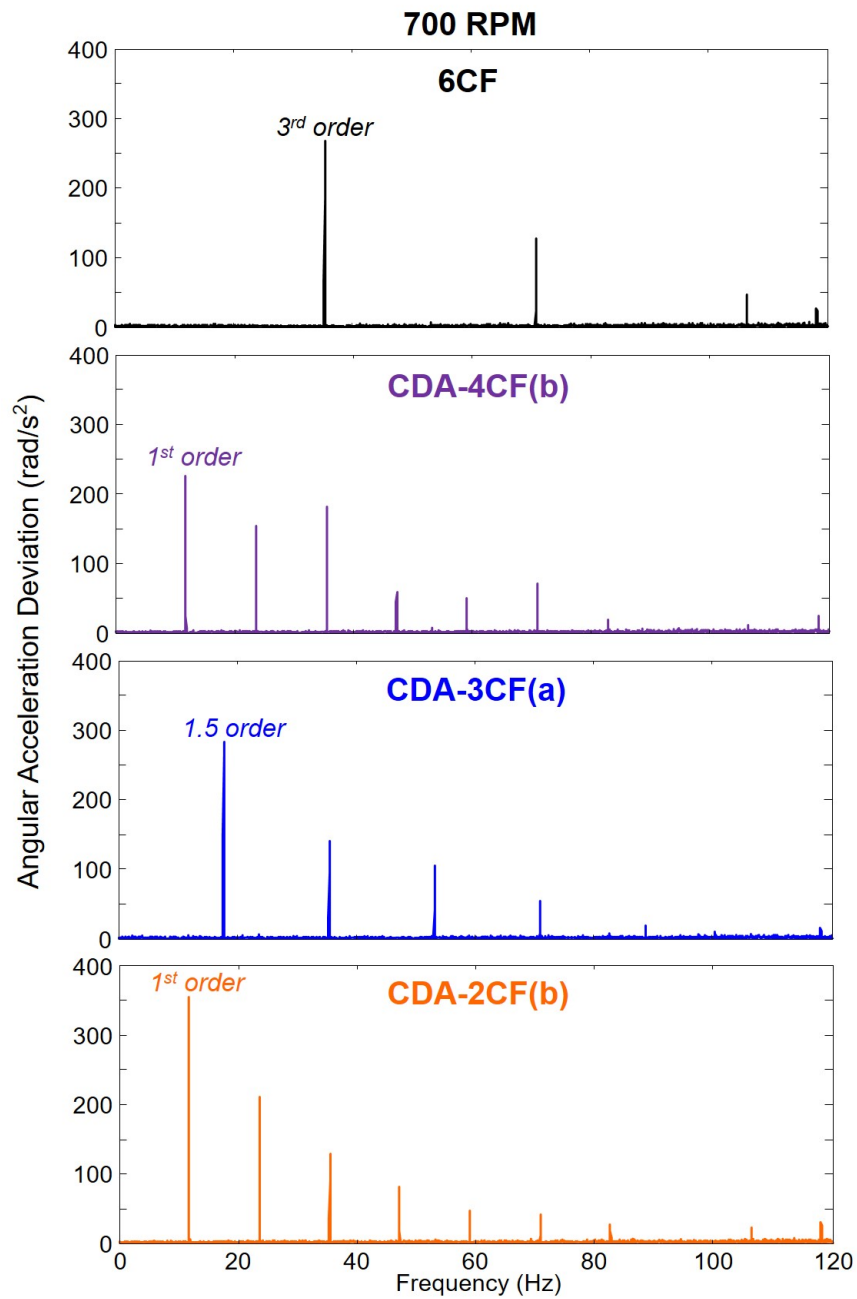
Figure 5.5.   Angular acceleration frequency analysis for loaded idle at 700 RPM conventional and CDA operations.

5.2.3 Speed Sweep Results

The speed sweep tests result in the torsional vibrations variation over the speed range shown in Figure 5.6. These plots depict order cuts for the speed sweeps. An order cut is the magnitude, in this case the magnitude of angular acceleration deviation, at a given order. These plots show order cut for the firing order of each CDA mode and conventional 6CF operation. CDA-2CF is omitted from the 3 bar BMEP and 3.75 bar BMEP conditions due to inability to reach those loads with two cylinders active.

Literature suggests that operations with angular acceleration magnitudes lower than 500 rad/s^2 at all frequencies are typically acceptable for torsional vibrations [66]. CDA is shown to be below this threshold for all speeds and loads tested. However, ultimately, the frequency response of the drivetrain must also be considered.

The magnitude of the angular acceleration deviation stays relatively constant over the speed sweep for a given load for the CDA modes. However, the magnitude decreases during 6CF mode. The torsional magnitudes increase with increasing load, as expected due to the greater impact of the combustion at the firing engine order.

Speed sweeps also can be thought of as firing frequency sweeps over the range of firing frequencies that the engine outputs. CDA changes this range, as shown by the order cut of the 1.3 bar BMEP speed sweep in Figure 5.7. CDA extends the range of firing frequencies lower than conventional operations, as discussed in the previous section. The firing frequencies for CDA reach 11.6 Hz at 700 RPM during the speed sweep, whereas conventional operation at 700 RPM has a firing frequency of 35 Hz. Similarly, the upper range of firing frequencies for CDA is reduced by an even larger amount. Conventional operation has firing frequencies as high as 110 Hz at 2200 RPM, however the 2200 RPM firing frequency for CDA is 55 Hz for CDA-3CF and 36.6 Hz for CDA-4CF and CDA-2CF.

The CDA configurations shown in Figure 5.3 have equivalent firing frequencies for each mode. For instance, CDA-4CF(a), CDA-4CF(b), and CDA-4CF(c) have

the same firing pattern and firing frequency, however the geometric configurations of the firing cylinders vary. It was previously unknown whether the magnitude of torsional vibration varies depending on this firing configuration. Figure 5.8 shows the configurations with equivalent firing frequencies have little to no effect on the magnitude of torsional vibrations. For this reason, the results in this chapter primarily focus on CDA-4CF(b), CDA-3CF(a), and CDA-2CF(b) as the standards for each CDA mode.

Also notable in Figure 5.8 is the slight, but distinct, discontinuity in torsional amplitude for the CDA-4CF and CDA-2CF modes at approximately 1050 RPM. This is due to these modes passing through a linear resonance at this speed, which will be discussed in more detail in the next section. This shows some apparent coupling between the linear and torsional vibrations or measurements.
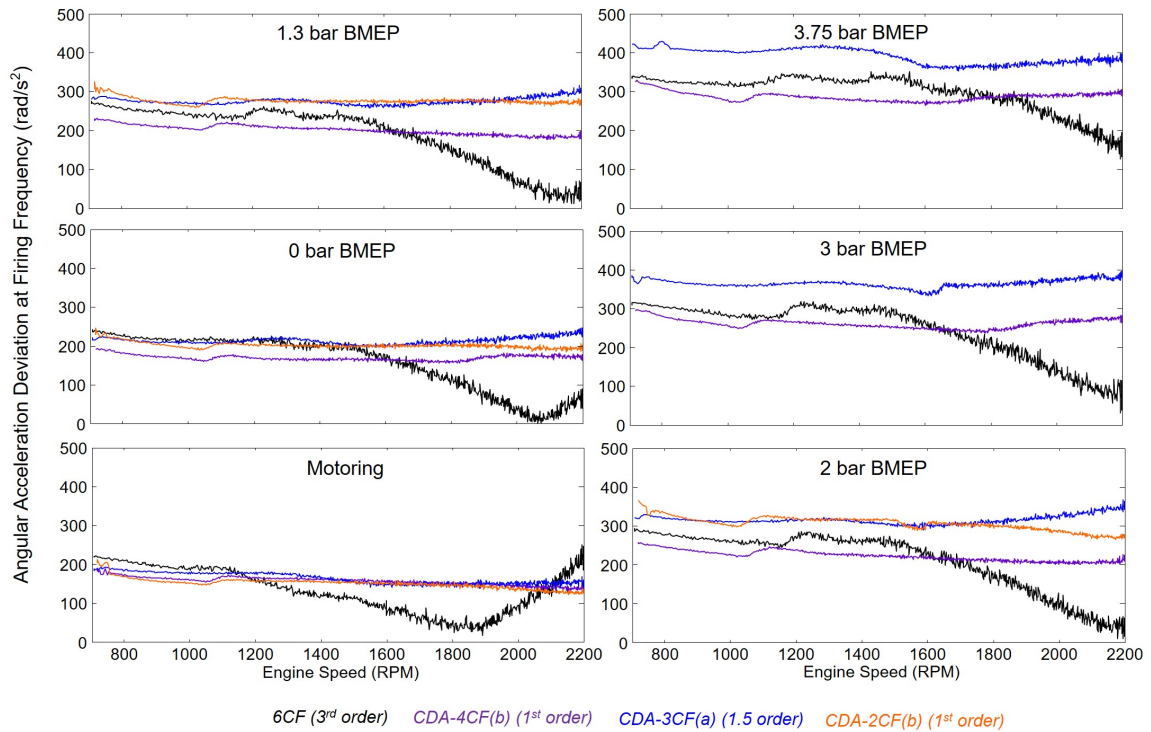
Figure 5.6. Order cut torsional analysis for the speed sweeps.
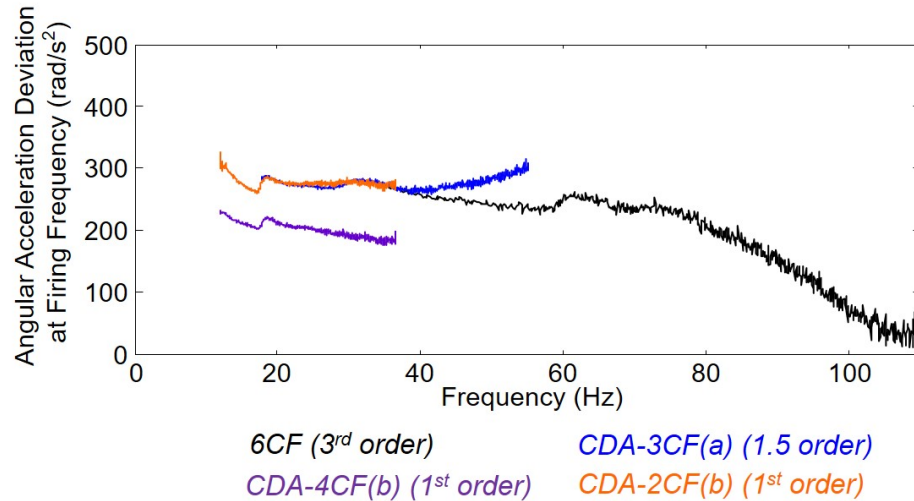
Figure 5.7. Fundamental order angular acceleration magnitudes plotted against frequency for the speed sweeps.

The configurations in Figure 5.3 were tested because these represent the maximum firing frequencies for a given CDA mode. This is thought to be preferable in order to maintain as high a firing frequency as possible to ease/enable drivetrain design and avoid low-frequency regions of particular human body resonance. However, two additional speed sweeps with 'non-standard' firing orders were conducted to examine torsional vibrations for these firing orders. Any non-standard fixed CDA firing configuration will inherently be 0.5 engine order for the firing frequency, meaning that its firing order takes two full engine revolutions to repeat. This is equivalent to the firing frequency of deactivating only one cylinder or five cylinders. As shown in Figure 5.9, the magnitude of angular acceleration for the firing frequency is lower than the magnitudes of equivalent CDA modes. While this may seem beneficial at first, it is important to reiterate that the frequency associated with these non-standard configurations is much lower than standard fixed CDA configurations, reaching as low as 5.8 Hz at 700 RPM, which could be problematic. For example, the speed sweeps were not performed during this study below 1200 RPM to avoid the engine-dynamometer driveline resonance of 5.4 Hz. Additionally, non-standard CDA also has content at

more frequencies due to the harmonics. This contributes to the lower primary firing frequency torsional magnitude to maintain equivalent load but also makes avoiding resonances difficult.
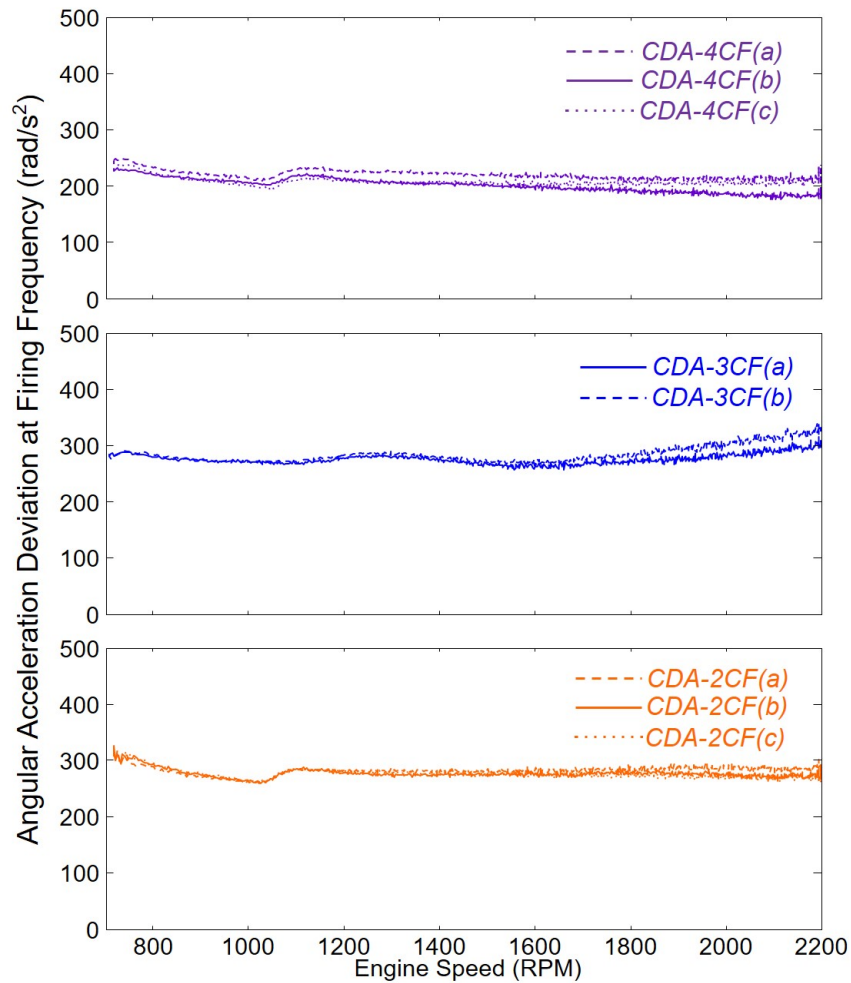
Figure 5.8.   Comparison of torsional vibration order cuts for each CDA configuration tested.
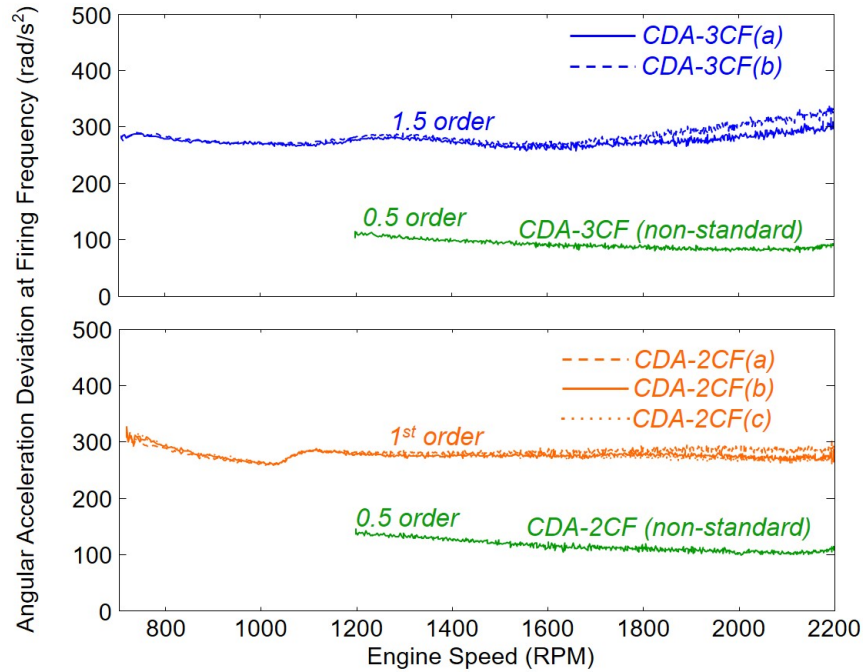
Figure 5.9.   Comparison of standard and non-standard fixed CDA firing configurations.

5.2.4   Load Sweep Results

The order cuts for the load sweep results at 800 RPM and 1200 RPM are shown in Figures 5.10 and 5.11, respectively. All modes were taken to their respective motoring torques. The achievable motoring load decreases with greater number of cylinders deactivated due to the lower pumping work.

There is a monotonic increase in the magnitude of angular acceleration at the firing frequency as the load increases, as expected due to the larger combustion events. Similarly, the slopes of the trend lines increase with greater number of cylinders deactivated and proportionally larger combustion events. For instance, CDA-2CF has a steeper rate of change of angular acceleration per increase in load than CDA-3CF because each cylinder, which is firing at the firing frequency depicted, must produce a proportionally greater load for CDA-2CF.
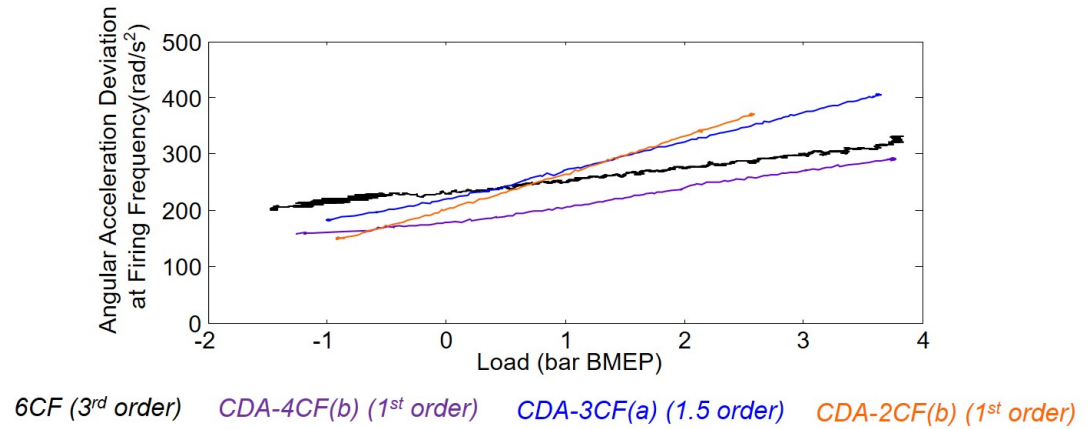
Figure 5.10. Order cut analysis for load sweeps at 800 RPM.
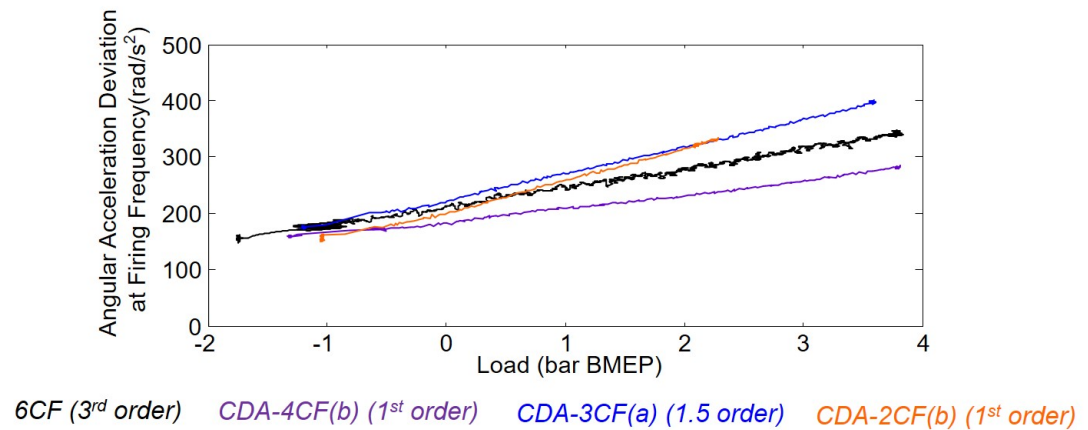
Figure 5.11. Order cut analysis for load sweeps at 1200 RPM.

5.2.5 Summary of CDA Torsional Vibration Characterization

The torsional vibrations effects of CDA are characterized across the engine speed range for a variety of loads. The analysis of this section demonstrates that CDA affects torsional vibrations by decreasing the fundamental frequency of the firing events and causing variation in the magnitude of angular acceleration deviation at a

given rotational speed and load. CDA configurations can create firing patterns that do not follow typical firing frequency calculation. One must consider the actual firing pattern and analyze for periodicity. The range of forcing frequencies from the engine is reduced during CDA, however the lower range limit is lowered. This means that CDA at low speeds can excite driveline frequencies that were previously only excited briefly during starting and shutdown of the engine.

The magnitudes of torsional vibrations can increase with reduced number of active cylinders, especially during increased loads. Literature suggests that operations with angular acceleration magnitudes lower than 500 rad/s^2 at all frequencies are typically acceptable for torsional vibrations [66]. CDA was shown to be below this threshold for all speeds and loads tested. However, ultimately, the frequency response of the drivetrain must also be considered. For example, the testbed used for these results has a driveline that was specifically designed for CDA applications by specifying a driveshaft with a lower resonant frequency. A driveshaft with rubber couplings and prescribed dimensions creates a driveline resonant frequency of 5.4 Hz, well below the frequency range of the standard CDA modes in Figure 5.7. A non-standard CDA at idle, for instance, could not be run on this driveline due to the resonance. A vehicle application of CDA would likely also require driveline-specific design and operating mode constraints.

5.3   Linear Vibration Effects of CDA

5.3.1   Introduction and Methodology

Linear vibrations refer to the translational movement of the engine block in the Cartesian directions. These vibrations, sometimes called longitudinal vibrations, are caused by imbalances in the rotating engine and are transmitted to the rest of the vehicle through the engine mounts. The driver receives these vibrations through the seat rail, steering wheel, and pedals. Since CDA effectively alters the balance of the engine, it is important to understand these effects on linear vibrations to

create a more complete vibration characterization of CDA. Linear vibration data was acquired parallel to the torsional vibration data discussed in the previous section using three PCB Piezotronics A33 triaxial accelerometers installed on the engine block. The mounting positions were determined in collaboration with industry partners and are shown in Figure 5.12. The mounting configuration of the engine in the test cell contributes to the resultant vibration levels, so it is diagrammed in Figure 5.13 alongside a coordinate diagram of the accelerometers. From a driver's viewpoint, the X-direction is fore-aft/longitudinal, the Y-direction is vertical, and the Z-direction is lateral. Accelerometer data was acquired by a Rotec DAQ system with a 12.5 kHz sampling rate. A low-pass Butterworth filter with bandwidth of 2 kHz was applied to attenuate high-frequency content for analysis. This is a useful frequency range, especially for idle analysis, per reference [69]. Thus, signal root mean square (RMS) values shown are the RMS of the content less than 2 kHz. Similar to the torsional vibration analysis, spectrum and order cut comparisons of linear vibrations for CDA and conventional operation are explored. These order cuts are expressed as root sum square (RSS) of the three axes at the given accelerometer location.

Similar testing should be performed in-vehicle for production scenarios, so these tests serve as a comparative study. The conventional 6CF operation is in production and therefore serves as a point of reference. However, it is important to note that this is not equivalent to 6CF serving as the threshold for acceptance.
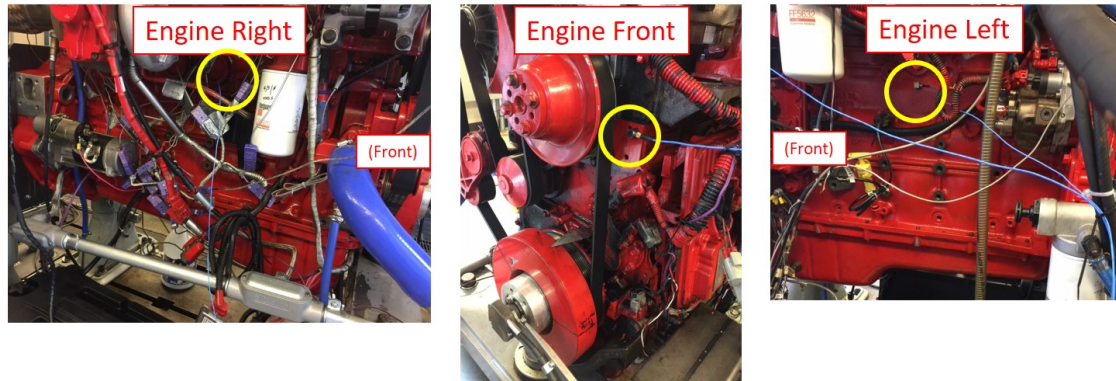
Figure 5.12.   Photographs of the accelerometers mounted to the engine block.
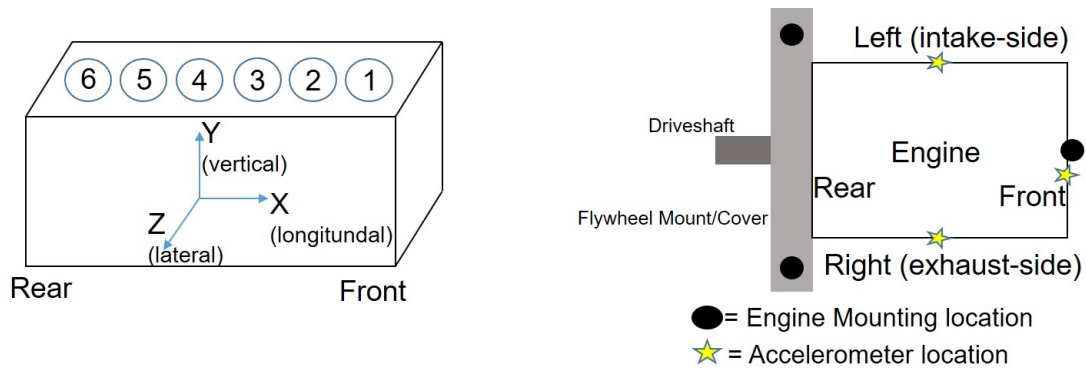
Figure 5.13.   Diagrams of accelerometer mounting locations and the coordinate system used to describe the linear vibration results.

5.3.2   Loaded Idle Results

RMS accelerations are used to characterize and compare the vibration levels in each direction for each accelerometer location. Figure 5.14 shows the resulting RMS values for the 800 RPM loaded idle tests. CDA has consistently lower RMS linear vibrations than 6CF operation at this condition with the exception of the front Z case, where the mount resonance causes increased lateral vibrations for CDA-3CF. This resonance effect will be discussed more below. CDA-2CF and CDA-4CF show consistently reduced linear vibrations compared to 6CF operation.

In general, the X-direction has the lowest RMS accelerations due to the majority of the crank-slider motions causing primarily vertical and lateral block motion. CDA-3CF has the highest vertical motion of the CDA modes. This was expected due to the physical asymmetry that results from the deactivation configuration for CDA-3CF. Vibration levels were similar for CDA-2CF and CDA-4CF, with both modes having lower vibration levels than CDA-3CF. This trend aligns with visual observations during engine testing.

Visual observations also align well with the order cut linear acceleration values shown in Figure 5.15, where CDA-3CF shows elevated vibrations for all accelerometer locations and directions. These plots are equivalent to taking the magnitude of an FFT at the fundamental frequency of the given mode. CDA-2CF and CDA-4CF have lower linear accelerations than 6CF in the longitudinal and vertical directions, however they are higher in the lateral direction. Trends could also change with higher loads, as the larger combustion events cause greater asymmetry.

The vibration levels for the tested active cylinder configurations at a given CDA mode vary slightly between configuration. These variations are shown in the RMS linear accelerations in Figures 5.16 to 5.18. Some of the variations are intuitive. Based on the layout of active and inactive cylinders for CDA-2CF and CDA-4CF, it would be expected that there would be less fore-aft rocking as the active cylinders move closer towards the center of the engine. This manifests as reducing vertical vibration at the front accelerometer location for CDA-2CF(b) than CDA-2CF(c) than CDA-2CF(a). A similar effect occurs for CDA-4CF. CDA-3CF has block asymmetry, with the front half of the engine cylinders active for CDA-3CF(a) and the rear half of the cylinders active for CDA-3CF(b). However, there is also mounting asymmetry in the test setup, as described earlier. This causes reduced vertical vibration at the front accelerometer when the rear bank of cylinders.
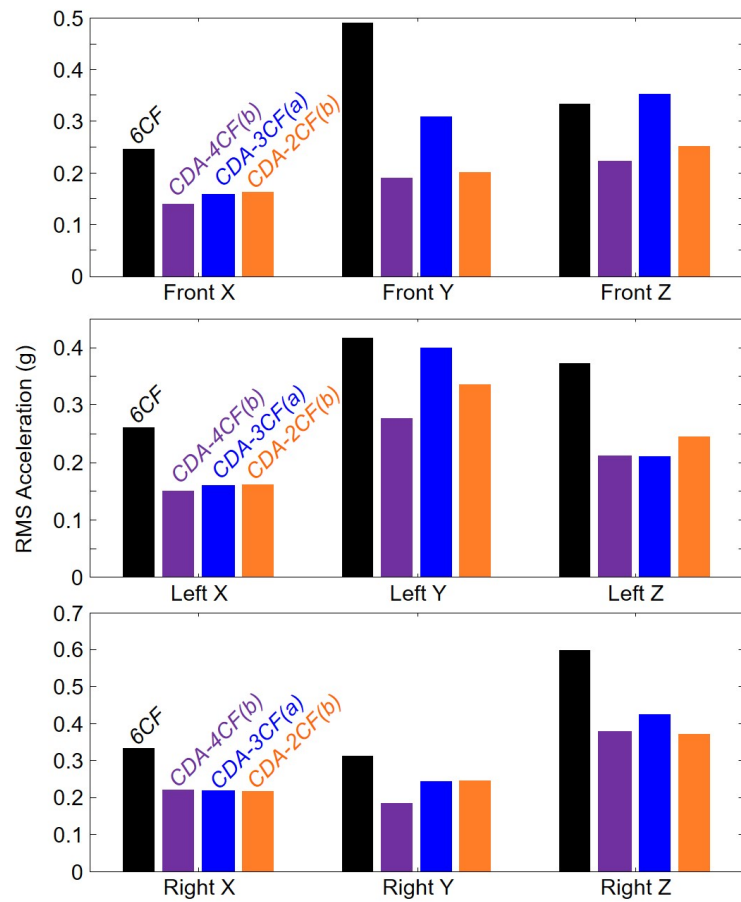
Figure 5.14. RMS linear accelerations for the CDA modes and 6CF operation at 800 RPM, 1.3 bar BMEP loaded idle.
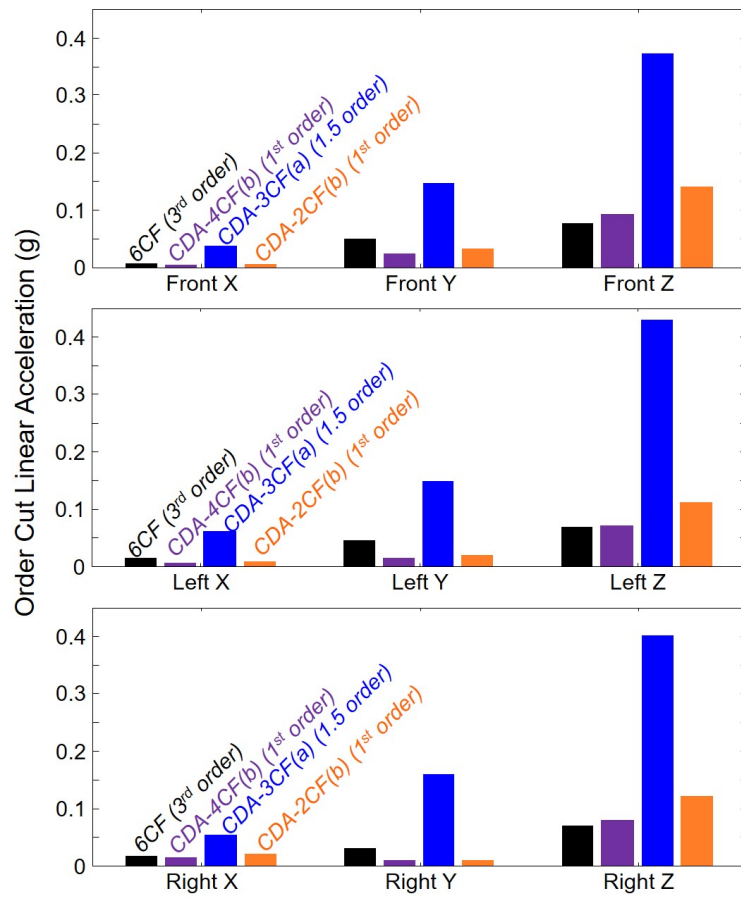
Figure 5.15.   Linear acceleration order cut comparisons for CDA modes and 6CF operation at 800 RPM, 1.3 bar BMEP loaded idle.
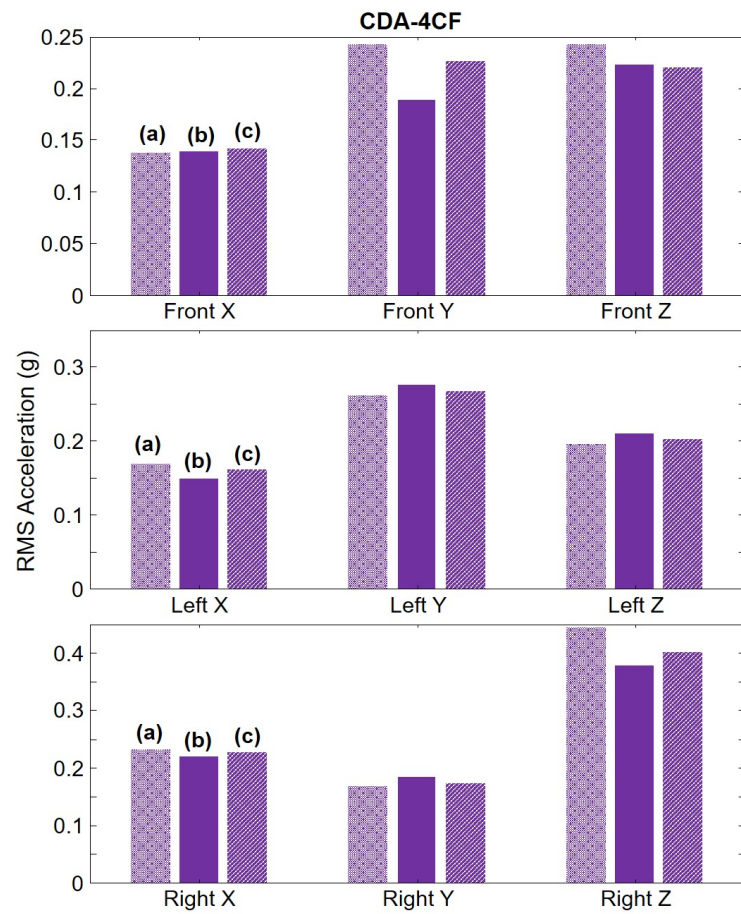
Figure 5.16. RMS linear accelerations for the tested CDA-4CF configurations at 800 RPM, 1.3 bar BMEP loaded idle.
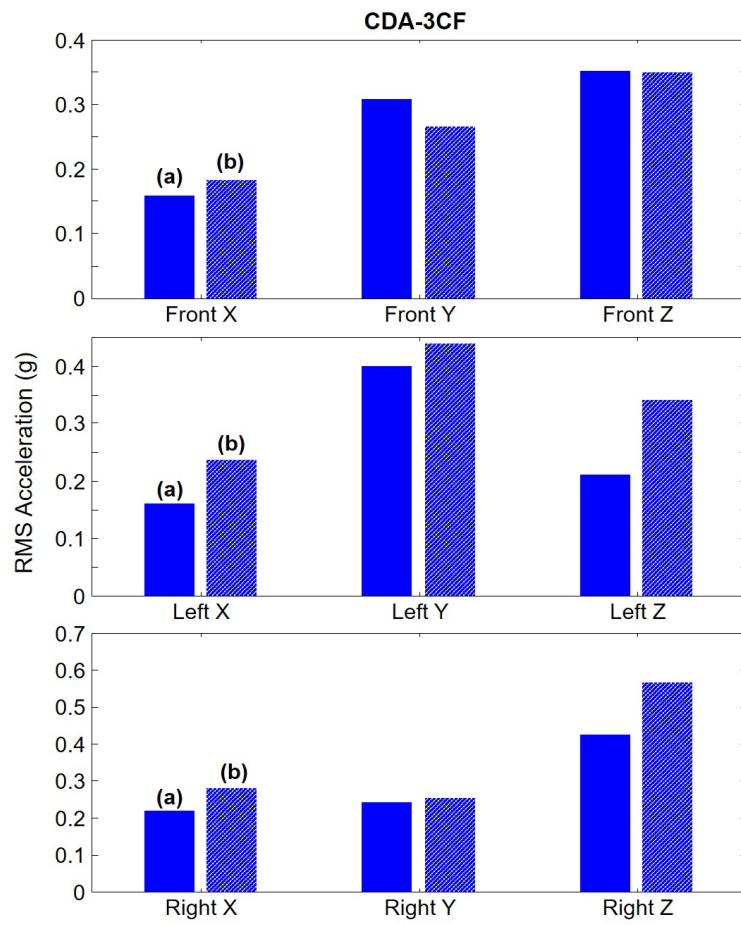
Figure 5.17. RMS linear accelerations for the tested CDA-3CF configurations at 800 RPM, 1.3 bar BMEP loaded idle.
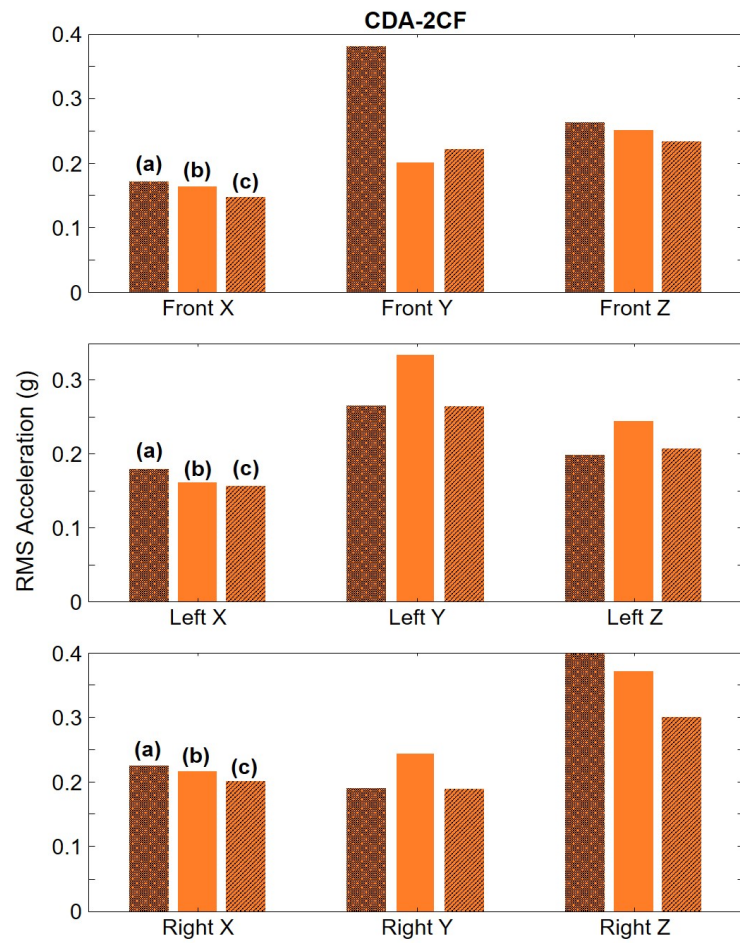
Figure 5.18. RMS linear accelerations for the tested CDA-2CF configurations at 800 RPM, 1.3 bar BMEP loaded idle.

5.3.3   Speed Sweep Results

The speed sweep results are characterized by the order cut RSS values of each accelerometer location for each CDA mode and load in Figure 5.19. The order cuts show the magnitudes at the fundamental frequency for each mode, as these are the primary source of the vibrations. The magnitudes at each accelerometer location are similar, with the front accelerometer location being consistently greatest. 6CF operation has linear vibration levels below 0.25g throughout all the speed sweeps. The CDA modes have similar linear vibration levels at higher speeds, however noticeable peaks greater than 0.5g and as high as 1.2g occur for the CDA modes at lower speeds. This data correlates with visual observations of the engine vibration during tests.
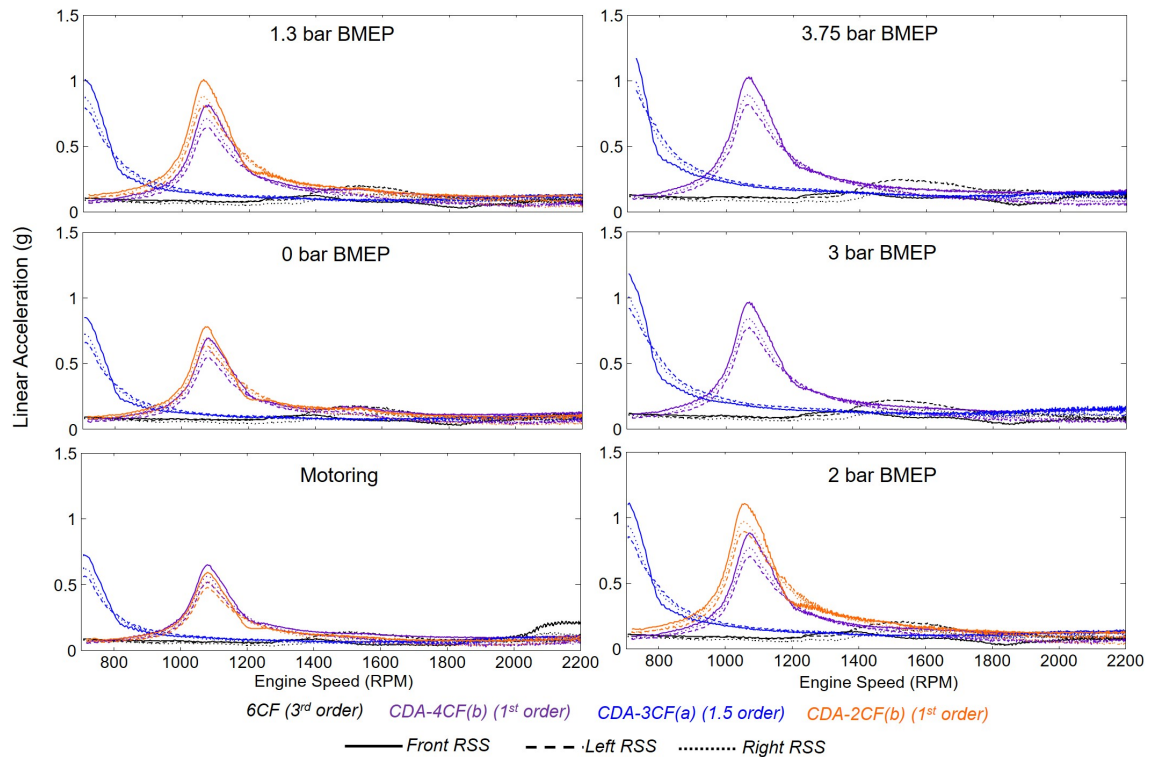
Figure 5.19.   Linear vibration order cuts for the conventional and CDA speed sweeps.

These peaks in vibration magnitude occur at approximately 1050 RPM for the CDA-2CF and CDA-4CF modes and 700 RPM for the CDA-3CF mode due to resonant excitation of the engine mounts at the corresponding firing frequencies. The engine mounts were found to have a resonance of approximately 17.5 Hz by examining the frequency domain representation in Figure 5.20. 6CF operation never reaches low enough frequency to excite resonance in the system, as shown in the zoomed out version of the frequency domain representation in Figure 5.21.

The resonance occurs primarily in the lateral direction as the mounts vibrate. This is demonstrated by the speed sweep order cuts in each direction shown in Figure 5.22. Increased vibrations in the longitudinal and vertical direction also appear. However, this could be artificially due to slight accelerometer or engine mounting misalignment. The figure shows only the front accelerometer data, though similar trends appear for the left and right accelerometers also.

The CDA configurations shown in Figure 5.3 have equivalent firing frequencies for each mode. For instance, CDA-4CF(a), CDA-4CF(b), and CDA-4CF(c) have the same firing pattern and firing frequency, however the geometric configurations of the firing cylinders vary. It was previously unknown whether the magnitude of torsional vibration varies depending on this firing configuration. Figure 5.8 shows the configurations with equivalent firing frequencies have little to no effect on the magnitude of torsional vibrations. For this reason, the results in this chapter primarily focus on CDA-4CF(b), CDA-3CF(a), and CDA-2CF(b) as the standards for each CDA mode.

As discussed in the previous torsional vibration section, the CDA configurations shown in Figure 5.3 have equivalent firing frequencies for each mode. And similar to the torsional vibrations, there is negligible variation in the magnitude of linear acceleration depending on firing configuration for equivalent firing frequency configurations. This is demonstrated by the front accelerometer vibration levels in Figure 5.23 for each configuration.
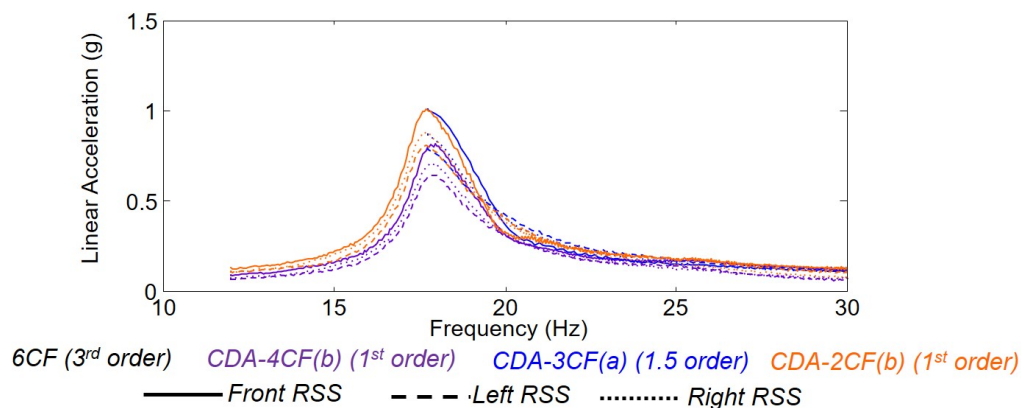
Figure 5.20. Zoomed in section of the linear vibration order cuts plotted versus frequency for the conventional and CDA speed sweeps at 1.3 bar BMEP to highlight the system resonance.
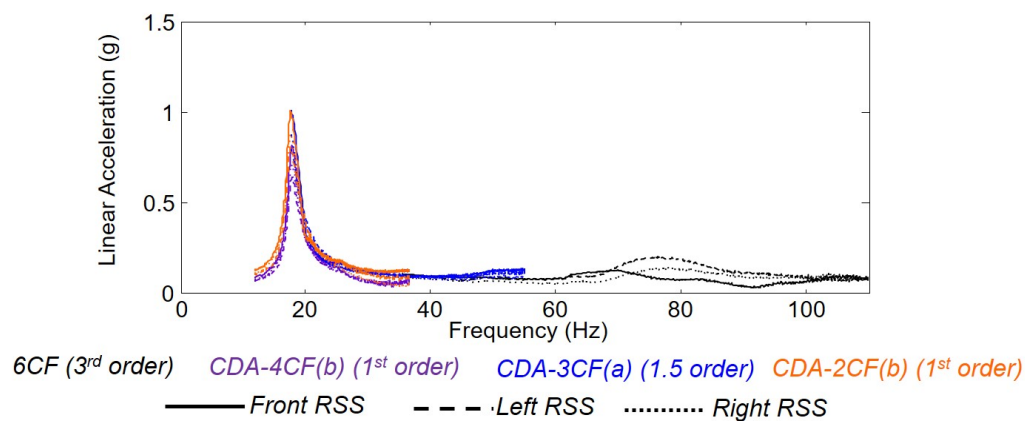
Figure 5.21. Linear vibration order cuts plotted versus frequency for the conventional and CDA speed sweeps at 1.3 bar BMEP.
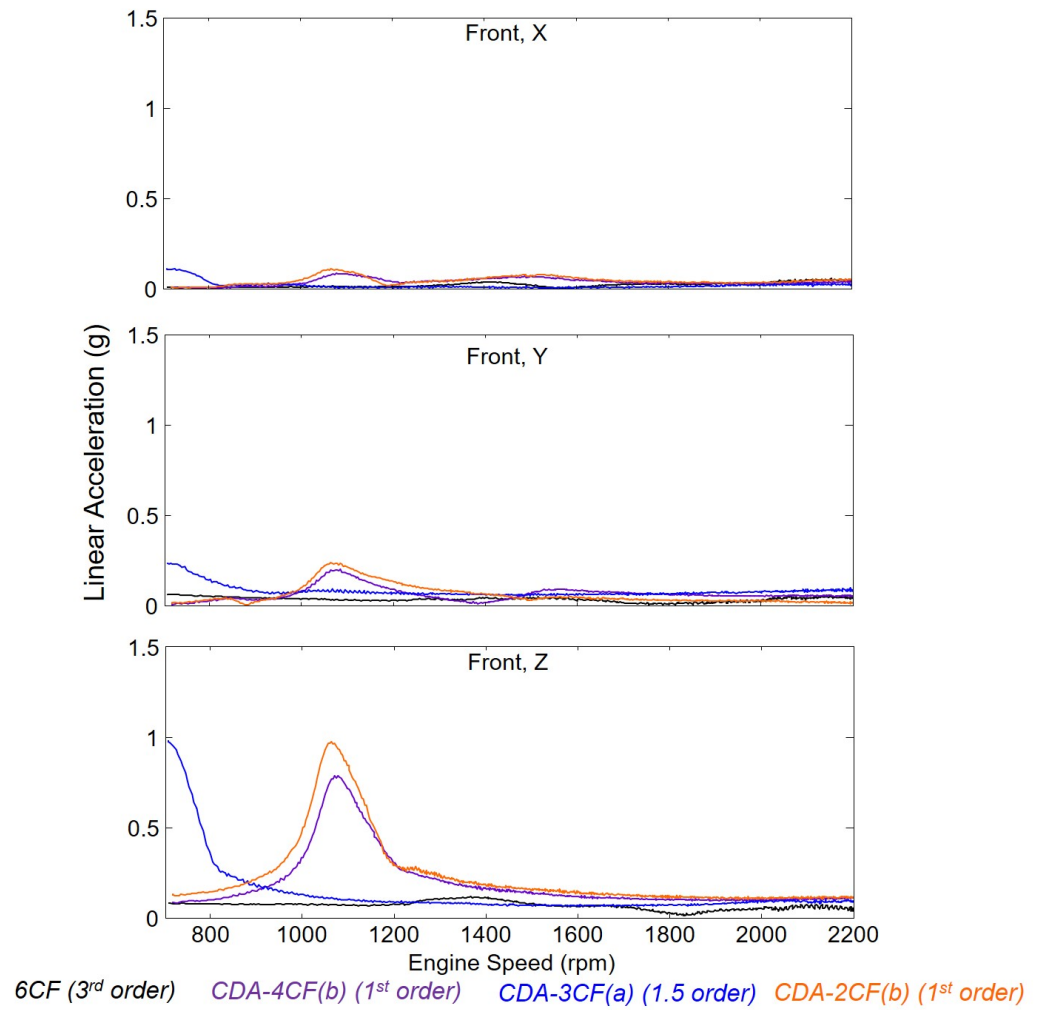
Figure 5.22. Linear vibration order cuts in each direction for the front accelerometer location during the speed sweeps at 1.3 bar BMEP.
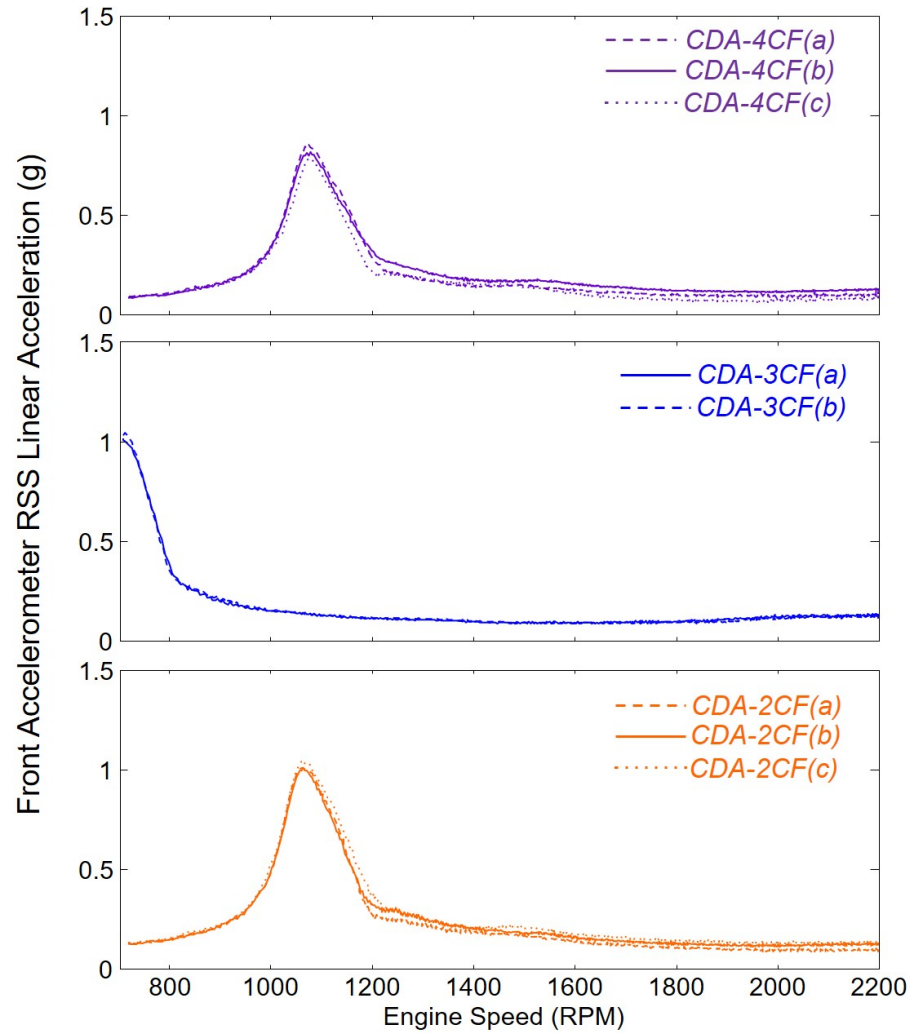
Figure 5.23. Comparison of the linear vibrations of various equivalent CDA configurations during the speed sweep at 1.3 bar BMEP.

The linear vibration effect of non-standard CDA firing configurations are shown in Figure 5.24. The non-standard CDA configurations have 0.5 order firing frequency, causing the mount resonance of 17.5 Hz to occur at 2100 RPM. The linear vibration of non-standard CDA is lower than the standard fixed CDA modes until after 1900 RPM. However, as mentioned in prior torsional vibration discussion, the low firing frequency of non-standard CDA firing orders can cause dangerous driveline resonance

on this test setup, emphasizing the need for both linear and torsional vibrations to be considered in production designs.
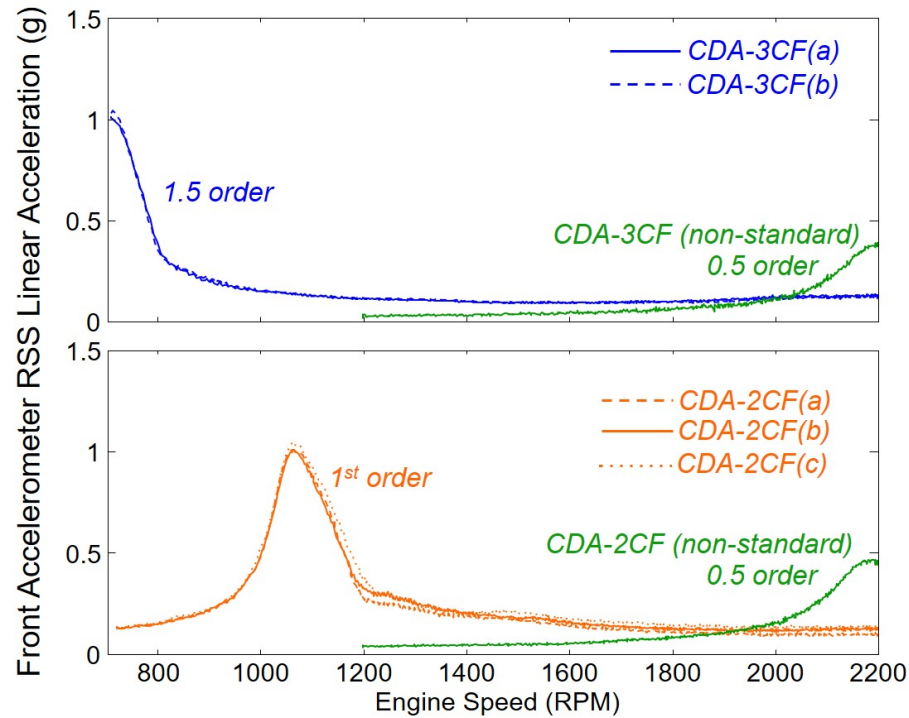
Figure 5.24. Comparison of linear vibration order cuts for standard and non-standard fixed CDA modes during the speed sweep at 1.3 bar BMEP.

5.3.4 Load Sweep Results

The linear vibration amplitudes for varying load at constant speeds of 800 RPM and 1200 RPM are shown in Figures 5.25 and 5.26. There is a general linearly proportional correlation between load and linear vibration, even during negative motoring conditions. However, the increase in linear vibration for increasing loads is not substantial. The amplification from the mount resonance appears at the 800 RPM for CDA-3CF and 1200 RPM for CDA-4CF and CDA-2CF, elevating the corresponding linear vibrations and magnifying any increase in load.
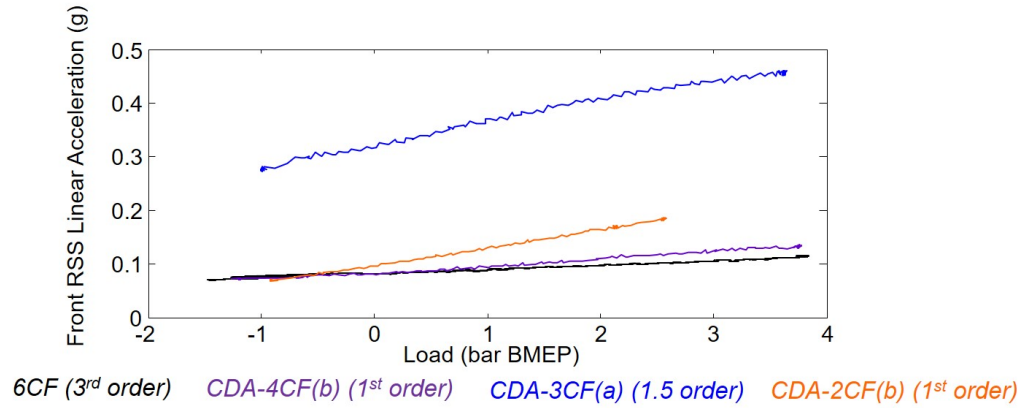
Figure 5.25. Linear vibration order cut analysis for a load sweep at 800 RPM.
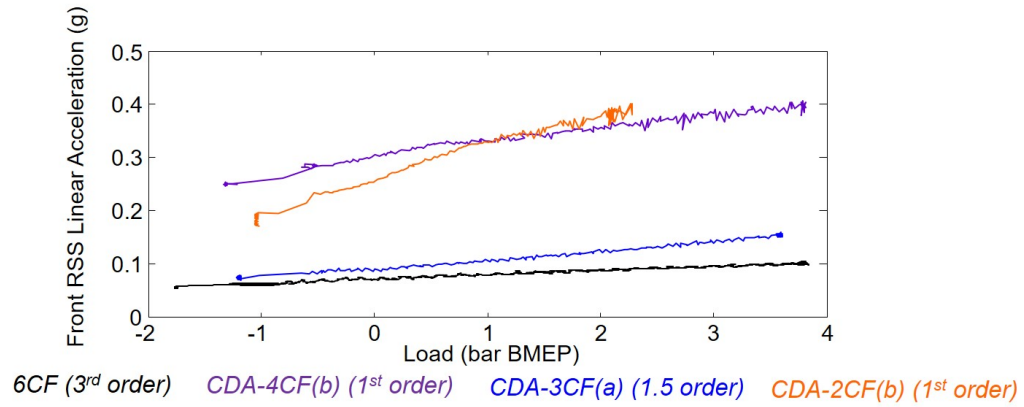
Figure 5.26. Linear vibration order cut analysis for a load sweep at 1200 RPM.

5.3.5   Summary of CDA Linear Vibration Characterization

Linear vibration experimentation and analysis is presented in this section. CDA has similar linear vibration levels for most of the operating range in the three directions. However, CDA is shown to excite the engine mount resonance for particular engine speeds and CDA modes, causing markedly higher linear vibrations for CDA-3CF at/around 700 RPM and for CDA-2CF at/around 1050 RPM. While the resonant

frequency of the engine mount is specific to this test setup, the scenario does demonstrate the importance of considering the frequency of vibration content in addition to the magnitudes. Non-standard CDA firing patterns also provide potential to change the speed location of resonance, however these patterns cause the low half-order vibration content that may excite other resonant frequencies. Load sweeps of CDA and conventional operation at different speeds show slight increases in vibration levels for CDA over conventional operation at each load when no resonant frequency is excited.

5.4 Acoustic Characterization of CDA

5.4.1 Introduction and Methodology

A brief study on the noise characteristics of CDA was conducted in order to attempt to explain the effects caused by the deactivation. Sound measurements were taken with an integrated circuit piezoelectric microphone sampled using a portable HEAD Acoustics SQuadriga data acquisition system sampling at 48 kHz. The microphone was calibrated prior to experimentation using a 94 dB, 1 kHz calibration tone. The microphone was positioned facing the exhaust side of the engine, as shown in Figure 5.27. The test chamber housing the engine was hard-walled and not suitable for lab-grade acoustics characterization, therefore the results should be taken as relative comparisons of the sound quality of CDA versus conventional engine operation.

The acoustics study was conducted prior and separate to the combined torsional and linear vibration experimentation. Therefore, a more limited set of CDA configurations is examined, however trends are not expected to vary depending on CDA configuration. Measurements were taken for 30 seconds at each of the operating scenarios shown in Table 5.1. The 800 RPM, 0 bar BMEP unloaded idle condition was chosen as the primary focus of the study due to the fuel performance results described previously in this document at that operating condition. That operating condition was also the only loading condition able to run with CDA-4CF and CDA-2CF at the time of testing due to torsional driveline considerations.

Figure 5.27.   Microphone setup for acoustic testing of the engine.

Table 5.1.   Tested operating conditions and cylinder configurations for acoustics study.

Mode	Speed (RPM)	Load (bar BMEP)	Number of Cylinders Active
6CF	800	0	6
CDA-4CF	800	0	4 (2,3,4,5)
CDA-3CF	800	0	3 (1,2,3)
CDA-2CF	800	0	2 (3,4)

Sound levels are depicted in terms of SPL and occasionally A-weighted SPL, which accounts for greater human susceptibility to some frequencies. This is the metric by which safety standards are typically indicated. However, many characteristics other than the overall level combine to create the eventual sensation heard by a person, and sound quality cannot be categorized by a single metric [70]. Therefore, additional analysis was done with the goal of describing the effects of CDA on a sound quality basis. Sound quality is a more abstract way to qualitatively describe sound that uses a variety of empirical relationships, therefore HEAD Acoustics Artemis software was used for analysis. For this study, the psychoacoustic metrics loudness, sharpness, and roughness were used in order to quantify human-perceived differences in sound quality due to CDA. These metrics are commonly used to analyze engine sounds [71].

Loudness is the human perceived value of sound strength on a linear scale. While SPL values measure the power of a sound based solely on amplitudes, the perceived loudness of a sound is also dependent on the frequency locations of the amplitude content. Therefore, SPL values are combined with frequency weightings based on variations in human-perceived loudness at different frequencies. This study uses weightings according to DIN 45631/A1 procedure [72]. The procedure, developed in part by Zwicker, specifies the weightings that are applied to the third octave levels of the signal. The total loudness is then the integrated value of these weighted levels. The units of loudness are sone. A sine tone of 1 kHz frequency at 40 dB has, by definition, a loudness of 1 sone.

Sharpness is the relative sensation caused by high-frequency sound content and is a primary driver in many annoyance metrics [73]. The sharpness metric linearizes the response of the human reaction to high-frequency noise. The unit of sharpness is the acum. 1 acum is defined as the sharpness of a narrow band noise one critical band wide at a center frequency of 1 kHz having a sound level of 60 dB. There are various procedures that have been developed to measure sharpness, including by von Bismark in reference [74]. Like loudness, sharpness uses a weighting scale to create the linearization.

Lastly, roughness is a measure of the temporal human perception of variations in sound. Increases in roughness are typically perceived as more annoying. Roughness occurs when temporal structures exist within a critical frequency band. When these variations occur in a low-frequency band, the human ear is able to better track the changes and the roughness increases. A 17% difference in roughness is generally taken to be the limit of detectability [75]. The unit of roughness is the asper, defined as a 1 kHz sine tone with a level of 60 dB, amplitude-modulated at a frequency of 70 Hz. Roughness is calculated using the model developed by Sottek [76].

5.4.2 Results

The acoustic sound pressure level (SPL) of the data is first examined in the frequency domain. Much like the torsional and linear vibration studies described earlier in this chapter, CDA has an effect on the acoustic frequency content based on the number of cylinders active. Many of the important operating characteristics of the engine can be extracted from the lower frequency range of the acoustic plots. The 800 RPM, 0 bar BMEP tests at each CDA level are used to demonstrate the effect of the deactivations. The frequency spectrum of the background noise, which was taken with the engine off but all other utilities running, is shown in Figure 5.28. All of the engine running data also contains this background frequency content currently, therefore those peaks can be neglected.

The association of acoustic frequency content to its mechanical source is a complex area, particularly at higher frequencies. However, the lower frequency content can be attributed more intuitively. Because the six cylinders of the engine are configured such as in Figure 5.29, it would be expected that a large portion of the 6CF operation sound would be located in the third order with respect to engine rotation. This is because many events, such as the firings of cylinders, compression events, expansion events, and vibration events of the engine are happening three times per engine revolution. This is confirmed through the frequency spectrum of the SPL in Figure 5.30 that
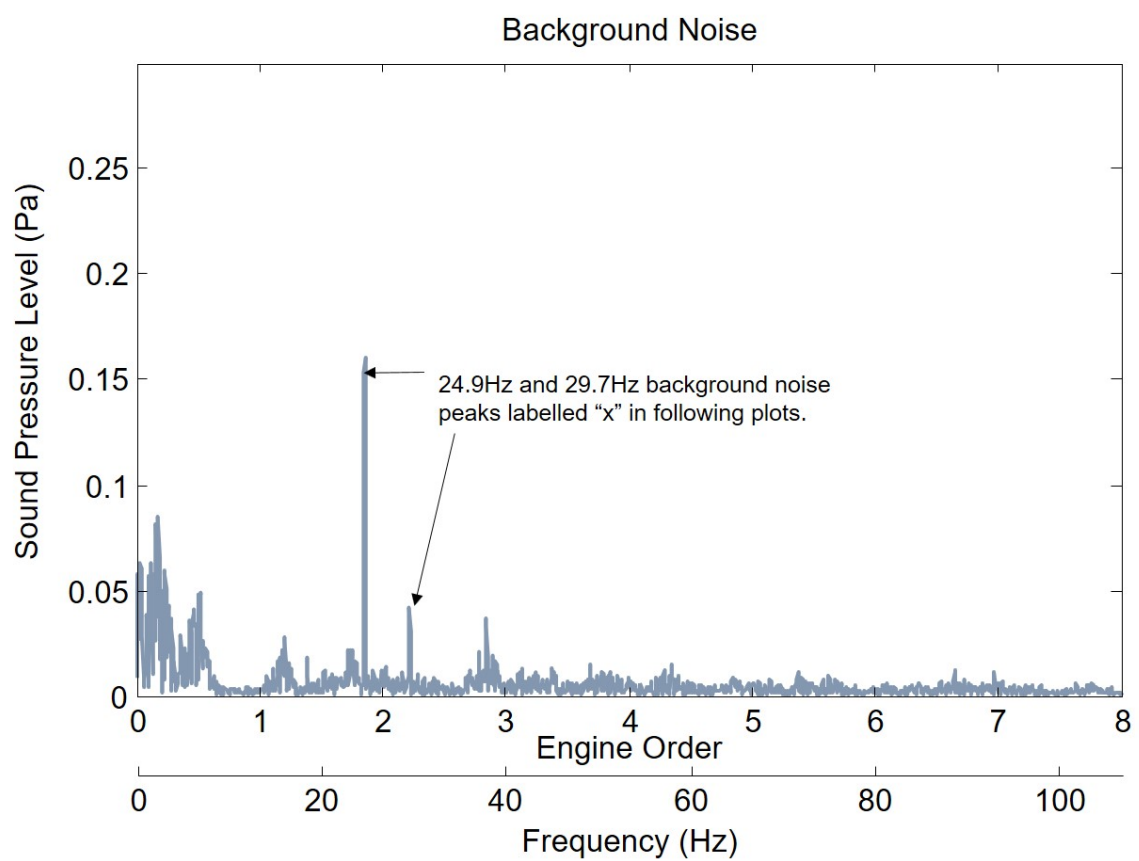
Figure 5.28. Frequency spectrum of the background noise levels during the acoustic tests.

shows the baseline 6CF operation at 800 RPM, 0 bar BMEP. A large third order peak occurs. A noticeable half order harmonic appears in this case, likely due to slight cylinder-to-cylinder imbalances. Finally, a prominent sixth order peak is present. While the second order firing harmonic contributes to this peak, the main driver is likely the motion of the pistons. There is upward piston motion occurring six times per engine revolution and downward piston motion occurring six times per engine revolution. This motion can contribute to the noise, particularly at the more lightly loaded operating conditions such as 0 bar BMEP.
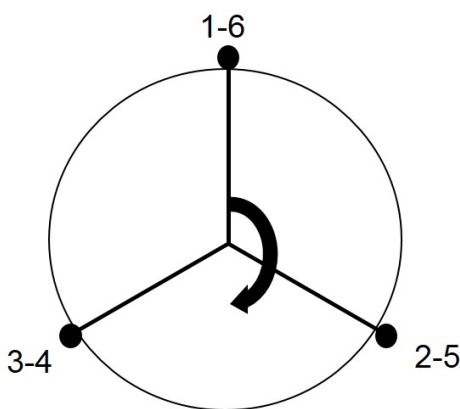
Figure 5.29. Crankshaft layout of the tested engine with the numbers corresponding to the cylinder numbers. The firing order of the engine is 1-5-3-6-2-4.

Deactivating cylinders changes the locations and magnitudes of the frequencies. CDA-3CF is shown in Figure 5.31. As discussed in the first section of this chapter, the firing frequency is half of 6CF operation during CDA-3CF. This drops the compression/expansion frequency and firing frequency to 1.5 engine order, resulting in more sound content at this frequency. The third order content is still larger, however, due to the physical layout of the engine and crankshaft still causing third order balance vibrations. Moreover, the inactive cylinders have compression and expansion events at twice their normal frequency due to the gas spring effect. This creates even more third order content. The combustion is also relatively small at this operating condition of 0 bar BMEP, diminishing its normal contribution to the 1.5 order. A sec-
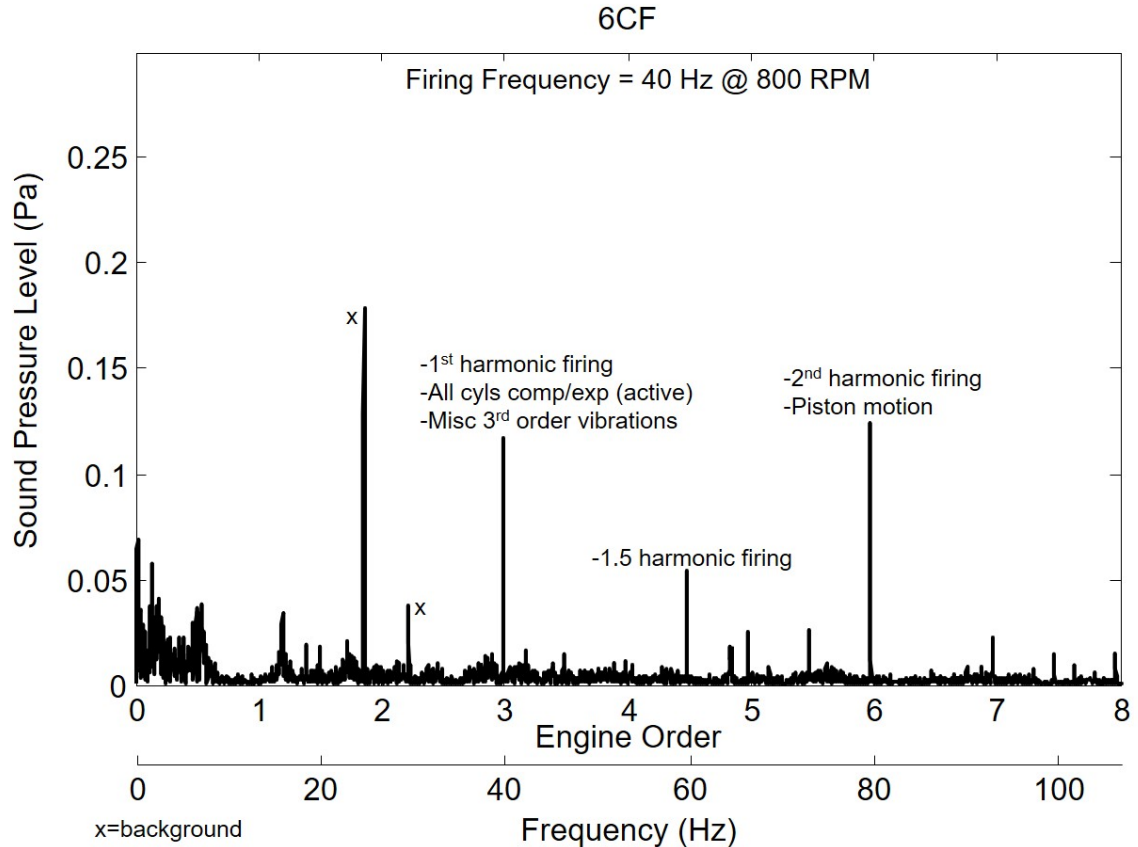
Figure 5.30.   Frequency spectrum for the sound pressure levels for 6CF operation at 800 RPM, 0 bar BMEP.

ondary compression/expansion frequency is also prominently displayed at 4.5 engine orders. This is the frequency that all cylinders, inactive and active, are combining to creating sound. Lastly, the piston motion seems to provide content at the same sixth order frequency as 6CF operation piston motion.

Figures 5.32 and 5.33 depict the sound pressure frequency spectrum for CDA-4CF and CDA-2CF, respectively. These CDA modes have sound content at more frequencies on this analyzed range than CDA-3CF and 6CF operation due to their configurations creating events at normally quiet orders. For instance, both modes have content at the fourth order, which was quiet for the previously described modes,
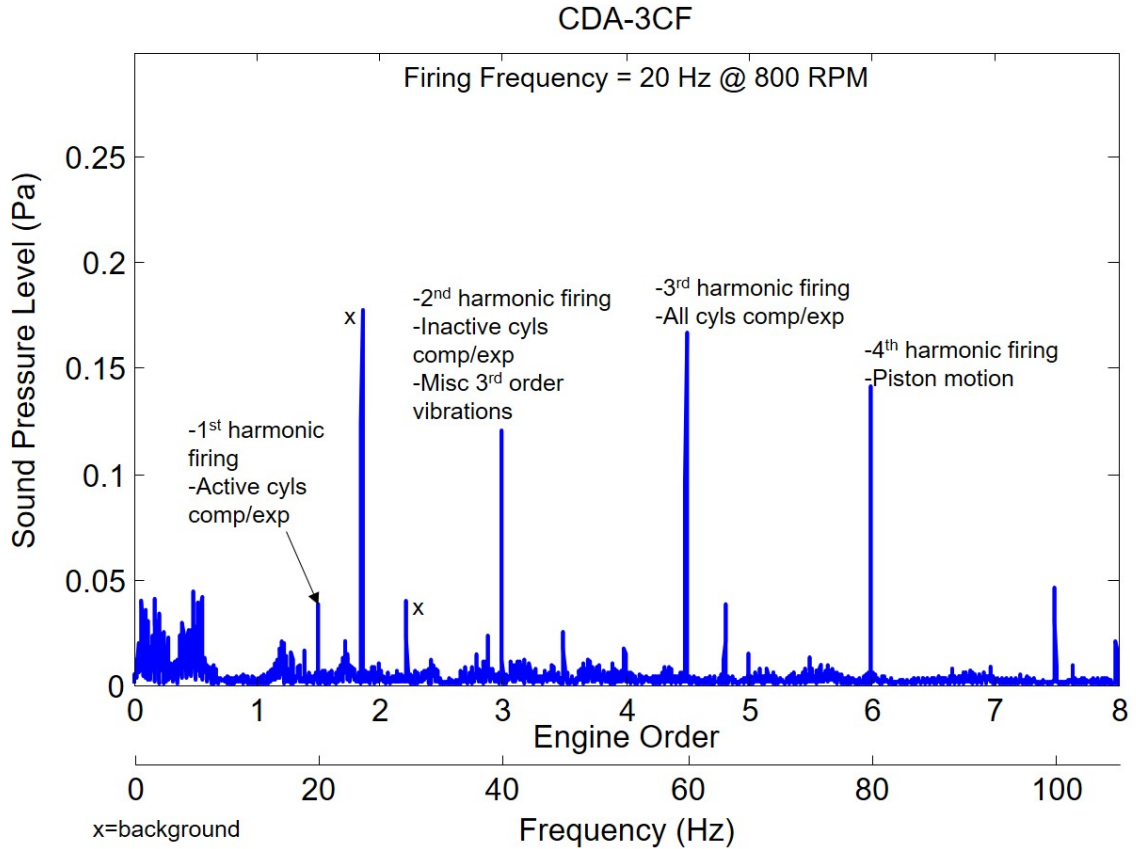
Figure 5.31. Frequency spectrum for the sound pressure levels for CDA-3CF at 800 RPM, 0 bar BMEP.

due to either all cylinders compressing and expanding (CDA-4CF) or the inactive cylinders compressing and expanding (CDA-2CF). This means in a vehicle application, these operations have the potential to excite more structural frequencies in the cabins and exterior. As is the case for 6CF and CDA-3CF, the piston motion sixth order content produces a large portion of the sound. CDA-4CF also has a component that is not present for the other modes due to its firing order (*nonfire-fire-fire-nonfire-fire-fire*). Similar to what was described in the torsional analysis section of this work, CDA-4CF does not necessarily follow traditional logic due to its asymmetric firing. Though there are two firings per engine rotation, the firing pattern causes these events

to have the spectral effect of a first order firing (courtesy of the *nonfire-fire-fire* period).
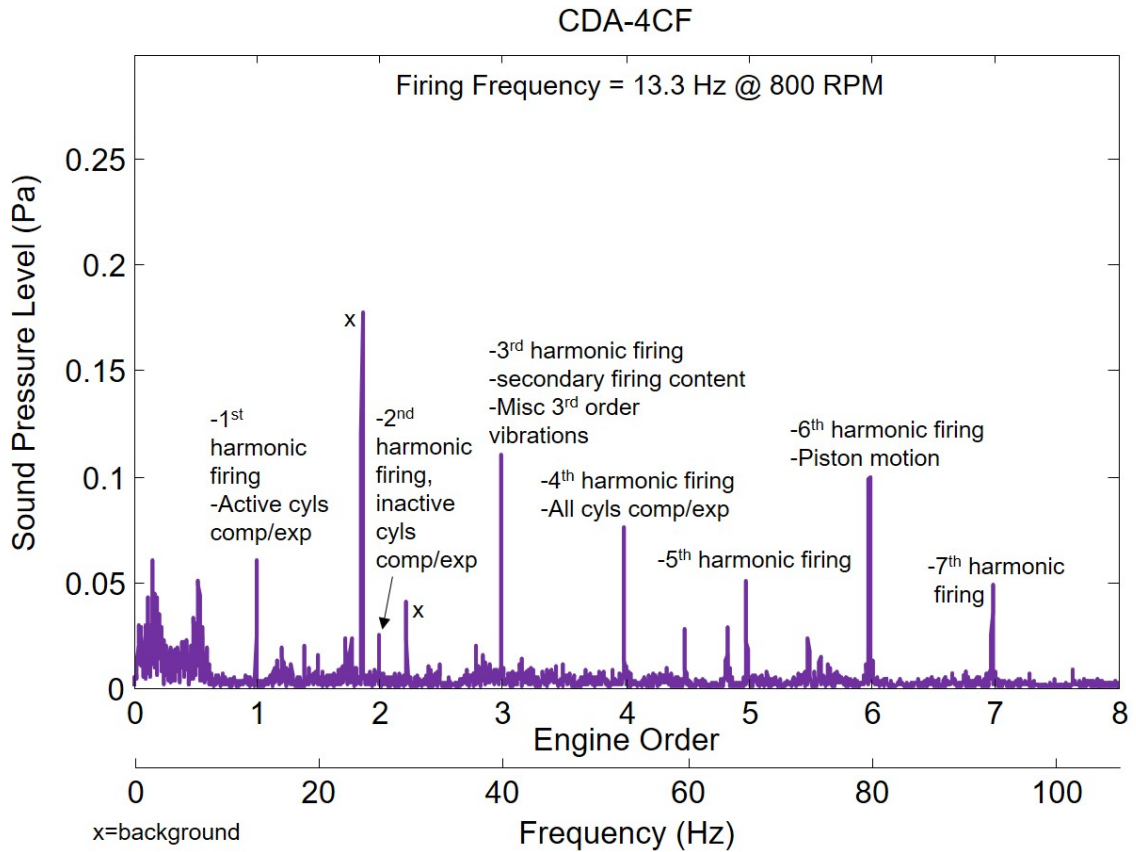
Figure 5.32.   Frequency spectrum for the sound pressure levels for CDA-4CF at 800 RPM, 0 bar BMEP.

The power spectrum of the entire audible frequency range for each of the above conditions can be shown in terms of third octave SPL bands. The result is shown in Figure 5.34. CDA of all modes results in less high-frequency content and greater low-frequency content on the acoustic spectrum.
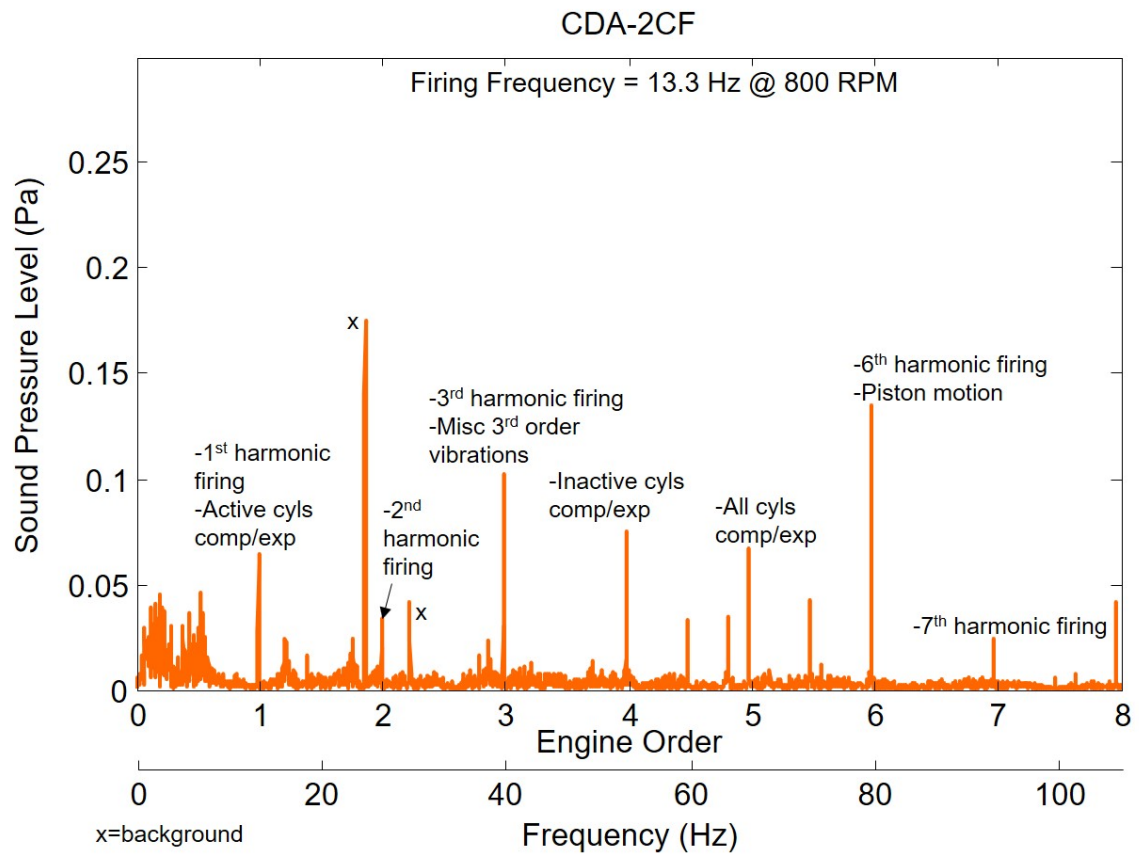
Figure 5.33. Frequency spectrum for the sound pressure levels for CDA-2CF at 800 RPM, 0 bar BMEP.
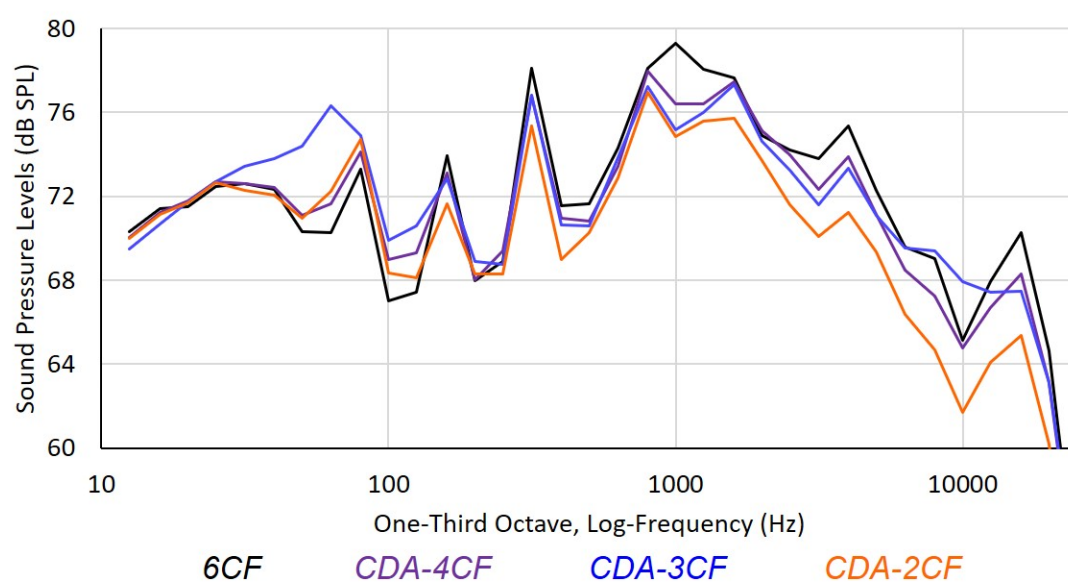
Figure 5.34.   Third octave SPL of each CDA mode at 800 RPM, 0 bar BMEP.

Psychometric values can help describe the spectral trends described above in addition to some of the temporal trends in the sounds. Due to the hard-walled test cell, the psychometric values are obtained with the assumption of a diffuse sound field, one where the reflected sound dominates the direct point source sound. This environment is still not ideal for acoustic testing, so all results are taken as comparative. The resulting overall sound pressure level (OASPL) values and average sound quality metric values for 800 RPM, 0 bar BMEP are shown in Table 5.2. As more cylinders are deactivated, the OASPL values decrease. This decreasing trend holds true for both the unweighted OASPL and the A-weighted OASPL, a frequency weighting commonly used for safety standards. A similar trend appears for the sound quality metrics, with CDA-2CF showing significant improvements in all metrics. However, CDA-3CF does diverge slightly from the trend for both loudness and sharpness. This divergence can be correlated with the third octave SPL data depicted in Figure 5.34 that shows higher levels of lower frequency content to increase loudness and a band around 10 kHz with higher frequency content to increase the sharpness and loudness. The CDA-3CF configuration has higher average SPL values than CDA-4CF for much of the higher-frequency bands. This, by definition, results in a higher overall sharpness value for CDA-3CF. Higher frequencies are weighted more heavily in the loudness metric calculations, so the CDA-3CF loudness value becomes closer to the CDA-4CF loudness even though CDA-4CF has an additional cylinder active. Roughness differences for all cylinder deactivations can be considered negligible, as they are well within the 17% limit described above.

Table 5.2. Acoustic metrics results for 800 RPM, 0 bar BMEP with various cylinder configurations.

CDA Mode	OASPL (dB)	OASPL (dBA)	Loudness (sone)	Sharpness (acum)	Roughness (asper)
6CF	89.1	87.2	78.4	5.21	5.60
CDA-4CF	88.4	86.2	74.2	4.99	5.25
CDA-3CF	88.6	85.8	74.4	5.18	5.18
CDA-2CF	87.5	84.7	67.4	4.57	5.12

A similar analysis is summarized in Table 5.3 for all operating conditions tested. These values show the effect of deactivating cylinders at additional loading conditions. The input variables (SOI, Rail Pressure, VGT and EGR positions) remain identical during a given loading condition with the exception of 1200 RPM, 7.6 bar BMEP, where this is not feasible due to the mechanical constraints of the engine.

A similar trend with respect to the number of cylinders activated appears for all tested loading conditions. CDA operations have comparable SPL and psychoacoustic metric values to conventional operation, even with larger combustion events in the active cylinders during CDA at more elevated loads. Loudness slightly decreases for the CDA operations, indicating a perceived quieter operation. Differences are not significant, however, leading to the conclusion that deactivating cylinders does not greatly affect the engine sound levels and sound quality.

Table 5.3. Acoustic metrics results at all tested conditions.

Setpoint	CDA Mode	OASPL (dB)	OASPL (dBA)	Loudness (sone)	Sharpness (acum)	Roughness (asper)
800/0	6CF	89.1	87.2	78.4	5.21	5.60
800/0	CDA-4CF	88.4	86.2	74.2	4.99	5.25
800/0	CDA-3CF	88.6	85.8	74.4	5.18	5.18
800/0	CDA-2CF	87.5	84.7	67.4	4.57	5.12
800/0.3	6CF	89.3	88.0	80.4	5.18	5.66
800/0.3	CDA-3CF	89.4	87.5	77.7	4.72	5.69
800/2.5	6CF	90.7	88.9	85.4	5.13	5.84
800/2.5	CDA-3CF	91.3	88.4	83.9	4.76	5.44
1200/7.6	6CF	97.1	95.9	130.8	6.59	6.84
1200/7.6	CDA-4CF	96.7	95.8	125.9	6.63	6.91
1200/7.6	CDA-3CF	96.7	95.6	128.8	7.01	6.65

5.4.3 Summary of CDA Acoustic Characterization

The acoustic results discussed in this section show how CDA changes the acoustic content of the diesel engine. In general, CDA produces low-frequency content at more frequencies. Overall, the sound quality analysis indicates little perceivable differences between CDA operation and conventional operation at the tested conditions. The acoustic testing indicated that this aspect of CDA can be considered acceptable no matter the condition and CDA mode. While this could change in a vehicle where the engine compartment amplifies certain frequencies, the acceptability holds for the test cell.

5.5 Dynamic Cylinder Activation for Additional NVH Control

5.5.1 Overview

Dynamic cylinder activation (DCA) is an alternate method of implementing CDA. The CDA operations previously described in this document will be referred to as fixed CDA during this section to avoid confusion. Fixed CDA keeps the same set of cylinders deactivated throughout the given mode of CDA operation. DCA differs from fixed CDA by actively changing the cylinder combination that is deactivated. An example of DCA operation is diagrammed in Figure 5.35. The graphic on the left shows fixed CDA-3CF operation. Notice that the same three cylinders are firing for all cycles. The DCA operation on the right, however, changes the order and number of cylinders that are active during each engine cycle. However, the total firing density for both fixed CDA and DCA in this example is 50%, making these operations hypothetically have equivalent emissions, fuel consumption, and thermal management performance.

The equivalent performance hypothesis was proven true experimentally in [54] at loaded idle conditions of 800 RPM, 1.3 bar BMEP. The efficiency and thermal management performance characteristics, shown in Figure 5.36, remain equivalent
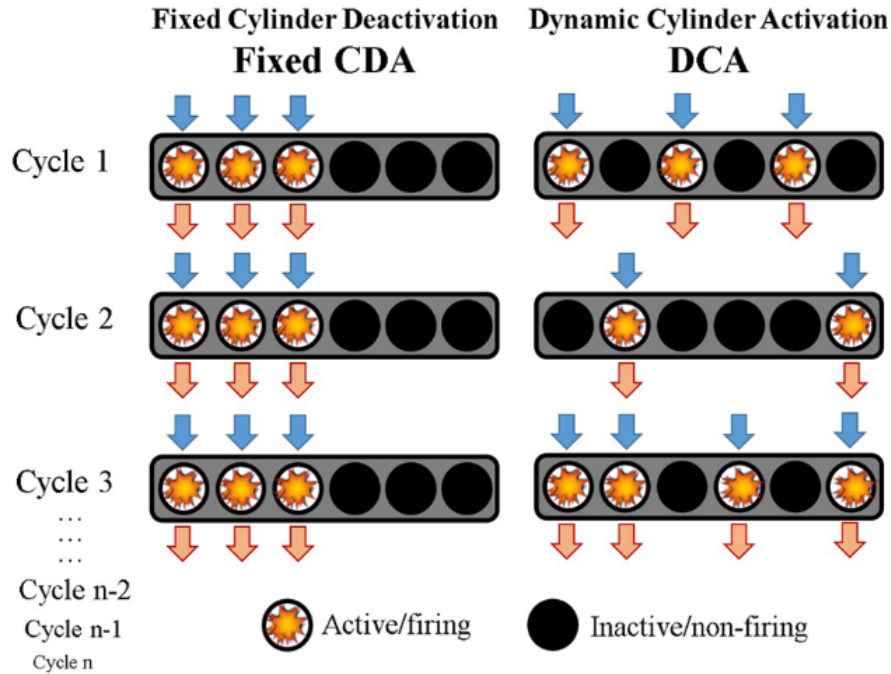
Figure 5.35. Example graphic showing fixed CDA-3CF versus DCA with 50% firing density.

for fixed CDA and DCA. Fixed CDA and both DCA patterns have improved fuel efficiency, elevated exhaust temperatures, and reduced airflow compared to conventional 6CF operation. Additionally, the NOx emissions for CDA and DCA are comparable to the shown 6CF operation, while the PM flows are reduced by almost half.

There are numerous combinations of DCA strategies and activation patterns that can be employed. However, the two studied in this section are referred to as either a 'long' pattern or 'alternating' pattern. The implementation of these patterns are described by Figure 5.37. The alternating pattern has an overall firing period that is (*fire-fire-inactive-inactive*). This creates a fundamental frequency that is 0.75 engine order. Notice that each cylinder during this pattern switches between firing and non-firing for each engine cycle. The long pattern implementation of DCA does not have a specified period. It is meant to be a pseudo-random combination of active and inactive events that average out to the desired firing density. This work implements
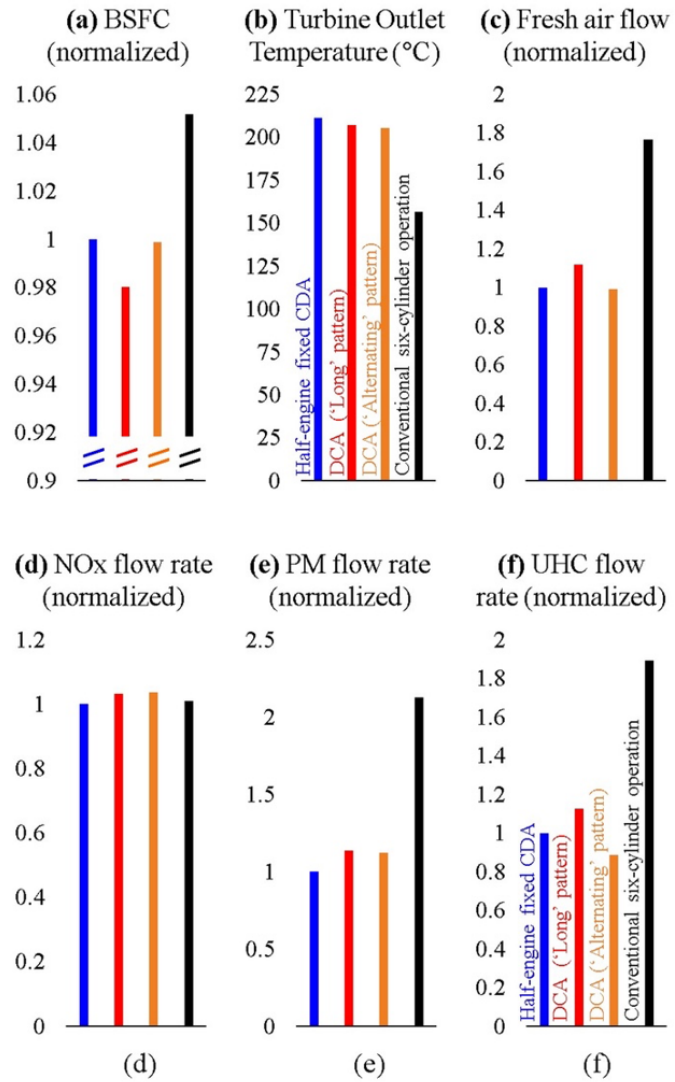
Figure 5.36. Performance of DCA compared to fixed CDA and 6CF operations at loaded idle (800 RPM, 1.3 bar BMEP). [54]

Figure 5.37. Comparison of the 'long' and 'alternating' forms of DCA firing sequences.

'long' DCA form as firing sequences with a period of 100 cycles, hence the pseudo-random classification.

DCA allows for greater flexibility in firing density than fixed CDA. Fixed CDA is constrained to a given set of firing densities. CDA-2CF has 33.3% firing density, CDA-3CF has 50% firing density, and CDA-4CF has 66.7% firing density. Fixed CDA is unable to achieve firing densities in between these discrete densities. However, there are DCA implementations that enable this effect. For example, the firing patterns shown in Table 5.4 provide 25% firing density, 40% firing density, 60% firing density, and 75% firing density in periodic manners. Moreover, long pattern implementations of DCA can provide any firing density. While the ability to vary firing density is used with great impact in gasoline engine fuel efficiency, it is unknown whether it will be needed in diesel engines for fuel economy or thermal management. However, DCA provides the capability should the need arise.

Table 5.4. Various periodic DCA firing sequences.

Label	Firing Density	Period
DCA-1.5eCF	25%	*fire-inactive-inactive-inactive*
DCA-2.4eCF	40%	*fire-inactive-fire-inactive-inactive*
DCA-3.6eCF	60%	*inactive-fire-inactive-fire-fire*
DCA-4.5eCF	75%	*fire-fire-fire-inactive*

Charge trapping, discussed in detail for fixed CDA in Chapter 4 of this document, is especially important for DCA. The frequent deactivation and reactivation of each cylinder can cause considerable efficiency performance degradation to occur if charge is trapped in the cylinder due to losses from additional pumping events. Therefore, low-pressure trapping is implemented for DCA. This implementation, along with the pumping loss mechanism during fresh charge trapping, is shown in Figure 5.38. Low-pressure trapping deactivates the valves after the exhaust stroke of the given cylinder, causing a low pressure to be present from the start of the deactivation. Fresh charge trapping, which is commonly used in fixed CDA, uses an additional intake event before the deactivation to capture a fresh charge in the cylinder with the motivation of reducing oil accumulation. As described in Chapter 4, the pressure of this trapped fresh charge decays quickly, which causes an eventual pumping loss due to the lack of air spring. This single pumping loss is very minimal compared to the total efficiency gains of fixed CDA. However, the frequent trapping and releasing of fresh charge during DCA is substantial enough to make a performance impact. This impact is shown in Figure 5.39, where low-pressure charge trapping has consistently

improved efficiency, reduced airflow, and elevated exhaust temperatures compared to fresh charge trapping at 800 RPM, 1.3 bar BMEP.
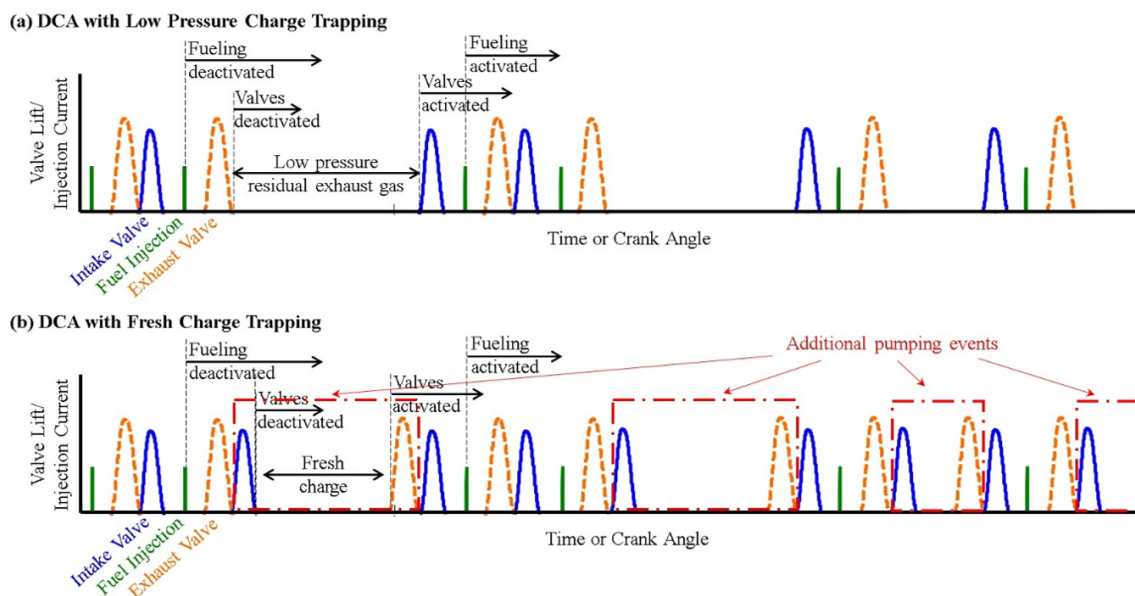
Figure 5.38.   Charge trapping implementation during DCA.
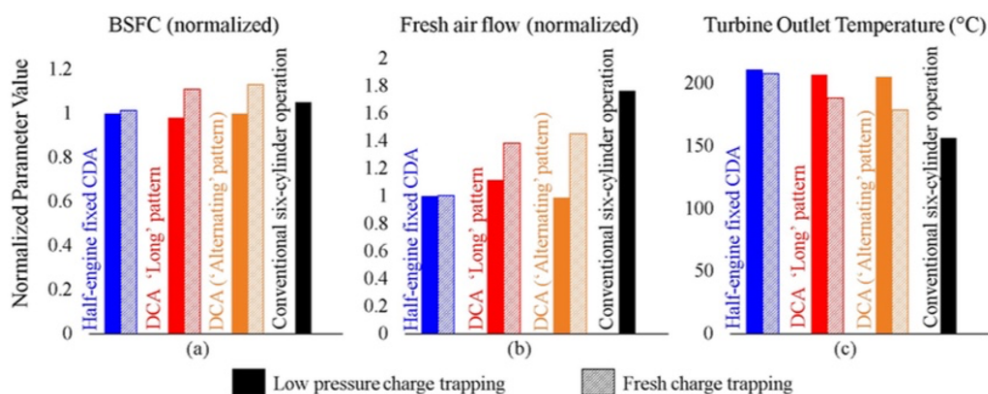
Figure 5.39.   Performance comparison between low-pressure charge trapping and fresh charge trapping for DCA at loaded idle (800 RPM, 1.3 bar BMEP). [54]

5.5.2   DCA NVH Results

DCA Torsional Vibrations

Torsional vibrations could be a motivator for DCA in diesel engines. As discussed in Section 5.2, fixed CDA reduces the firing frequency of the engine. At idle and low speeds, this often results in firing frequencies lower than ever experienced during conventional 6CF operation (except during starting and shutdown of the engine). This could cause the firing frequency of the engine in fixed CDA to excite a resonant frequency of the driveline. DCA provides the potential to mitigate this issue while maintaining equivalent fuel economy and thermal management performance by shifting the firing frequency of the engine away from the resonant frequency. Therefore, an experimental exploration of torsional vibrations during DCA was conducted. These torsional vibration measurements at 800 RPM, 1.3 bar BMEP loaded idle were taken during the torsional and linear vibration experimentation introduced in Sections 5.2 and 5.3.

Figure 5.40 shows FFTs of flywheel angular acceleration at loaded idle (800 RPM, 1.3 bar BMEP) for the fixed CDA operation of CDA-3CF(a) and two equivalent DCA operations. DCA-3eCF-alt is an equivalent 50% firing density operation using the alternating pattern discussed in this section. DCA-3eCF-long(a) is an equivalent 50% firing density operation using pseudo-random long pattern discussed in this section. Fixed CDA-3CF(a) has a firing frequency at 1.5 engine order, which corresponds to 20 Hz at this condition. However, if the vehicle driveline has a resonance frequency at or around 20 Hz, this operation may not be possible. One option would be to switch to fixed CDA-2CF or CDA-4CF operation, however the thermal management and fuel economy effects would change. In order to maintain equivalent 3CF performance while avoiding the hypothetical 20 Hz resonance, DCA-3eCF-alt shifts the firing frequency to 0.75 engine order, which corresponds to 10 Hz at this condition.

DCA-3eCF-long(a) provides a similar, albeit fundamentally different, effect. The pseudo-random long pattern spreads the normally 20 Hz content throughout the

low-frequency spectrum, only at lower magnitudes. This provides the potential to avoid multiple resonant frequencies, depending on the allowable content at those frequencies. There are infinitely many firing combinations to create these pseudo-random long patterns. Two different implementations are shown in Figure 5.41, however the spectrums appear similar for these particular cases.
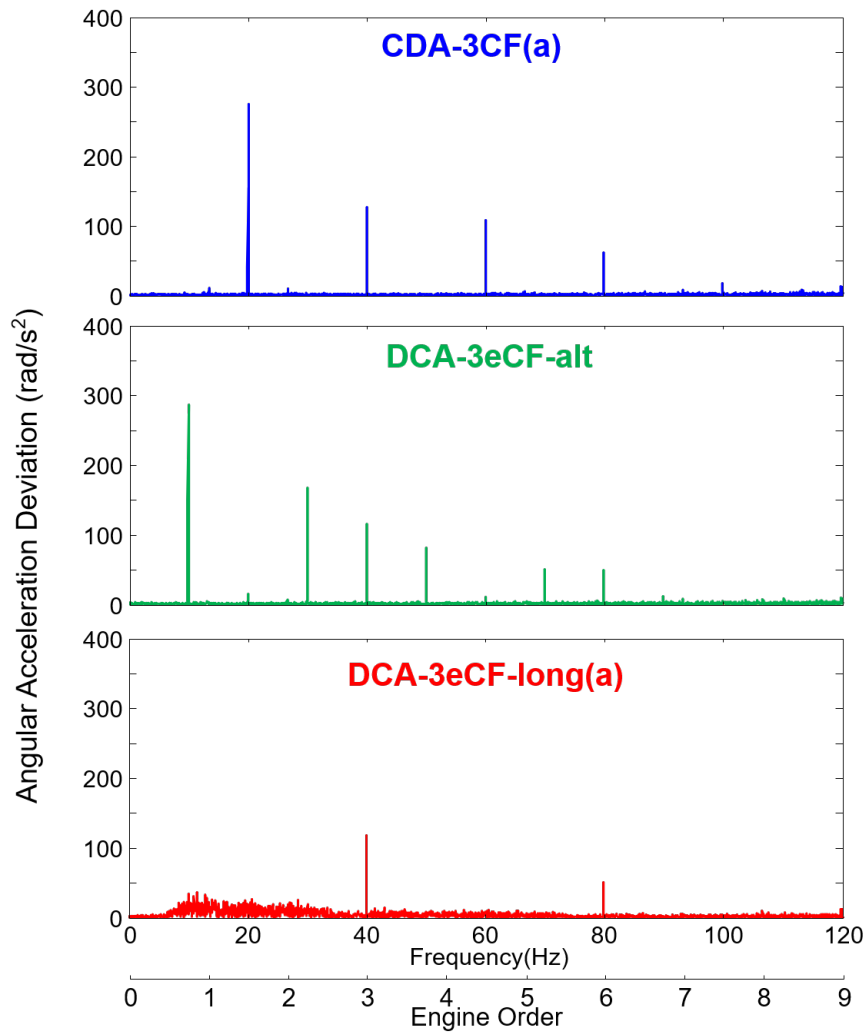
Figure 5.40.   Torsional vibration spectrums of fixed CDA and DCA 50% firing density operations at 800 RPM, 1.3 bar BMEP loaded idle.
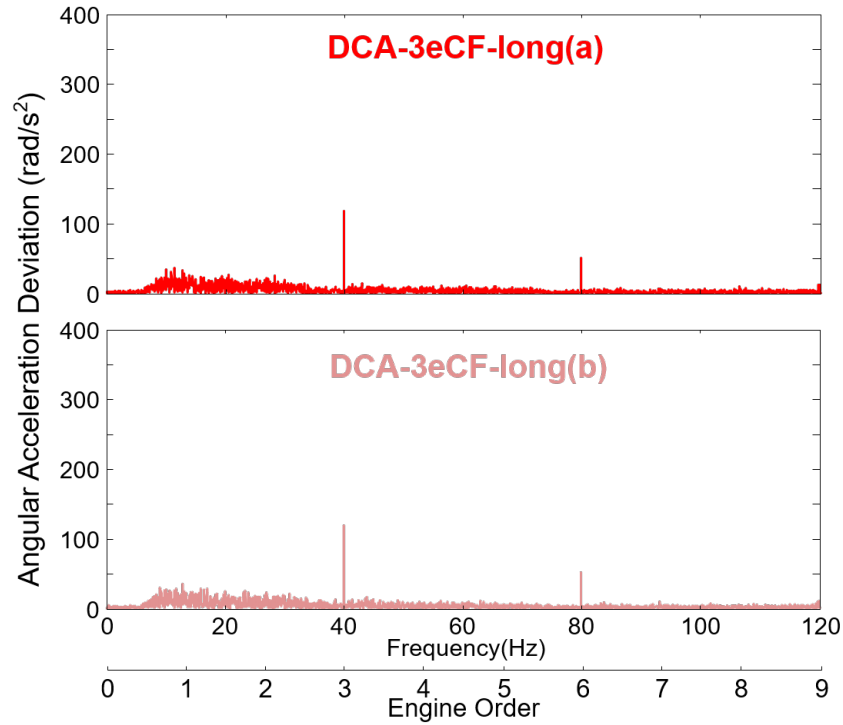
Figure 5.41.   Torsional vibration spectrums of two different DCA-3eCF-long implementations at 800 RPM, 1.3 bar BMEP loaded idle.

Firing densities that are not achievable with fixed CDA also exist for periodic (alternating-type) DCA implementations. Variation in firing density also changes the frequency content. Figure 5.42 shows a few of these implementations at 25%, 40%, 60%, and 75% firing density.
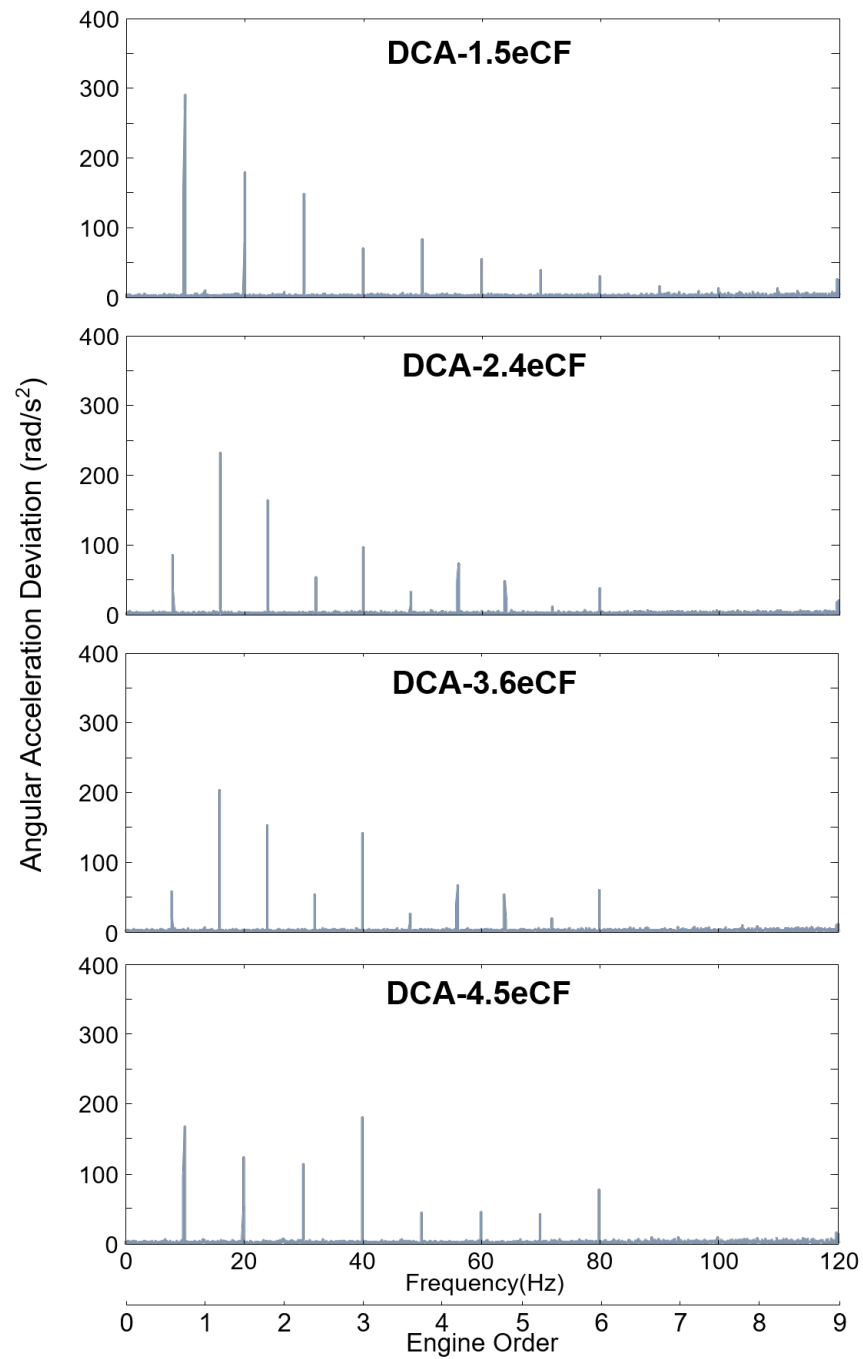
Figure 5.42. Torsional vibration spectrums of various periodic DCA implementations of intermediate firing densities not achievable with fixed CDA at 800 RPM, 1.3 bar BMEP loaded idle.

DCA Linear Vibrations

Linear vibrations are also affected by DCA. Experimental linear vibration measurements at 800 RPM, 1.3 bar BMEP loaded idle were taken during the torsional and linear vibration experimentation introduced in Sections 5.2 and 5.3 of this chapter.

RMS linear accelerations for each accelerometer location and direction at loaded idle are shown in Figure 5.43 for four equivalent 50% firing density operations. As a reminder, fixed CDA-3CF operation excites a mount resonance in the tested engine setup due to its firing frequency (20 Hz) proximity to the mount resonant frequency (17.5 Hz), and the resonance was shown to appear primarily in the lateral (Z) direction for the fixed CDA results. DCA-3eCF-alt helps alleviate the increase in lateral vibration by shifting the firing frequency to 10 Hz. This is a good example of the merits of DCA to avoid undesirable frequencies while maintaining fuel efficiency and thermal management performance of CDA-3CF.

The long pattern DCA operations have elevated vibration levels compared to DCA-3eCF-alt in the lateral (Z) direction. It is likely that the frequency content at the mount resonant frequency, though lower in amplitude for the long pattern DCA operations, still excites some resonance. However, there is still a reduction compared to fixed CDA in all directions. These trends correlate with visual observations during testing.

The DCA operations have similar longitudinal (X) vibration as fixed CDA-3CF, however there is consistently lower vertical (Y) vibration for the DCA operations. Fixed CDA-3CF operation creates a physical asymmetry in the engine by activating only the front half or rear half of the cylinders. It is hypothesized that DCA restores some balance by utilizing cylinders in both engine halves, thus reducing the rocking and vertical motions.
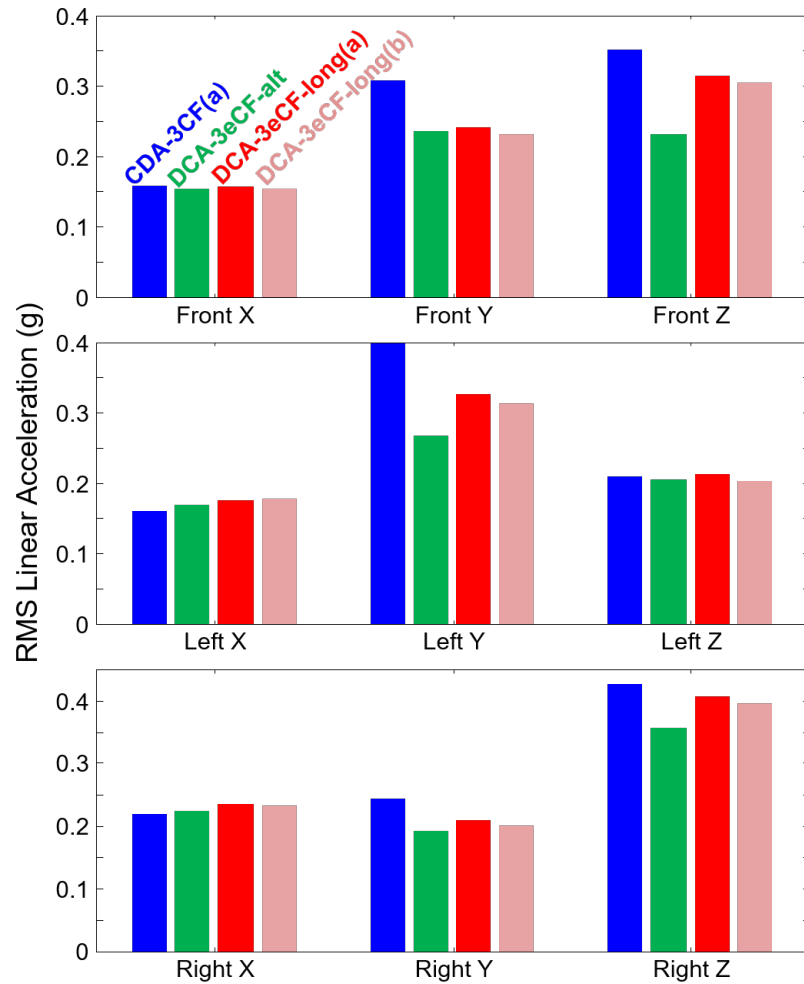
Figure 5.43. RMS linear accelerations for the equivalent fixed CDA and DCA 50% firing densities operations at loaded idle (800 RPM, 1.3 bar BMEP).

5.5.3 Summary of DCA

DCA in diesel engines has been demonstrated to achieve similar efficiency, emissions, and thermal management performance as fixed CDA. This work characterizes the NVH performance effects of DCA compared to traditional 6CF and fixed CDA operation. The NVH of various firing density operations were explored, including firing densities which cannot be achieved via fixed CDA. DCA enables the frequency

content of equivalent firing density operations to vary according to the firing pattern. This firing pattern can be periodic, as was shown during the alternating pattern example, or aperiodic, as was shown during the long pattern example. DCA provides a possible option of avoiding undesirable frequencies in a driveline while maintaining the desired nominal engine fuel efficiency, emissions, and thermal management performance of fixed CDA. This was demonstrated by the alternating DCA operation avoiding the linear vibration resonance that fixed CDA excites on the experimental setup.

6. CONCLUSION

6.1 Summary

This work advances the forthcoming technology of diesel engine CDA by demonstrating fuel efficiency and thermal management performance, providing a comparison of deactivation strategies, and characterizing trends in NVH. Chapter 3 demonstrated fuel efficiency improvements enabled by CDA at unloaded idle (800 RPM, 0 bar BMEP) and loaded idle (800 RPM, 1.3 bar BMEP). Both CDA-3CF and CDA-2CF were studied. DOE-based fuel efficiency optimizations combined with further screening at unloaded idle demonstrate:

- Optimized CDA-3CF improves fuel efficiency by 15% over optimized 6CF operation at equivalent emissions constraints when using periodic intake recharges. Improvements of 20% over 6CF operation are possible without intake recharges.

- Optimized CDA-2CF improves fuel efficiency by 23% over optimized 6CF operation at equivalent emissions constraints when using periodic intake recharges. Improvements of 28% over 6CF operation are possible without intake recharges.

- The CDA fuel efficiency improvements are accompanied by modest exhaust temperature increases of 14°C for CDA-3CF and 33°C for CDA-2CF over 6CF operation.

Screening at the loaded idle operating condition based on the unloaded idle DOE was conducted. These results demonstrate:

- CDA-3CF provides 13% improvement in fuel efficiency over baseline 6CF operation under the same emissions constraints.

- CDA-2CF provides 6% improvement in fuel efficiency over baseline 6CF operation under the same emissions constraints. Note that, contrary to unloaded idle, CDA-2CF was not as efficient as CDA-3CF due to the increased load.

- CDA fuel efficiency improvements are accompanied by exhaust temperature increases of 41°C for CDA-3CF and 107°C for CDA-2CF over 6CF operation.

The CDA-3CF strategies were implemented over the HD-FTP for fuel consumption testing. This resulted in CDA-3CF providing 0.7% fuel efficiency improvement over baseline 6CF operation.

Detailed studies of CDA fuel efficient thermal management performance during low-load cycles were conducted for (i) extended idle operation at 800 RPM, 1.3 bar BMEP and (ii) creep operation. Modified CDA strategies for improved thermal management maintained higher SCR outlet temperatures than conventional thermal management operation for 34 minutes during extended idle for CDA-2CF and is comparable during much of the creep operation. The thermal management for all components is notably improved for CDA operations compared to the more fuel neutral conventional fuel efficient operation. The fuel consumption reduction for CDA was up to 40% during extended idle and 31% during creep operation. This is achieved with typically comparable or improved engine-out emissions. CDA-3CF and CDA-2CF operations show 72% and 50%, respectively, lower soot than TM-6CF during extended idle. This coincides with 52% and 38% reductions in NOx for CDA-3CF and CDA-2CF, respectively.

In Chapter 4, an experimental investigation into CDA transition strategies provides a comparison of fresh charge trapping and combusted charge trapping. In-cylinder pressure measurements indicate disparities between the two strategies directly after the deactivation, specifically that combusted charge trapping can create recompression pressures greater than even the combustion pressures. Although the greater initial deactivation pressures associated with combusted charge trapping would theoretically mitigate the loss of gas spring and eventual oil accumulation in

the cylinder, the experimental results indicate this is not the case. Blow-by around the piston rings and heat loss through the cylinder walls and pistons result in similar rapidly decaying in-cylinder pressures for both fresh charge and combusted charge trapping CDA that cause the cylinder pressures to converge as quickly as 0.8 seconds after deactivation. This indicates that there is minimal performance difference expected between fresh charge trapping and combusted charge trapping strategies for conventional CDA.

Chapter 5 characterizes the NVH effects of CDA, specifically torsional vibrations, linear vibrations, and acoustics. CDA causes frequency content at reduced frequencies compared to conventional operation. This has effects on all aspects of NVH. Torsional vibrations are shown to remain below magnitude limits from literature, however the frequency content must ultimately be considered. Linear vibrations are shown to be similar to conventional operation when engine mount resonance is not excited on this experimental setup. Psychoacoustic analysis of CDA noise indicates similar or improved characteristics to conventional operation. Finally, the NVH of DCA is explored in detail. DCA is shown to provide a possible option of avoiding undesirable frequency output while maintaining the desired engine performance of CDA.

6.2   Recommendations

Future work to advance CDA in diesel engines should focus on possible system-level modifications to optimize benefits from CDA. Possible modifications could include more optimal turbomachinery for CDA, potential for CDA to extend the operating ranges of alternate combustion modes, and reconfigured/next generation aftertreatment. For example, close-coupled aftertreatment components could help maximize the temperature benefits of CDA. The effects of CDA during active SCR dosing may also have potential for interesting study, as lower space velocity from CDA will likely have an effect. The impact of CDA should also be studied for various engine sizes. Ultimately, on-vehicle testing must be conducted to fully understand many of

the real-world benefits. On-vehicle testing will also allow more thorough investigation of the NVH impact of CDA. However, further analysis on these impacts can still be conducted with more information on the given driveline.

REFERENCES

REFERENCES

[1] United States Environmental Protection Agency. Draft Inventory of U.S. Greenhouse Gas Emissions and Sinks 1990-2017. Technical report, United States Environmental Protection Agency, 2019.

[2] United States Department of Transportation Federal Highway Administration. Freight Quick Facts Report 2016. Technical report, United States Department of Transportation, 2016.

[3] United States Department of Transportation. Beyond Traffic: 2045 Final Report. Technical report, United States Department of Transportation, 2017.

[4] National Petroleum Council. Advancing Technology for America's Transportation. Technical report, Washington, DC: National Petroleum Council, 2012, 2012.

[5] Energy Information Administration U.S. Department of Energy. Annual Energy Outlook 2008: With Projections to 2030. 202(202):202–586, 2008.

[6] Y. Najjar. Gaseous Pollutants Formation and Their Harmful Effects on Health and Environment. *Ashdin Publishing Innovative Energy Policies*, 1(8), 2011.

[7] United States Environmental Protection Agency. and United States Department of Transportation. Greenhouse Gas Emissions and Fuel Efficiency Standards for Medium- and Heavy-Duty Engines and Vehicles - Phase 2. Regulatory Impact Analysis. 2016.

[8] United State Environmental Protection Agency and National Highway Traffic Safety Administration. Greenhouse Gas Emissions and Fuel Efficiency Standards for Medium- and Heavy-Duty Engines and Vehicles Phase 2. *Rules and Regulations*, 81(206), 2016.

[9] Y. Zeldovich, D. Frank-Kamenetskii, and P. Sadovnikov. *Oxidation of Nitrogen in Combustion*. Publishing House of the Acad of Sciences of USSR, 1947.

[10] R.C. Flagan and J.H. Seinfeld. *Fundamentals of Air Pollution Engineering*. Prentice-Hall, Inc., Englewood Cliffs, NJ, 1988.

[11] D.W. Stanton. Systematic development of highly efficient and clean engines to meet future commercial vehicle greenhouse gas regulations. *SAE International Journal of Engines*, 6(3):1395–1480, 2013.

[12] S. McConnell. Heavy-duty diesel engine nox reduction with nitrogen-enriched combustion air. Technical Report 02-VTCE-GS-009, Argonne National Laboratory, Lemont, IL, July 2010.

[13] H. Jääskeläinen and W.A. Majewski. Heavy-duty diesel engines with aftertreatment. Technical report, DieselNet Technology Guide, 2018.

[14] T. Johnson and A. Joshi. Review of Vehicle Engine Efficiency and Emissions. *SAE Technical Paper 2017-01-0907*, 2017.

[15] T. Johnson. *Review of Selective Catalytic Reduction (SCR) and Related Technologies for Mobile Applications*, pages 3–31. Springer New York, New York, NY, 2014.

[16] Y. Zheng, M. Li, M. Harold, and D. Luss. Enhanced low-temperature nox conversion by high-frequency hydrocarbon pulsing on a dual layer lnt-scr catalyst. *SAE International Journal of Engines*, 8(3):1117–1125, 2015.

[17] D. Carder, R. Ryskamp, M. Besch, and A. Thiruvengadam. Emissions control challenges for compression ignition engines. *Procedia IUTAM*, 20:103 – 111, 2017. 24th International Congress of Theoretical and Applied Mechanics.

[18] F. Gao, X. Tang, H. Yi, S. Zhao, C. Li, J. Li, Y. Shi, and X. Meng. A review on selective catalytic reduction of nox by nh3 over mnbased catalysts at low temperatures: Catalysts, mechanisms, kinetics and dft calculations. *Catalysts*, 7(7), 2017.

[19] D. Zhong, S. He, P. Tandon, M. Moreno, and T. Boger. Measurement and prediction of filtration efficiency evolution of soot loaded diesel particulate filters. In *SAE Technical Paper*. SAE International, 2012.

[20] R. Allansson, P.G. Blakeman, B.J. Cooper, H. Howard, P.J. Silcock, and A.P. Walker. Optimising the low temperature performance and regeneration efficiency of the continuously regenerating diesel particulate filter (cr-dpf) system. In *SAE Technical Paper*. SAE International, 2002.

[21] P. Phlips and T. Megli. Powertrain Efficiency in the US Fleet on Regulatory Drive Cycles and with Advanced Technologies. *SAE International Journal of Fuels and Lubricants*, 10(2):2017–01–0895, 2017.

[22] A. Radulescu, J. McCarthy Jr, and S. Brownell. Development of a Switching Roller Finger Follower for Cylinder Deactivation in Gasoline Engine Applications. *SAE Technical Paper 2013-01-0589*, 91:347–360, 2013.

[23] T.G. Leone and M. Pozar. Fuel Economy Benefit of Cylinder Deactivation - Sensitivity to Vehicle Application and Operating Constraints. *SAE Technical Paper Series*, 1645(724):10–11, 2001.

[24] M. Stabinsky, W. Albertson, J. Tuttle, D. Kehr, J. Westbrook, H. Karbstein, and M. Kuhl. Active fuel management technology: Hardware development on a 2007 gm 3.9l v-6 ohv si engine. In *SAE World Congress and Exhibition*. SAE International, 2007.

[25] M. Fujiwara, K. Kumagai, M. Segawa, R. Sato, and Y. Tamura. Development of a 6-Cylinder Gasoline Engine with New Variable Cylinder Management Technology. 2008(724), 2008.

[26] K.J. Douglas, N. Milovanovic, J.W.G. Turner, and D. Blundell. Fuel Economy Improvement Using Combined CAI and Cylinder Deactivation (CDA)-An Initial Study. *Training*, 2013:6–11, 2005.

[27] S.C. Davis, S.E. Williams, R.B. Boundy, and S. Moore. 2015 vehicle technologies market report. Technical report, Oak Ridge National Laboratory, Oak Ridge, TN, 2015.

[28] Transportation Research Board, Engineering National Academies of Sciences, and Medicine. *Identification and Evaluation of Freight Demand Factors*. The National Academies Press, Washington, DC, 2012.

[29] A. Papson and M. Ippoliti. Key performance parameters for drayage trucks operating at the ports of los angeles and long beach, 2013.

[30] C. Ding, L. Roberts, D.J. Fain, A.K. Ramesh, G.M. Shaver, J. McCarthy Jr, M. Ruth, E. Koeberlein, E.A. Holloway, and D. Nielsen. Fuel efficient exhaust thermal management for compression ignition engines during idle via cylinder deactivation and flexible valve actuation. *International Journal of Engine Research*, 2015.

[31] M.C. Joshi, D.B. Gosala, C.M. Allen, K. Vos, M. Van Voorhis, A. Taylor, G.M. Shaver, J. McCarthy Jr, D. Stretch, E. Koeberlein, and L. Farrell. Reducing diesel engine drive cycle fuel consumption through use of cylinder deactivation to maintain aftertreatment component temperature during idle and low load operating conditions. *Frontiers in Mechanical Engineering*, 3:8, 2017.

[32] S. Pillai, J. LoRusso, and M. Van Benschoten. Analytical and experimental evaluation of cylinder deactivation on a diesel engine. In *SAE 2015 Commercial Vehicle Engineering Congress*. SAE International, 2015.

[33] H. Mo, Y. Huang, X. Mao, and B. Zhuo. The effect of cylinder deactivation on the performance of a diesel engine. *Proceedings of the Institution of Mechanical Engineers, Part D: Journal of Automobile Engineering*, 228(2):199–205, 2014.

[34] D.B. Gosala, C.M. Allen, A.K. Ramesh, G.M. Shaver, J. McCarthy Jr, D. Stretch, E. Koeberlein, and L. Farrell. Cylinder deactivation during dynamic diesel engine operation. *International Journal of Engine Research*, 18(10):991–1004, 2017.

[35] J. McCarthy Jr. *Cylinder deactivation improves Diesel aftertreatment and fuel economy for commercial vehicles*, pages 1013–1039. Springer Fachmedien Wiesbaden, Wiesbaden, 2017.

[36] A.N. Bharath, Y. Yang, R.D. Reitz, and C. Rutland. Comparison of Variable Valve Actuation , Cylinder Deactivation and Injection Strategies for Low-Load RCCI Operation of a Light Duty Engine. 2015.

[37] X. Lu, C. Ding, A. Ramesh, G. Shaver, E. Holloway, J. McCarthy Jr, M. Ruth, E. Koeberlein, and D. Nielsen. Impact of cylinder deactivation on active diesel particulate filter regeneration at highway cruise conditions. *Frontiers in Mechanical Engineering*, 1(9), 2015.

[38] A.K. Ramesh, G.M. Shaver, C.M. Allen, S. Nayyar, D.B. Gosala, D. Caicedo Parra, E. Koeberlein, J. McCarthy Jr, and D. Nielsen. Utilizing low airflow strategies, including cylinder deactivation, to improve fuel efficiency and aftertreatment thermal management. *International Journal of Engine Research*, 18(10):1005–1016, 2017.

[39] M. Halbe, B. Pietrzak, D. Fain, A.K. Ramesh, G.M. Shaver, J. McCarthy Jr, M. Ruth, and E. Koeberlein. Oil accumulation and first fire readiness analysis of cylinder deactivation. *Frontiers in Mechanical Engineering*, 3:1, 2017.

[40] M. Rebbert, G. Kreusen, and S. Lauer. A new cylinder deactivation by fev and mahle. In *SAE World Congress and Exhibition*. SAE International, 2008.

[41] W. Gottschalk, R. Fink, and M. Schultalbers. Investigations on ventilation strategies for si cylinder deactivation based on a variable valve train. In *SAE 2016 International Powertrains, Fuels and Lubricants Meeting*. SAE International, 2016.

[42] M. Wilcutts, J. Switkes, M. Shost, and A. Tripathi. Design and Benefits of Dynamic Skip Fire Strategies for Cylinder Deactivated Engines. *SAE Int. J. Engines*, 6:278–288, 2013.

[43] A. Ihlemann and N. Nitz. Cylinder Deactivation A technology with a future or a niche application? *10th Schaeffler Symposium*, 2014.

[44] Qianfan Xin. Chapter 11 - noise, vibration, and harshness (nvh) in diesel engine system design. In *Diesel Engine System Design*, pages 759 – 821. Woodhead Publishing, 2013.

[45] B.M. Spessert and H.A. Kochanowski. *Diesel Engine Noise Emission*, pages 487–504. Springer Berlin Heidelberg, Berlin, Heidelberg, 2010.

[46] T. Ramachandran and K.P. Padmanaban. Review on internal combustion engine vibrations and mountings. *International Journal of Engineering Sciences and Emerging Technologies*, 3(1):2231–6604, 2012.

[47] T. Wellmann, K. Govindswamy, and D. Tomazic. Impact of the Future Fuel Economy Targets on Powertrain, Driveline and Vehicle NVH Development. *SAE International Journal of Vehicle Dynamics, Stability, and NVH*, 1(2):2017–01–1777, 2017.

[48] T. Wellman, K. Govindswamy, E. Braun, and K. Wolff. Aspects of Driveline Integration for Optimized Vehicle NVH Characteristics. *SAE Technical Paper*, (724), 2007.

[49] C. Schenk and P. Dekraker. Potential Fuel Economy Improvements cEGR and CDA on Atkinson Engine. *SAE Technical Paper 2017-01-1016*, 2017.

[50] P. Lee and A. Rahbar. Active tuned absorber for displacement-on-demand vehicles. In *SAE 2005 Noise and Vibration Conference and Exhibition*. SAE International, 2005.

[51] J. Serrano, G. Routledge, N. Lo, M. Shost, V. Srinivasan, and B. Ghosh. Methods of Evaluating and Mitigating NVH when Operating an Engine in Dynamic Skip Fire. *SAE International Journal of Engines*, 7(3), 2014.

[52] E. Watanabe and I. Fukutani. Cylinder cutoff of 4-stroke cycle engines at part-load and idle. In *SAE Technical Paper*. SAE International, 1982.

[53] Q. Xin. Chapter 9 - advanced diesel valvetrain system design. In *Diesel Engine System Design*, pages 529 – 650. Woodhead Publishing, 2013.

[54] D.B. Gosala, C.M. Allen, G.M. Shaver, L. Farrell, E. Koeberlein, B. Franke, D. Stretch, and J. McCarthy Jr. Dynamic cylinder activation in diesel engines. *International Journal of Engine Research*, 0(0):1468087418779937, 2018.

[55] D.B. Gosala, A.K. Ramesh, C.M. Allen, M.C. Joshi, A.H. Taylor, M. Van Voorhis, G.M. Shaver, L. Farrell, E. Koeberlein, J. McCarthy Jr, and D. Stretch. Diesel engine aftertreatment warm-up through early exhaust valve opening and internal exhaust gas recirculation during idle operation. *International Journal of Engine Research*, 19(7):758–773, 2018.

[56] M.C. Joshi, D.B. Gosala, C.M. Allen, S. Srinivasan, A.K. Ramesh, M. Van Voorhis, A. Taylor, K. Vos, G.M. Shaver, J. McCarthy Jr, L. Farrell, and E. Koeberlein. Diesel engine cylinder deactivation for improved system performance over transient real-world drive cycles. In *WCX World Congress Experience*. SAE International, 2018.

[57] K.R. Vos, G.M. Shaver, X. Lu, C.M. Allen, J. McCarthy Jr, and L. Farrell. Improving diesel engine efficiency at high speeds and loads through improved breathing via delayed intake valve closure timing. *International Journal of Engine Research*, 20(2):194–202, 2019.

[58] C.M. Allen, D.B. Gosala, G.M. Shaver, and J. McCarthy Jr. Comparative study of diesel engine cylinder deactivation transition strategies. *International Journal of Engine Research*, 2018.

[59] C. Lindhjem, L. Chan, A. Pollack, and C. Kite. Applying Humidity and Temperature Corrections to On and Off-Road Mobile Source Emissions. *13th International Emission Inventory Conference "Working for Clean Air in Clearwater"*, pages 6–7, 2004.

[60] F. Stodolsky, L. Gaines, and A. Vyas. Analysis of technology options to reduce the fuel consumption of idling trucks. Technical Report ANL/ESD-43, Argonne National Laboratory, Lemont, IL, June 2000.

[61] I.N. Vuchkov and N.L. Boyadjieva. *Quality Improvement with Design of Experiments: A Response Surface Approach*. Topics in Safety, Risk, Reliability and Quality. Springer Netherlands, 2001.

[62] Environmental Protection Agency. 40 cfr 86.1342-90 - calculations; exhaust emissions, July 2002. 54 FR 14605, Apr. 11, 1989, as amended at 62 FR 47135, Sept. 5, 1997.

[63] C.A. Sharp, C.C. Webb, G.D. Neely, Sr., and I. Smith. *Evaluating Technologies and Methods to Lower Nitrogen Oxide Emissions from Heavy-Duty Vehicles*. 2017.

[64] E.G. Giakoumis. *Heavy-Duty Vehicles and Engines*, pages 193–284. Springer International Publishing, Cham, 2017.

[65] National Renewable Energy Laboratory. Nrel drivecat - chassis dynamometer drive cycles, 2018.

[66] A. Archer and J. McCarthy Jr. Quantification of diesel engine vibration using cylinder deactivation for exhaust temperature management and recipe for implementation in commercial vehicles. In *WCX World Congress Experience*. SAE International, 2018.

[67] Michael K. Neylon, Mario J. Castagnola, Norma B. Castagnola, and Christopher L. Marshall. Coated bifunctional catalysts for nox scr with c3h6: Part i: water-enhanced activity. *Catalysis Today*, 96(1):53 – 60, 2004.

[68] C.E. Goering, M.L. Stone, D.W. Smith, and P.K. Turnquist. *ENGINE DESIGN*. ASAE, St. Joseph, MI, 2003.

[69] M. Ajovalasit and J. Giacomin. Analysis of variations in diesel engine idle vibration. *Proceedings of the Institution of Mechanical Engineers, Part D: Journal of Automobile Engineering*, 217(10):921–933, 2003.

[70] G. Ebbitt and P. Davies. The role of sound quality assessment in noise control engineering. *INTER-NOISE and NOISE-CON Congress and Conference Proceedings*, 1998(1):23–40, 1998.

[71] H. Schiffbnker, F.K. Brandl, and G.E. Thien. Development and application of an evaluation technique to assess the subjective character of engine noise. In *SAE Technical Paper*. SAE International, 05 1991.

[72] Deutsches Institut fur Normung. *DIN DIN45631/A1 - Calculation of loudness level and loudness from the sound spectrum*, 2010.

[73] H. Fastl and E. Zwicker. *Psychoacoustics: Facts and Models*. Springer series in information sciences. Springer Berlin Heidelberg, 2007.

[74] G. von Bismarck. Sharpness as an attribute of the timbre of steady sounds. *Acta Acustica united with Acustica*, 30(3):159–172, 1974.

[75] P. Daniel and R. Weber. Psychoacoustical roughness: Implementation of an optimized model. *Acta Acustica united with Acustica*, 83(1):113–123, 1997.

[76] R. Sottek. *Modelle zur Signalverarbeitung im menschlichen Gehör*. RWTH Aachen, 1993.

APPENDIX

A. CYCLE ANALYSIS METHODOLOGY

In-cylinder pressure acquisition allows for characterizing the engine cycle through standard mean effective pressure (MEP) metrics. MEPs represent the mean pressure acting on the piston during that portion of the cycle. The three MEPs of concern in this work are net indicated mean effective pressure (NIMEP), gross indicated mean effective pressure (GIMEP), and pumping mean effective pressure (PMEP). The PV diagram in Figure A.1 can be used to illustrate these MEPs. GIMEP is the integrated area of the loop labeled "Gross work" divided by the cylinder displacement. It represents the work done during the compression and expansion strokes. PMEP is the integrated area of the loop labeled "Pumping work" divided by the cylinder displacement. This represents the work to pump gas from the intake to exhaust manifolds during the gas exchange process. PMEP is typically less than zero for diesel engines with high pressure EGR. Finally, NIMEP is the sum of the GIMEP and PMEP.

The brake thermal efficiency of an engine is a dimensionless parameter that describes how efficient the engine is at converting fuel energy to useful work. It is formulated in Equation (A.1). Though the BTE is ultimately of singular importance, the MEP metrics metrics can be utilized to deconstruct the brake thermal efficiency (BTE) of the engine into subcomponents of open cycle efficiency (OCE), closed cycle efficiency (CCE) and mechanical efficiency (ME) for further analysis via Equation (A.2) [11]. The OCE of the engine quantifies the ability of the engine to exchange the charge into the cylinder and exhaust products out of the cylinder. It is defined per Equation (A.3). Factors that affect OCE include turbocharger efficiency, manifold and port design, and volumetric efficiency. The CCE quantifies the efficiency of the combustion and heat transfer processes that occur during the compression and expansion. It is defined per Equation (A.4). The main factors that affect CCE can be generally categorized as combustion efficiency and in-cylinder heat transfer. Fi-
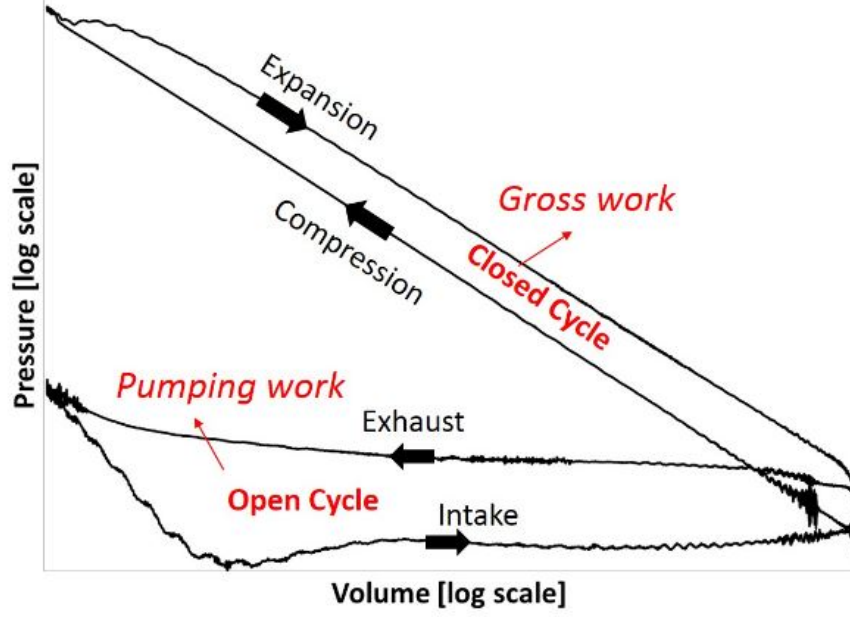
Figure A.1. LogP-LogV diagram annotated with cycle characteristics.

nally, ME describes the efficiency of the work transmission of the engine. As shown in Equation (A.6), ME often back-calculated from BTE using but can also be determined using the brake mean effect pressure (BMEP) of the engine in conjunction with NIMEP. These are the most effective methods of calculating ME when combustion is occurring because the combustion pressure increase can increase friction in the cylinders. However, relative comparisons can also be obtained by using motoring tests to determine frictional losses with different accessory configurations. Numerous factors influence ME, but among the most prevalent are mechanical friction, accessory loads, and high pressure fuel pump load.

$$BTE = \frac{P_{brake}}{\dot{m}_{fuel}Q_{LHV}} \tag{A.1}$$

where P_{brake} is the brake power of the engine, $\dot{m}_{fuel}$ is the fuel flow rate, and Q_{LHV} is the lower heating value of the fuel.

$$BTE = OCE \cdot CCE \cdot ME \tag{A.2}$$

$$OCE = \frac{NIMEP}{GIMEP} = 1 - \frac{PMEP}{GIMEP} \tag{A.3}$$

$$CCE = \frac{GIMEP}{\frac{\dot{m}_{fuel}Q_{LHV}}{C \cdot N \cdot V_d}} \tag{A.4}$$

where $\dot{m}_{fuel}$ is the fuel flow rate, Q_{LHV} is the lower heating value of the fuel, N is the engine speed, V_d is the displacement of the engine, and C is a constant for unit conversion.

$$BMEP = \frac{P_{brake}}{C \cdot V_d \cdot N} \tag{A.5}$$

where P_{brake} is the brake power of the engine, V_d is the engine displacement, N is the engine speed, and C is a constant for unit conversion.

$$ME = \frac{BTE}{OCE \cdot CCE} = \frac{BMEP}{NIMEP} \tag{A.6}$$

VITA

VITA

EDUCATION:

Purdue University, West Lafayette, IN

Ph.D. in Mechanical Engineering, May 2019

M.S. in Mechanical Engineering, December 2016

University of Illinois at Urbana-Champaign, Champaign, IL

B.S. in Mechanical Engineering, May 2014

EMPLOYMENT EXPERIENCE:

Purdue University, Herrick Laboratories: Graduate Research Assistant, September 2014-May 2019.

Purdue University, Mechanical Engineering: Graduate Teaching Assistant, September 2016-December 2017.

SGS: Intern, May-August 2016.

Caterpillar Inc: Intern, May-August 2013.

SELECT PUBLICATIONS:

C. Allen, D. Gosala, G. Shaver, and J. McCarthy, Jr. *Comparative study of diesel engine cylinder deactivation transition strategies.* International Journal of Engine Research. 146808741876811. 10.1177/1468087418768117. 2018.

D. Gosala, C. Allen, G. Shaver, L. Farrell, E. Koeberlein, B Franke, D. Stretch, and J. McCarthy, Jr. *Dynamic cylinder activation in diesel engines.* International Journal of Engine Research. https://doi.org/10.1177/1468087418779937. 2018.

C. Allen, M. Joshi, D. Gosala, G. Shaver, L. Farrell, and J. McCarthy, Jr. *Experimental assessment of diesel engine cylinder deactivation performance during load load transient operations.* Submitted.